ERASMUS MUNDUS MSC PROGRAMME

COASTAL AND MARINE ENGINEERING AND MANAGEMENT
COMEM

THE INFLUENCE OF THE DIQUE CHANNEL DISCHARGE ON THE SEA WATER LEVEL OF CARTAGENA BAY - COLOMBIA

Supervisor: Ph.D Marc Mestres

UNIVERSITAT POLITECNICA DE CATALUNYA
2011

Ricardo Molares Babra

The Erasmus Mundus MSc Coastal and Marine Engineering and Management is an integrated programme organized by five European partner institutions, coordinated by Delft University of Technology (TU Delft).

The joint study programme of 120 ECTS credits (two years full-time) has been obtained at three of the five CoMEM partner institutions:

- Norges Teknisk- Naturvitenskapelige Universitet (NTNU) Trondheim, Norway
- Technische Universiteit (TU) Delft, The Netherlands
- City University London, Great Britain
- Universitat Politècnica de Catalunya (UPC), Barcelona, Spain
- University of Southampton, Southampton, Great Britain

The first year consists of the first and second semesters of 30 ECTS each, spent at NTNU, Trondheim and Delft University of Technology respectively. The second year allows for specialization in three subjects and during the third semester courses are taken with a focus on advanced topics in the selected area of specialization:

- Engineering
- Management
- Environment

In the fourth and final semester an MSc project and thesis have to be completed.

The two year CoMEM programme leads to three officially recognized MSc diploma certificates. These will be issued by the three universities which have been attended by the student. The transcripts issued with the MSc Diploma Certificate of each university include grades/marks for each subject. A complete overview of subjects and ECTS credits is included in the Diploma Supplement, as received from the CoMEM coordinating university, Delft University of Technology (TU Delft).

Information regarding the CoMEM programme can be obtained from the programme coordinator and director

Prof. Dr. Ir. Marcel J.F. Stive
Delft University of Technology
Faculty of Civil Engineering and geosciences
P.O. Box 5048
2600 GA Delft
The Netherlands

TABLE OF CONTENTS

LIST OF FIGURES

LIST OF TABLES

AKNOWLEDGMENT

I thank the Colombian Navy who provided me the time to make possible this Master studies, and the COMEM program who provided the funds for my scholarship. I also thank the Centro de Investigaciones Oceanográficas e Hidrográficas who provided me the most of the information and data I used for the thesis, and to Dr. Serguei Lonin who provided me an executable version of MECCA and helped me with the model configuration.

I would like to thanks the people of the UPC, especially Dr. Cesar Mösso whose help was invaluable, Dr.Marc Mestre for the advice, supervision and the interest given to this project, and to Pep Ciuraneta from the UPCLinux Group for helping me with the software installation, as well as the people of the administration of the Faculty, Genoveva and Gorka. I also want to thank all the teachers I had during this two years in NTNU, TUDELFT and UPC.

Finally, I deeply thank my wife Maria Eugenia and my daughter, Laura, whose helps, love and understanding supported me not only during the thesis but during the entire Master, and for the sacrifice they had to make, to stay with me during this two years, far from their friends and family.

INTRODUCTION

The sea level rise (SLR) due to climate change is one of the most important concerns in the coastal zone and particularly in low lying areas, not only in those natural areas but also in developed urban cities at the coast. Normally, the SLR is related to the increase of the volume of water due to the increasing temperatures that trigger thermal expansion of the sea water, and to the melting of the glaciers. The vertical movement of the land (subsidence) due to geological or man-induced causes is taken into consideration with the sea level rise to derive the relative sea level rise.

Climate change is generally related to the increase of the temperature since this is a basic measurable parameter of it, but it also causes changes in wind patterns, storm severity or frequency, as well as in the rainfall and run-off. The increase of river discharges will change salinity and, if not controlled, also the nutrients loads in coastal areas that can result in future eutrophication. What about the impacts in the sea level rise due to the possible increase in the river discharge in specific situation like semi enclosed bays or small estuaries?

Cartagena de Indias is a colonial city in the Colombian Caribbean coast situated along Cartagena Bay. This bay is flanked by an island (Tierrabomba) that creates two entrances or inlets to the bay. The entrances had been modified throughout the time by deepening the main entrance in the southwest for navigational purposes and shallowing the northern entrance for military defensive purposes during the Spanish colonization times in the fifteenth century. In 1850 a channel was dug in the south of the bay to connect Cartagena with the Magdalena River, the main fluvial artery of the country. The original marine life associated to the coral reef in the bay as well as the currents regime are no longer the same, and nowadays the bay is considered an estuary.

The sea level rise has attracted a lot of attention in Cartagena since the city is situated in a low lying area and in the last years it has been suffering flooding during the yearly higher tides. The relative sea level rise estimation for the Cartagena Bay is around 5.98 mm/yr and since the flooding is already happening during October and November, an additional few centimetres in the water level due to meteorological effects (including river discharges) will have important effects.

The Marine and Coastal Research Institute (INVEMAR) has explained this seasonal behaviour in Vides, M., 2008, as follows:

Sea-level is usually lowerr at the end of April when winds cease and increases during the time of transition until the arrival of the "Veranillo" in July or August when it has a slight and noticeable reduction reaching his maximum level in October.

At the end of the boreal summer, due to the seasonal thermal expansion, there is a shift of wind direction and intensity of the Crosscurrent of Panama-Colombia (Andrade 2000). The lower sea-level returns at the end of November with the arrival of the "wind time". This annual variation reaches around 40cm. Added to the 40cm of amplitude in a high tide in October, it produces during day hours an increase of almost a meter at the

Bay mean sea-level. The phenomenon translated into the well-known yearly floods of the low zones of the coast in Cartagena, the overflowing of pipes, and the opening of the bar of the Cienaga de la Virgen (from the sea inwards) among other aspects that have been observed and little studied"

In the project: "Environmental Restoration Plan for the Depleted Ecosystems around the Dique Channel" undertaken by UNINORTE (Universidad del Norte) and CIOH (Centro de Investigaciones Oceanograficas e Hidrograficas) in 1999, some numerical experiments were done in order to describe the hydrodynamic regime of the bay. The role of the river discharge was found one of the main contributors to the chemical processes, the circulation and the sea level behaviour, producing a water level slope higher at the mouth of the river and lower at the entrances of the bay (in the order of centimetres), producing barotropic currents.

This study aims at understanding the impact and the contribution of the river discharge on the sea level in Cartagena Bay and its role in the sea level rise due to climate change and strong meteorological phenomena such as ENSO (El Niño Southern Oscillation)

DESCRIPTION OF THE PROBLEM

Every year during the October - November period, Cartagena city experiences the highest sea water level that exceeds the inundation mark. Preliminary analysis of the water level data in Cartagena Bay shows a faster rising trend during the rainy season (October – November) that can not be related to storm surge because during this season the weakest wind regime is present. In order to assess future adaptation or mitigation measures due to the sea level rise in Cartagena, no real knowledge about the contributors and their contribution to the water level or to the sea level rise exists.

HYPOTESIS

The Dique Channel is one of the contributors to the water level and to the sea level behaviour in Cartagena Bay. Strong meteorological phenomena as ENSO can produce relative important elevation of the sea level in the Bay.

OBJECTIVES

- Description of the main meteorological and oceanographic forcing of the water level in the Caribbean Sea and the bay of Cartagena.
- Configuration of the ROMS model applied to the bay of Cartagena.
- Simulation of the hydrodynamic field of Cartagena Bay according the meteorological and hydrological yearly cycle (climatic seasons).
- Model results comparison between the ROMS and CODEGO models.
- Comparison of the modelled water level results with the water level data.
- Determination of the influence of the Dique Channel discharge in the water level of the Cartagena Bay.

METHODOLOGY

In order to achieve the proposed objectives a literature review is done to identify the possible contributors to the sea level in Cartagena Bay. In the geographical mesoscale, the oceanographic characteristics of the Caribbean Sea that can play a role in the sea level and could influence Cartagena Bay are revised considering aspects as currents, eddies, tides and meteorological components as cold fronts and hurricanes.

Even though the present study is focused on the role of the Dique Channel in the sea level of the bay of Cartagena, other aspects as the tides, sea level rise, subsidence and phenomena as the ENSO are considered taking into account the strong relationship between the fluctuation of the Dique Channel flow rate and El Niño or La Niña years.

In the first two chapters the available information of the system (Caribbean Sea and Cartagena Bay) is studied and presented in order to make a first qualitative approach to understand possible links between the Dique Channel discharge and the sea level behaviour in the bay of Cartagena.

To simulate the sea level in Cartagena Bay the Regional Ocean Model System (ROMS-Agrif 2.1) is used to include not only the tides as forcings of the sea level, but also the density gradient and surface slope due to the strong impact of the Dique Channel discharge on the temperature, salinity and density of the bay. Apart from the wind-driven and tidal currents, baroclinic currents are also simulated. In chapter IV the implementation of the input files is described.

To calibrate the ROMS model a comparison with the CODEGO (*Lonin, 1997)* model results is done. The CODEGO model was developed and calibrated by the CIOH (Oceanographic and Hydrographic Research Center); this model has been used in the bay as hydrodynamic component for ecological models (eutrophication – auto-depuration – Oil spill). Chapter V.

In order to find a link between the Dique Channel discharge and the sea level in the bay different scenarios were set up and the simulations were undertaken. These scenarios were designed with the objective of finding the differences in the sea level due to different conditions. The scenarios were focused on the detected mean differences of the bay water level along the year, to evaluate the fluctuation of the water level of the bay during the climatic seasons taking into consideration meteorological forcing (wind regime), oceanographic forcing (tides) and hydrological forcing (Dique Channel discharge). Chapter VI.

Finally the simulated water level time series in the bay obtained by the different simulated scenarios is compared with the available water level data measured in the bay, in order to determine the influence of the Dique Channel discharge.

DATA

Water level in the bay: the hourly time series data of the sea level in the bay between 1990 and 2010 is available in order to compare the model results. The bay water level was measured by the IDEAM (Institute of Hydrology, Meteorology and Environmental Studies) using a tide gauge situated in Naval Club (Castillogrande) during 1949 – 1995. In 1995 the tide gauge was moved to the CIOH facilities in the Manzanillo Island.

Bathymetry: the bathymetric data obtained by the CIOH during the 2008 hydrographic surveys for the publication of the Cartagena bay nautical chart COL 261 (7th ed. - 2009) is used for the bathymetric grid of the model, among others surveys, not only in Cartagena but in the surrounded area.

Dique Channel Flow Rates: The Dique Channel flow rate is measured by the IDEAM at four stations. The monthly variation of the average flow rate (1984-2000) and the 1988 – 1991 records are used.

Currents: Taking into consideration that the CODEGO model was validated by the CIOH for the bay of Cartagena, the currents data generated by that model is used for inter-comparison of the ROMS results.

Meteorological data: In the Manzanillo Island, facing Cartagena bay, the CIOH has measured the meteorological parameters and the information available for this study covers the period 2000 – 2010.

1 DESCRIPTION OF THE CARIBBEAN BASIN

The Caribbean Sea is a semi-enclosed sea surrounded by the greater and Lesser Antilles at the north and west respectively, and by the Central ad South American coastlines at the east and south. On the basis on the bottom topography in the Caribbean five different basins are evident. From east to west, the Grenada Basin lies between the Lesser Antilles Arc and Las Aves Ridge. The Beata Ridge crosses the central Caribbean, separating the Venezuela Basin in the east from the Colombian Basin in the west. The Central American Rise separates the Cayman and Colombian Basins. Finally, the Cayman Ridge divides the Cayman and Yucatan Basins, and the Caribbean ends in the Yucatan Strait (*Andrade, 2000*).

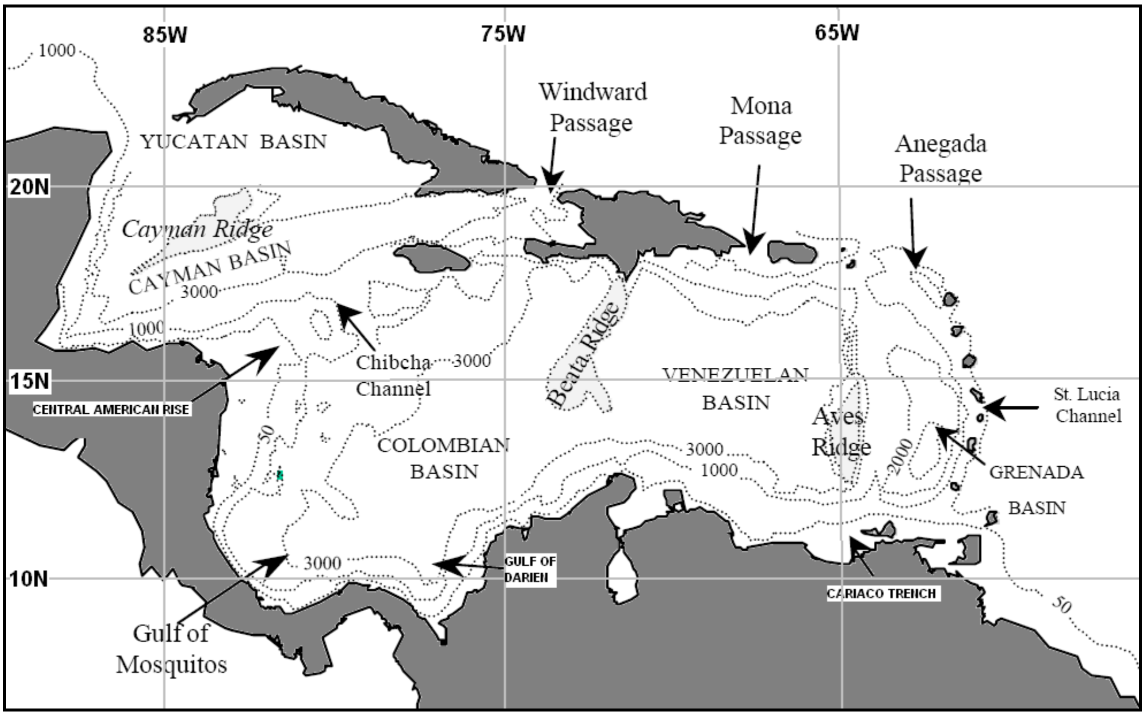

Figure 1. The Caribbean Sea shows important geological and geographical features. Adapted from Andrade (2000).

1.1 Relevant Oceanographic Features

1.1.1 Currents

The surface ocean in the region presents generally westward flowing currents which sweep the major crests of the Aves and Beata Ridges and the Colombian and Venezuelan Basin before this westward advection confronts the Central American Rise, and the flow turns northwest to the Gulf of Mexico. This main current called Caribbean Current has a northern and southern components (Southern Caribbean Current – sCC, Northern Caribbean Current – nCC) (*Jouanno et al., 2009*)

The sCC, which is the primary source of the Gulf Stream, begins where the Guyana Current and the North Ecuatorial Current (NEC) flows into the Lesser Antilles. It continues along the northern coast of Venezuela, Colombia and Central America, south of the Great Antilles Arc. Its westward continuation is known as the Yucatan Current and when it enters the Gulf of Mexico it takes the name of Loop Current. This flow then exits through the Straits of Florida as the Florida Current, starting the Gulf Stream. The westward flow north of the Antilles Islands is known as the Antilles Current or the nCC. The opposite deep movement beneath this current is part of a continuous deep western boundary current that flows outside of the basin *(Fine and Molinari, 1988).* The Deep Western Boundary Current of the Global Conveyor Belt flows equatorward at a depth of about 3000 m along the periphery of the IAS[1] continental slope, (*Stommel, 1965; Molinari et al., 1992* and *Lee et al., 1996*) with a volume transport of about 15Sv.

Close to the Colombian basin in the Caribbean, according to Andrade et al. (2003), using hydrographic transects, an eastward flow with a subsurface core along the entire southern boundary of the Caribbean Sea has been found. The transport of the coastal limb of the Panama-Colombia Gyre (PCG), known as the Panama-Colombia Countercurrent, decreases toward the east (from 6 Sv off Panama), as water is lost into the recirculation of the PCG. Off Panama, the flow is strongest at the surface, but, off Colombia, it is strongest at around 100 m. A portion of the counterflow (1 Sv) continues eastward along the Colombian coast as far as the Guajira region (12N, 72W), where it submerges to become an undercurrent beneath the coastal upwelling center there. The eastward flow also occurs in the Venezuela Basin, beneath the coastal upwelling region off Cariaco Basin and exits the Caribbean through the Grenada Channel at around 200 m depth. Numerical simulations suggest that this flow, opposite to the Caribbean Current, is a semi-continuous feature along the entire southern boundary of the Caribbean, and that it is associated with offshore cyclonic eddies.

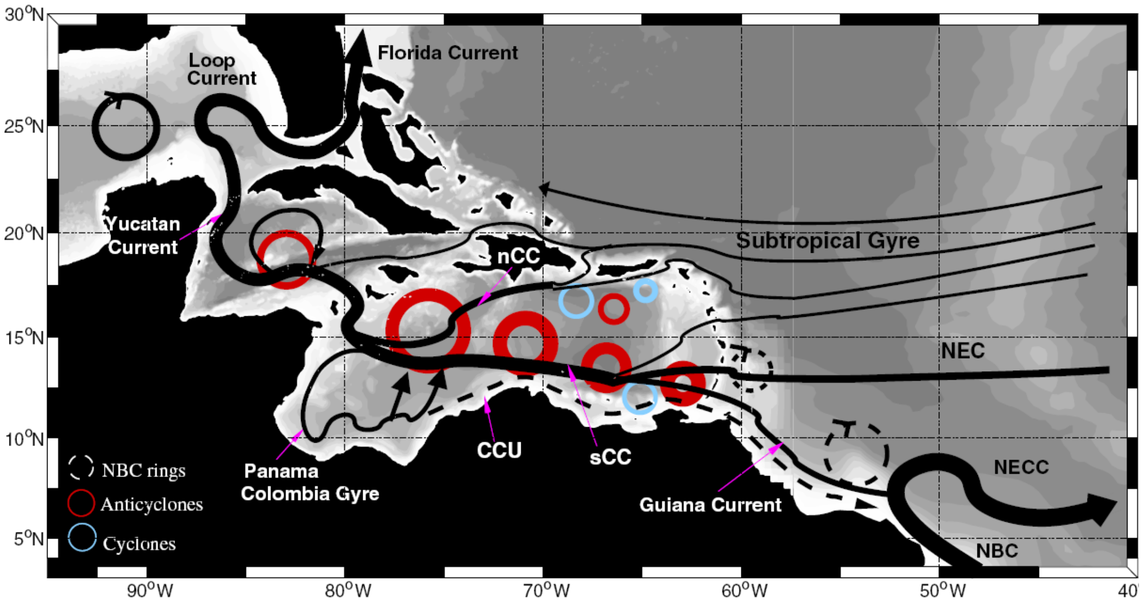

Figure 2. Main current paths: North Brazil Current (NBC), North Equatorial Current (NEC), southern Caribbean Current (sCC), northern Caribbean Current (nCC) and Caribbean Coastal Undercurrent (CCU). Circles represent structures moving westward: NBC rings (dashed), anticyclonic (red) and cyclonic (blue) Caribbean eddies.

---

[1] The Caribbean Sea together with the Gulf of Mexico and Straits of Florida make up a broader system called the Intra-Americas Sea (IAS).

1.1.2 Mesoscale Variability

An important feature of the Caribbean sea circulation is the existence of eddies that was recently described by Jouanno et al. (2008). The authors found that the Caribbean mean flow is organized in two intense jets flowing westward along the northern and southern boundaries of the Venezuela Basin, which merge in the center of the Colombia Basin. The width, depth and strength of the baroclinic eddies increase westward from the Lesser Antilles to the Colombia Basin. Although influenced by the circulation in the Colombia Basin, the variability in the Cayman Basin (which also presents a westward growth from the Chibcha Channel) is deeper and less energetic than the variability in the Colombia/Venezuela Basins.

In the production and the growth of the strong mesoscale eddy field in the Caribbean Sea the following characteristics have been identified (*Jouanno et al., 2008*):

- The mean currents in the Caribbean Sea are intrinsically unstable. The nature of the instability and its strength vary spatially due to strong differences of current structure among basins.

- The greatest and most energetic eddies of the Caribbean Sea originate in the Venezuela Basin by mixed barotropic-baroclinic instability of an intense jet, formed with waters mostly from the surface return flow of the Meridional Overturning Circulation and the North Equatorial Current which converge and accelerate through the Grenada Passage. The vertical shear of this inflow is enhanced by an eastward undercurrent, which flows along the South American Coast between 100 and 250 m depth. The shallow eddies (less than 200 m depth) formed in the vicinity of the Grenada Passage get rapidly deeper (down to 1000 m depth) and stronger by their interaction with the deep interior flow of the Subtropical Gyre, which enters through passages north of St. Lucia. These main eastern Caribbean inflows merge and form the southern Caribbean Current, whose baroclinic instability is responsible for the westward growth and strengthening of these eddies from the Venezuela to the Colombia Basin.

- Weaker eddies are produced in other regions of the Caribbean Sea. Their generation and growth is also linked with instability of the local currents. First, cyclones are formed in the cyclonic shear of the northern Caribbean Current, but appear to be rapidly dissipated or absorbed by the large anticyclones coming from the southern Caribbean. Second, eddies in the Cayman Sea, which impact the Yucatan region, are locally produced and enhanced by barotropic instability of the deep Cayman Current.

- The role of the North Brazil Current (NBC) rings is mostly to act as a finite perturbation for the instability of the mean flow. Their presence near the Lesser Antilles is ubiquitous and they appear to be linked with most of the Caribbean eddies.

1.1.3 Sea Level Variability

The Caribbean Sea has a microtidal range, for the most part between 10 and 20 cm (fig.3). The tide is primarily either mixed semidiurnal or mixed diurnal but a substantial section from Puerto Rico to Venezuela experiences diurnal tides (fig.4). The semidiurnal component of the tide is characterized for being an anticlockwise rotating amphidromic system centered in the eastern Caribbean (fig.5). The diurnal component of the tides is largely uniform in both phase and amplitude for most of the western and central Caribbean. However the diurnal phases increase rapidly toward the northwest and the Yucatan Channel (*Kjerfve, 1981*).

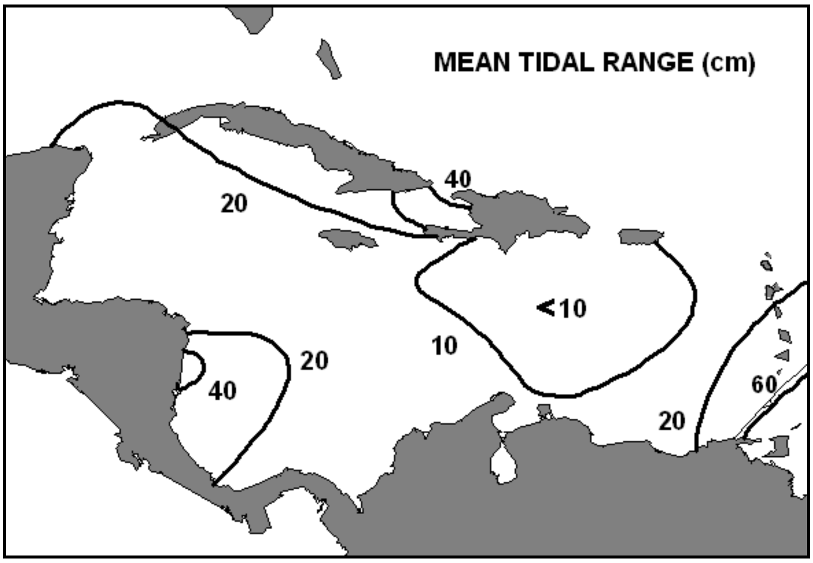

Figure 3. Spatial distribution of the mean tidal range in the Caribbean Sea (adapted from Kjerfve, 1981).

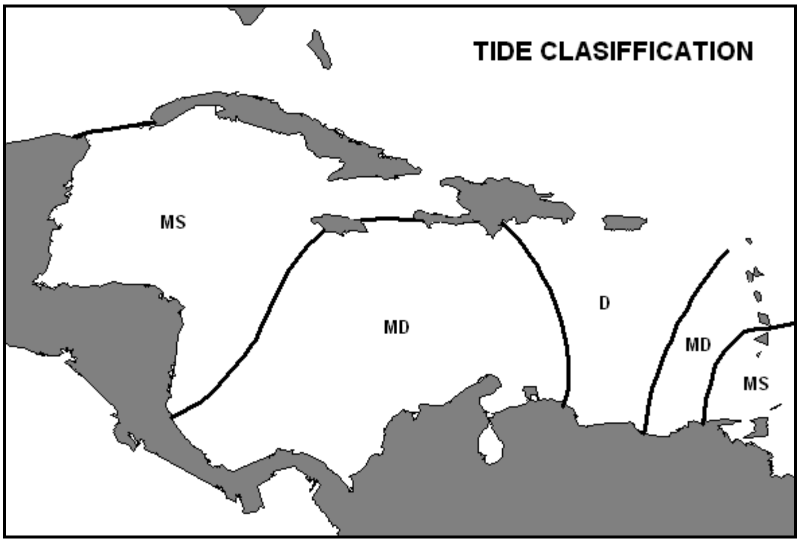

Figure 4. Tide classification in the Caribbean. MS: Mixed mainly semidiurnal. MD: Mixed mainly diurnal. D: Diurnal (adapted from Kjerfve, 1981).

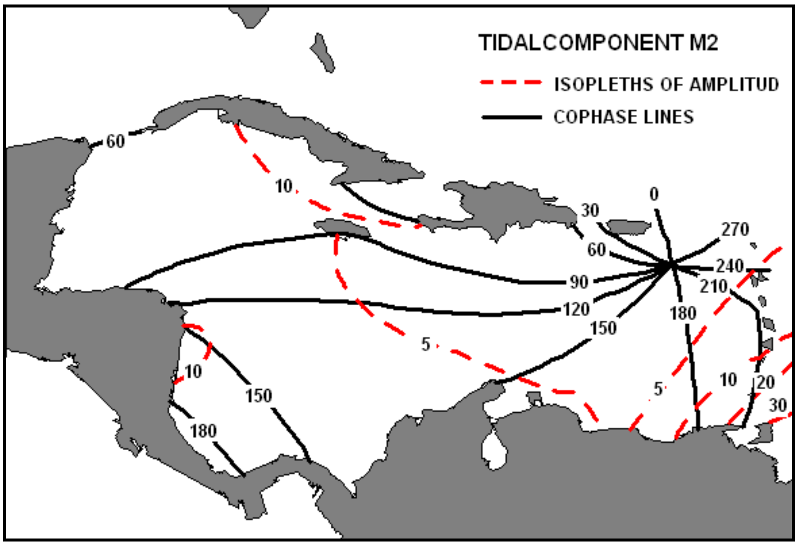

Figure 5. M_2 Tidal chart. Black solid lines represent lines of equal Greenwich phase expressed in degrees. Red dashed lines are isopleths of amplitude (H) in cm. (adapted from Kjerfve, 1981).

Cyclonic or anticyclonic circulation of surface water close to the coast may lower or rise the sea water level due to the converge or divergence of water off or to the center of rotation. Since there is a mesoscale variability in the Caribbean related with eddies travelling close to the coast (*Nystuen and Andrade, 1993; Andrade and Barton, 2000; Jouanno et al., 2008; Jouanno et al., 2009*) a sea level variability at the coast is expected (*Andrade, 2000*)

Sea level rise is one effect of both climate change and the subsidence of landmasses. According to Sutherland et al. (2008), sea level monitoring that has taken place in the Caribbean indicates that generally sea level is increasing in the region. According to some restrictions in the available data, sea level change relative to the land ranges from +8.6 mm/yr in Honduras to -6.4 mm/yr in Jamaica. The vertical motion of the land ranges from +34 mm/yr in Cuba to -27 mm/yr in Colombia, however in the case of Colombia it is necessary to highlight that the subsidence information was taken from Bogota (miles away from Cartagena, the place where the sea level data was measured). The authors estimated values of absolute change in sea level range from -4 mm/yr in Jamaica to +3 mm/yr in Barbados.

Another source of fluctuation (4 to 5 days - local inertial period) in the sea level is coherent and in phase with atmospheric waves in the Trade Winds (*Mofjeld and Wimbush, 1977- In Andrade, 2000*). The increase in the sea level due to storm surges is well known. In the Caribbean, important storm surge can occur during the hurricane season.

1.2 Relevant Meteorological Features

The winds and precipitation regime associated to their spatial variability are the main characteristics of the meteorology in the Caribbean. The precipitation is associated to the position of the Intertropical Convergence Zone (ITCZ) that can be defined as a low pressure cloudy belt around the globe. During the year the ITCZ moves from 5º S to 12º N defining the different seasons. In Colombia the season can be defined as dry, rainy and transition season (fig. 6). In his Ph.D Thesis, *Andrade (2000*) defined the climatic seasons as described below.

1.2.1 Seasons

Dry Season (December-April): or so-called the windy season; in this season the ITCZ can be found at its southernmost position around 0-5º S (fig. 6a). At this time the northern hemisphere Trade winds dominate the area with daily average speeds of about 8 m/s and up to 15 m/s during the diurnal maximum (*Andrade, 1993*). The Trade winds have a southward component in the Colombian Basin during this season. Little or no precipitation occurs during this period along the Colombian coast and the inner Antilles, although significant rain along the Panama and Costa Rican Caribbean coast is almost permanent throughout the year (*Andrade, 2000*).

Rainy Season (August – October): The ITCZ moves to 10-12º N permitting the Southern Trade winds, sometimes called "Southerlies", to cross the Central American Isthmus and to reach the Colombian Basin (fig. 6b). The associated winds are weak in the SWCS, promoting the highest rate of precipitation anywhere around the globe. These weaker (~4 m/s) and more irregular winds interact with the Northern Trades and, together with the high water vapour content, create propitious conditions for atmospheric instability. Consequently, explosive developments of cumulonimbus, with corresponding thunderstorms throughout the Colombian Basin are frequent. These conditions sometimes favour hurricane formation within the western Caribbean like the devastating Hurricane Mitch - October 1998.

Distinctive regimes occur on either side of 10º N in this season. Weak Southerlies are present south of 10º N while Northern Trade Easterlies are still strong over the central Caribbean Sea. A strong wind gradient occurs that inhibits precipitation in the north. As a result, the precipitation caused by the ITCZ climatic regime only affects the Colombian Basin south of 10º N and Easterlies occur off the Guajira Peninsula and farther east almost permanently (*Andrade, 2000*)

Transition Season (April – June): The Easterlies weaken and some precipitation occurs in the Colombian Basin (fig 6c). However, it is common for the Northern Trades to increase temporarily, inhibiting the increasing precipitation rate of the region. This Caribbean phenomenon is known as the "Veranillo" or "Mid summer drought" (*CLIVAR*, *1998*).

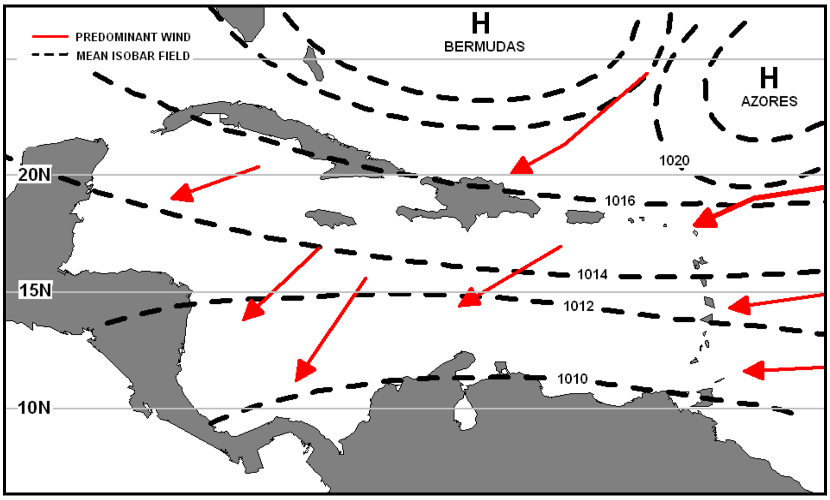

a)

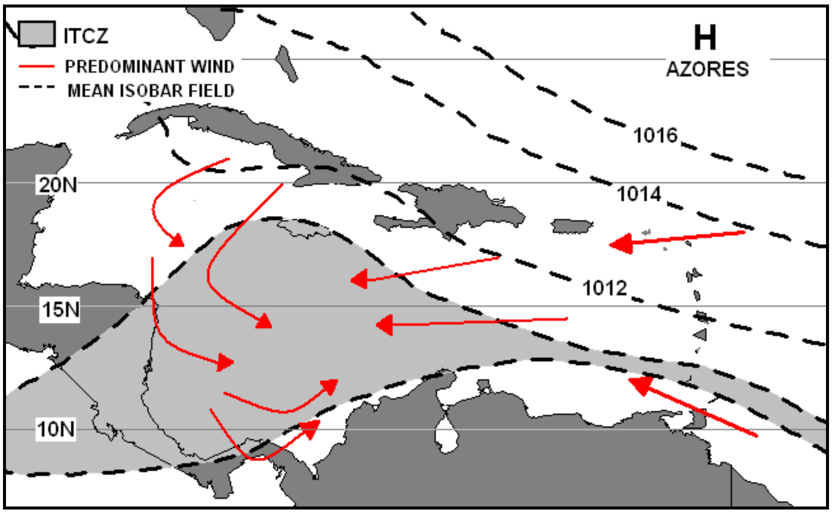

b)

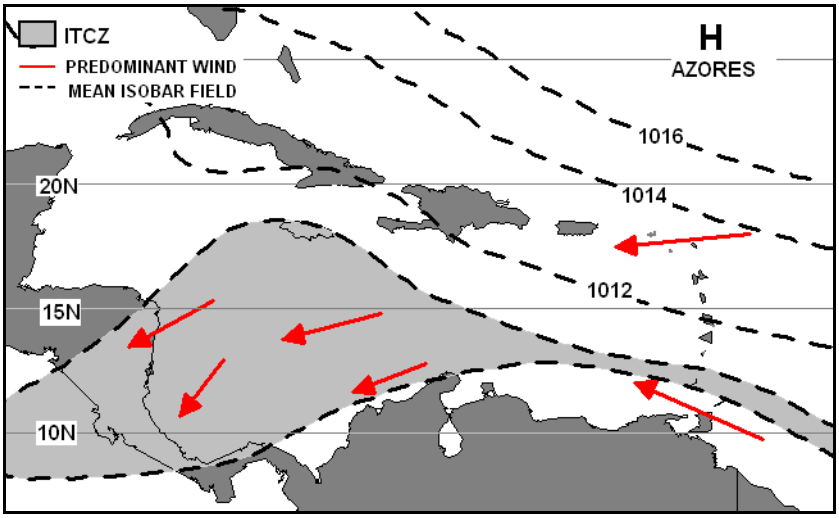

c)

Figure 6. Inter-tropical Convergence Zone. Positions for a) windy season. b) rainy season. c) transition season (adapted from *Pujos et al., 1986).*

1.2.2 Intraseasonal Oscillations

1.2.2.1 Easterly Tropical Waves

These are essentially disturbances of ondulatory type in the deep current of the tropical east, those that in their majority present cyclonal curvature and deform the pressure field. The importance of the waves from the east, frequent in the rainy season in the Colombian basin, lies in the fact that the passage of one of them through a given place alters the weather conditions, which are deteriorated gradually. Small number of these waves intensifies, originating a great part of the hurricanes.

In the Caribbean Sea, the tropical waves predominate between 20°N and 10°N. They have a thickness of 6 to 8 km and an average length of 2000 km, moving with speeds from 10 to 20 knots. The increase in cloudiness will take place in association with the ascent of the ITCZ, through which the tropical waves commonly travels.

Also, moderate precipitations in the east and northeast part of the Caribbean Sea will appear, as a result of the reactivation of a low pressure system predominant in the Gulf of Urabá, which interacts with the transit of the systems previously mentioned.These tropical waves can be experienced between May and November (table 1).

Table 1. Easterly Tropical Waves events in the Colombian coast (based on data from CIOH- Monthly Meteomarine Weather Report 2004 – 2010).

MONTH	EASTERLY TROPICAL WAVES						
	2004	2005	2006	2007	2008	2009	2010
JANUARY	0	0	0	0	0	0	0
FEBRUARY	0	0	0	0	0	0	0
MARCH	0	0	0	0	0	0	0
APRIL	0	0	0	0	0	0	2
MAY	5	5	3	0	0	2	9
JUNE	11	12	9	9	5	5	12
JULY	11	7	11	11	4	12	11
AUGUST	10	9	7	11	10	13	8
SEPTEMBER	4	6	6	6	9	5	5
OCTUBER	8	7	6	4	7	8	5
NOVEMBER	2	0	2	3	2	4	0
DECEMBER	0	0	0	0	0	0	0

1.2.2.2 Cold Fronts

Additionally, eastward cold fronts originating in North America invade the Caribbean with a 10-14 day periodicity (*Andrade, 2000*); an analysis of the CIOH- Monthly Meteomarine Weather Report (*MWR 2004/2010*) shows that the cold fronts enter the Caribbean Sea from October to April (table 2). They are especially strong during the boreal winter (*DiMego et al., 1976)* and that is why the Colombian Caribbean coast experiences one or two events of particularly strong swell from November to February, associated to these cold fronts.

Interaction between these two oscillations (cold fronts and easterly waves) affects wind velocity and produces subsequent effects in the precipitation and wind stress in the area *(Andrade, 1993; Alvarez et al., 1995: in Andrade 2000).*

Table 2. Cold fronts in the Caribbean vs Swell events in the Colombian coast. Empty cells: 0 – 0. N/A: Not available information (based on data from CIOH- Monthly Meteomarine Weather Report 2004 – 2010).

MONTH	COLD FRONT AND SWELL EVENTS IN THE COLOMBIAN COAST						
	2004	2005	2006	2007	2008	2009	2010
JANUARY	2 – 0	3 – 1	2 – 0	2 – 0	2 – 0	4 – 0	4 – 2
FEBRUARY	2 – 0	3 – 0	3 – 0	2 – 1	1 – 1	6 – 1	4 – 1
MARCH	1 – 1	5 – 0	2 – 0	2 – 0	4 – 0	1 – 0	4 – 1
APRIL	1 - 1			3 – 0	N/A	1 - 0	2 - 0
MAY				1 – 0			
JUNE							N/A
JULY							N/A
AUGUST							N/A
SEPTEMBER							N/A
OCTOBER			1 - 1	1 – 1	2 - 0	1 - 0	N/A
NOVEMBER		2 – 0	2 - 0	2 – 0	2 - 0	2 – 0	N/A
DECEMBER		4 - 0		1 - 0	4 – 0	4 – 0	N/A

1.2.2.3 Madden Julian Oscillations (MJO)

Other oscillations such as those with 40-50 day periodicities (MJO) have been detected in sea surface temperature and in precipitation data from Santa Marta, Colombia at 11ºN (*Rivera and Molares, 2003*). More recently, an 80-100 day period oscillation was found in the precipitation data in Panama (*Leaman and Donoso, 2001*). This oscillation has not been placed in a climate context yet, but it is important in the thermohaline regime in that particular region (*Andrade, 2000*).

1.2.2.4 El Niño-Southern Oscillation

The interannual variability associated with the El Niño-Southern Oscillation (ENSO), the sea surface warming in the Eastern Tropical Pacific Ocean associated with an inversion of the wind direction in the Walker Circulation in the Southern Hemisphere, has significant influence on the Caribbean Climate (*Maul, 1993*). Warm ENSO periods correlate with droughts in the north Colombian and Venezuelan Caribbean coast, while La Niña events (the inverse phase of ENSO) coincide with positive precipitation anomalies (*Alvarez et al., 1995*).

During the rainy season preceding the mature phase of a warm ENSO event the tendency is for drier than average conditions. The dry season that coincides with the mature phase of ENSO is wetter than average over the northwestern section of the Caribbean basin, that is, Yucatan, the Caribbean coast of Honduras, and Cuba, and drier than average over the rest of the basin, that is, Costa Rica and northern South America (*Gianinni et al., 2000*)

According to Poveda and Mesa (1997) the hydro climatology of tropical South America is strongly coupled to low-frequency large-scale oceanic and atmospheric phenomena occurring over the Pacific and the Atlantic Oceans. In particular, ENSO affects climatic and hydrologic conditions on timescales ranging from seasons to decades. With some regional differences in timing and amplitude, tropical South America exhibits negative rainfall and stream flow anomalies in association with the low–warm phase of the ENSO, and positive anomalies with the high–cold phase (La Niña). The ENSO effect on river discharges occurs progressively later for rivers toward the east in Colombia and northern South America. Also, the impacts of La Niña are more pronounced than those of El Niño.

The National Oceanographic and Atmospheric Administration (NOAA) have developed the Oceanic Niño Index (ONI) in order to identify such events. It is the running 3-month mean SST anomaly for the Niño regions. Events are defined as 5 consecutive months at or above the +0.5 °C anomaly for warm (El Niño) events and at or below the -0.5 ºC anomaly for cold (La Niña) events. The threshold is further broken down into Weak (with a 0.5 to 0.9 SST anomaly), Moderate (1.0 to 1.4) and Strong (≥ 1.5) events. Figure 7 shows ENSO events from 1992.

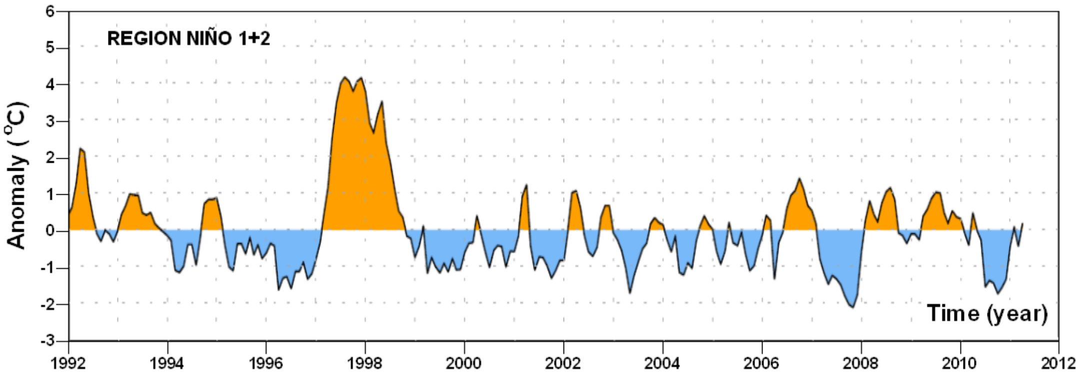

(a)

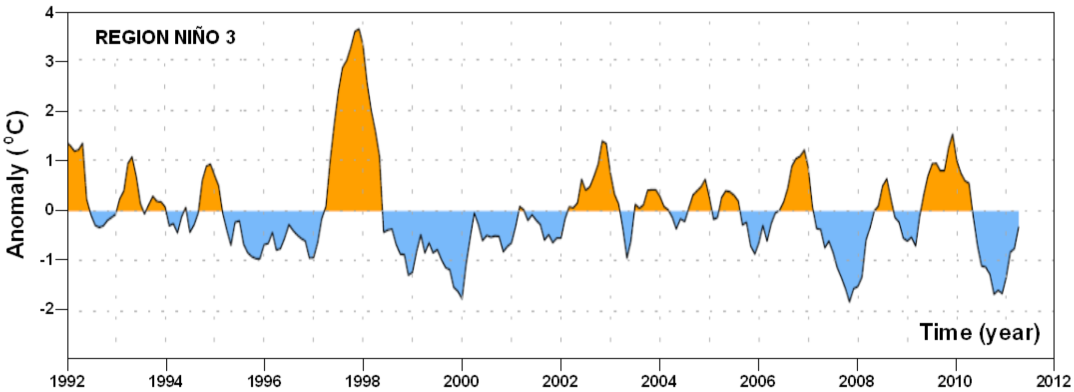

(b)

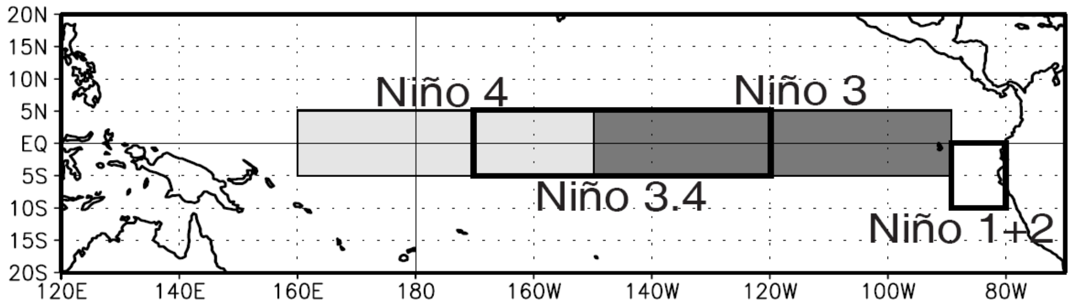

(c)

Figure 7. SST anomaly in region 1+2 (a) and region 3 (b) according to the international El Niño regions distribution (c) (*Shi et al., 2011*).

1.2.3 Storms and Hurricanes

The hurricane season runs from June 1st to November 30th. Through the Caribbean around 11 storms can travel (fig. 8) in highly random paths, being September the most active month (fig. 9). In figure 10 the path of hurricanes during the season is indicated.

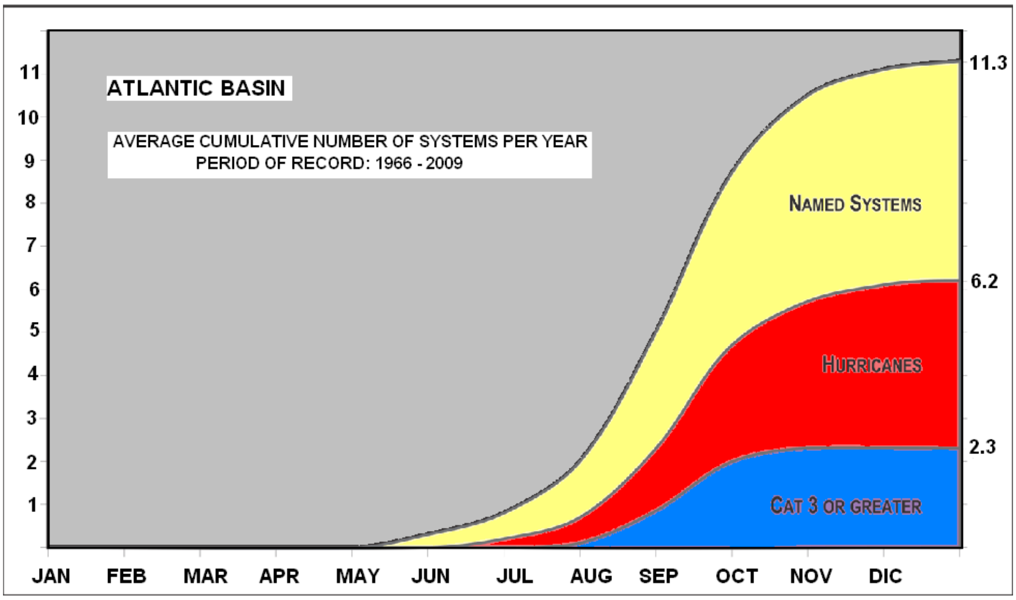

Figure 8. Average cumulative number of systems per year. Source: NOAA. http://www.nhc.noaa.gov/pastprofile.shtml (10/03/2011)

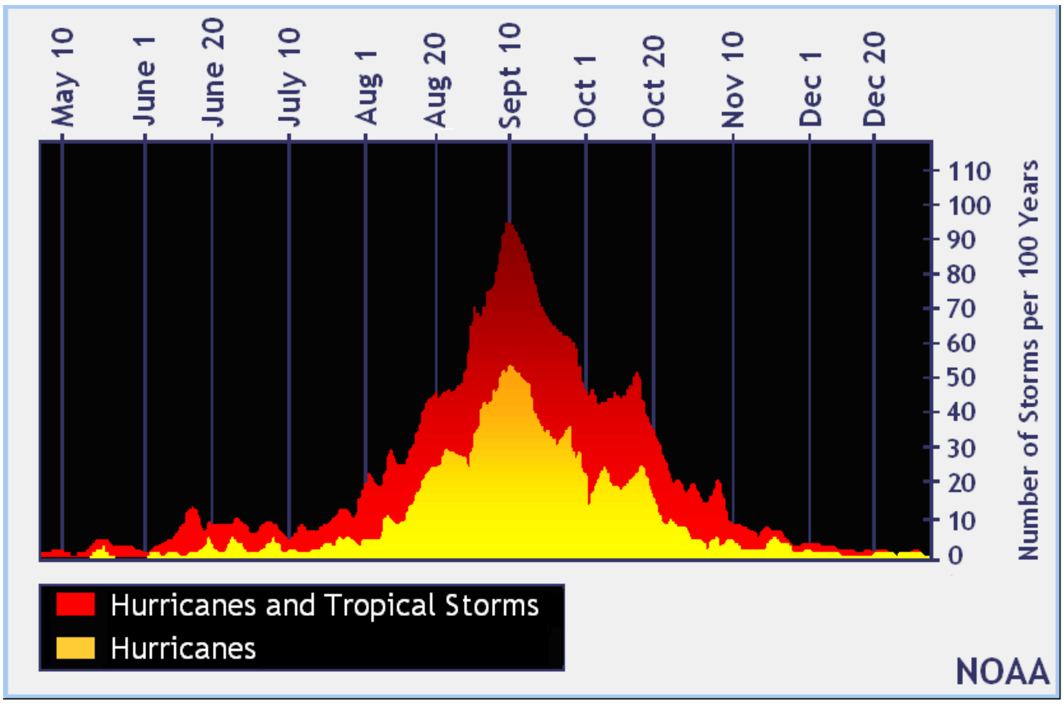

Figure 9. Number of storms per 100 years. As seen in the graph above, the peak of the season is from mid-August to late October. Source: NOAA. http://www.nhc.noaa.gov/pastprofile.shtml (10/03/2011)

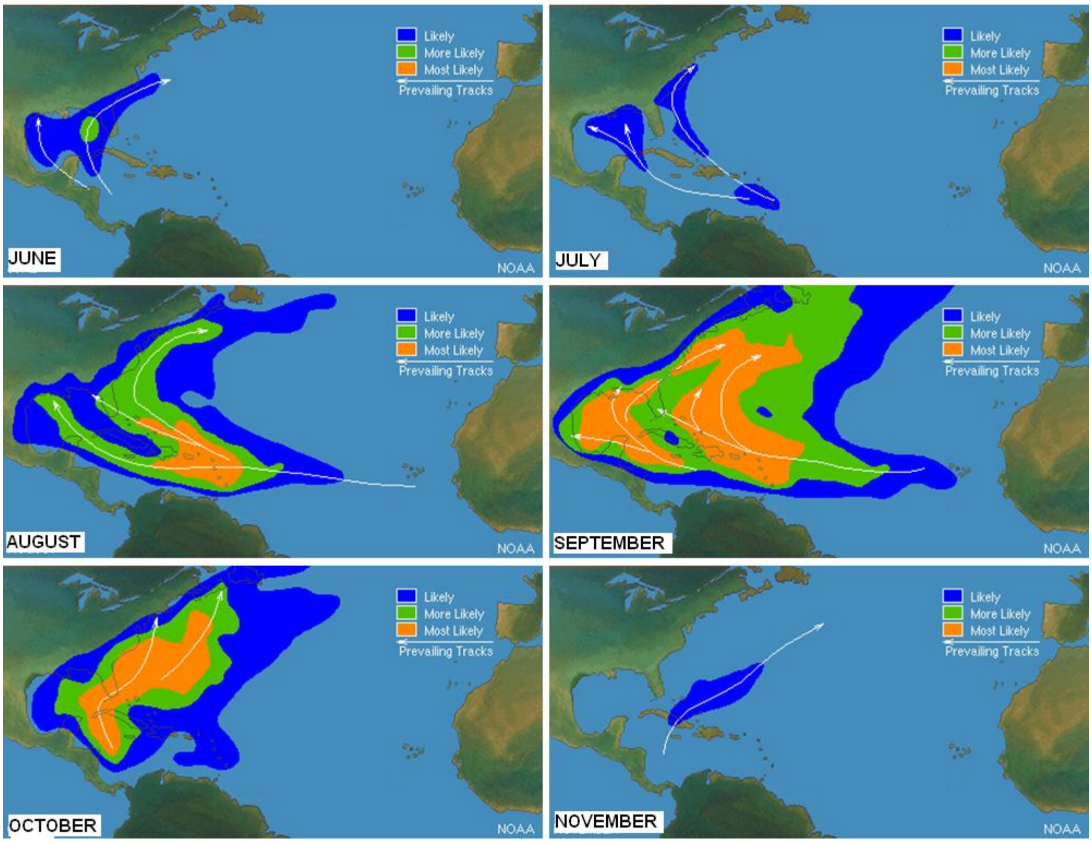

Figure 10. Climatological areas of origin and typical hurricane tracks. Source: NOAA. http://www.nhc.noaa.gov/pastprofile.shtml (10/03/2011)

The storm surge is produced by water being pushed toward the shore by the force of the winds moving cyclonically around the storm. The impact on surge of the low pressure associated with intense storms is minimal in comparison to the water being forced toward the shore by the wind. The classification of the hurricanes gives an insight of the wind involved. They are classified according to the Saffir-Simpson scale (table 3)

Table 3. Saffir-Simpson Scale for hurricane classification.

Saffir - Simpson Scale for Hurricane Classification		
Strength	**Wind Speed (knts)**	**Pressure (mbar)**
Category 1	64 - 82	> 980
Category 2	83 - 95	965 - 979
Category 3	96 - 113	945 - 964
Category 4	114 - 135	920 - 944
Category 5	> 135	919
Tropical Cyclone Classification		
Tropical Depression	20 - 34 knts	
Tropical Storm	35 - 63 knts	
Hurricane	> 64 knts	

Source: http://911weather.com/images/saffir-simpson_scale.jpg (09/03/2011)

The maximum potential storm surge for a particular location depends on a number of different factors. Storm surge is a very complex phenomenon because it is sensitive to the slightest changes in storm intensity, forward speed, size, angle of approach to the coast, central pressure (minimal contribution in comparison to the wind), and the shape and characteristics of coastal features such as bays and estuaries. In table 4 some examples of hurricanes are linked to the storm surge generated.

Table 4. Storm surge associated to some hurricanes. Data extracted from: http://www.nhc.noaa.gov/ssurge/ssurge_overview.shtml (09/03/2011)

Name	Year	Category	Storm Surge (m)	Place
IKE	2008	2	4.8 – 6.4	Texas
KATRINA	2005	5	8.0 – 9.0	Louisiana
DENNIS	2005	4	2.2 – 2.8	Florida
ISABEL	1995	4	2.56	Chesapeake
OPAL	1995	3	7.6	Pensacola
HUGO	1989	5	6.3	South Carolina
CAMILE	1969	5	7.6	Mississippi coast

The occurrence of storms in the Colombian Caribbean basin is described in detail in the next chapter.

2 CARTAGENA BAY

Cartagena de Indias was founded in 1533 and was built as a military fortress by the Spanish to protect it against pirates and the British Empire. It is the most important touristic city and one of the main ports of Colombia. It was designated a UNESCO world heritage in 1984. According to the 2005 population census undertaken by the National Department of Statistics, the population of Cartagena is 892545 inhabitants.

The bay of Cartagena de Indias is located in the Colombian Caribbean coast between 10^{o} 26’ N – 10^{o} 16’ N and 75^{o} 30’ W – 75^{o} 35’ W, it is 16 km long and 9 km wide, with an average depth around 16 m. The total area is 82 km^2. The bay is flanked by the Tierrabomba island (6.5 km long – 6.0 km wide) with a maximum height of 80 m.

The bay can be divided into two main parts. The external bay (in the white frame – fig.11) which connects to the sea through two entrances (Bocachica at the southwest and Bocagrande in the northwest), and the internal bay (in the red frame – fig. 11) in the north with no direct connection to the sea.

The exchange of the bay water with the open sea is done through two entrances. At the north (Bocagrande) the entrance is partially blocked by a submerged narrow wall (Escollera) with a depth between 0.6 to 2.1 m. The southern entrance has three narrows channels with depth between 0.5 and 3 m but one of them (the navigational access channel – Bocachica) is 30 m deep and 100 m wide.

During colonial times the main problem related to transportation and commerce through the New Reign of Granada (ancient name which includes the actual countries of Colombia, Panama, Ecuador and Venezuela) was that the main fluvial artery, the Magdalena river (300 km north-east from Cartagena), was practically impenetrable through its mouth, and the only two ports in the Caribbean were Santa Marta and Cartagena but neither of them had easy access to the river. In the first half of the XVII th century various governors of Cartagena became interested in the project of connecting Cartagena Bay to the Magdalena River through various lakes by digging a channel. After several years, on August 20^{th} 1650 the Dique Channel (as is known today) was finished. But not every one was happy with the project, and some people argued that there was a risk for Cartagena to be flooded with the new flow of water into the bay (*Lemaitre, 1998*). From those days on, Cartagena Bay would not be the same.

These works resulted in major changes in the entire aquatic system of the bay, transforming it from a clear water coralline bay to an estuary with a large amount of fresh water discharge and sediment in suspension which seasonally alter the salinity, oxygen and other physical and biological parameters (*Garay and Giraldo, 1997*).

During the last years, recurrent annual flooding due to high water levels between September-October had been occurring in the city. In Cartagena’s local newspaper the last inundation event of the city was titled: “High tide drives Cartagena’s inhabitants mad” (*El Tiempo, 23/09/2010*), and follows with:

> *“The daily increase of the sea level in Cartagena, had been so big during this year, that led the authorities to take emergency measures taking into consideration that it has spread more than expected.*

The increase of the tide has created a new and wet landscape for the locals and tourists, with the historical downtown flooded and foul odours, the entrance to the touristic zone completely overflowed, traffic jams all the day around, mad drivers whose cars are suffering the consequences of the salinity".

The climate in Cartagena de Indias is defined by the position of the ITCZ as was explained in the previous chapter, and the precipitation and wind (or the lack of) are the direct evidence of the ITCZ presence in the area of Cartagena.

The ITCZ has a latitudinal displacement following the apparent movement of the sun with respect to the earth. Over Colombia the ITCZ, its Pacific Ocean segment, reaches its extreme meridian position at 2^o N during January and February, while in December it is a little further to the north but it can reach 5^o S during El Niño events; the continental segment of the ITCZ is not constant and is located between 5^o to 10^o S. Between March and May in the Pacific the ITCZ moves toward the north and its position in the Pacific coast is between 2^o and 7^o N; the continental part is connected between March and April with the Atlantic Ocean, developing one system located between 5^o S and 1^o N. Between June and August the ITCZ moves from 8^o N toward 10^o N penetrating the Caribbean. In September – November the ITCZ starts moving to the south (from 11^o N to 7^o N).

In the ITCZ the Trade Winds (NE), originated as a flux around the high pressure centre of the Atlantic, join the Southeast Trade Winds (originated as a flux around South Pacific and South Atlantic highs). Due to this convergent flux, the ITCZ is where the weak winds and maximum rain and cloudiness can be found.

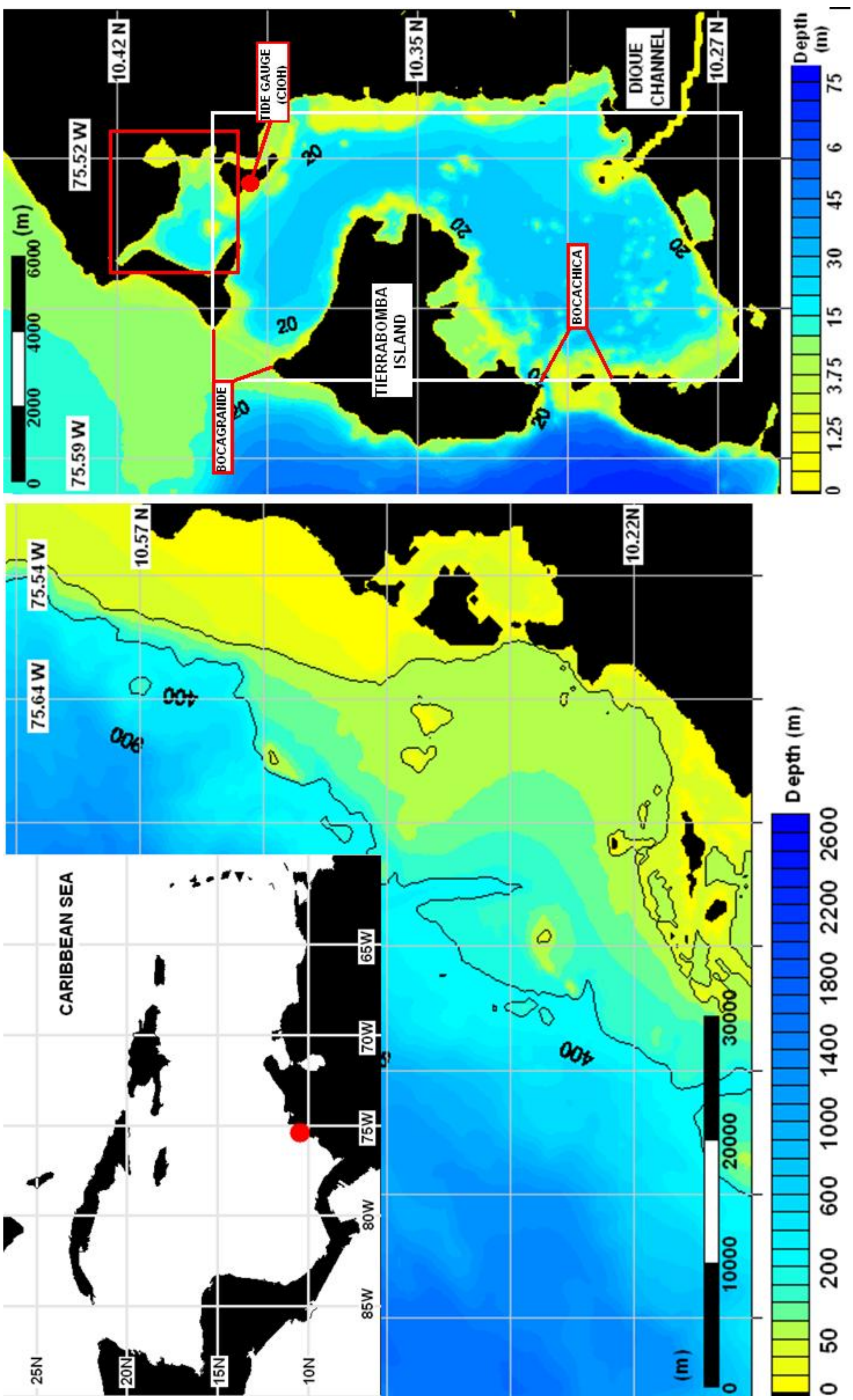

Figure 11. From left to right; The red dot shows the position of Cartagena in the Colombian Caribbean coast; A section of the Colombian Caribbean coast between Punta Canoas (north) and Rosario Islands (south); Cartagena Bay.

2.1.1 Precipitation

In Cartagena the rain begins in May with a steady increase. The peak is reached during October with around 250 mm (1971-2000 monthly average). At that time the ITCZ goes through the area heading south and then the rain decrease abruptly (fig. 12)

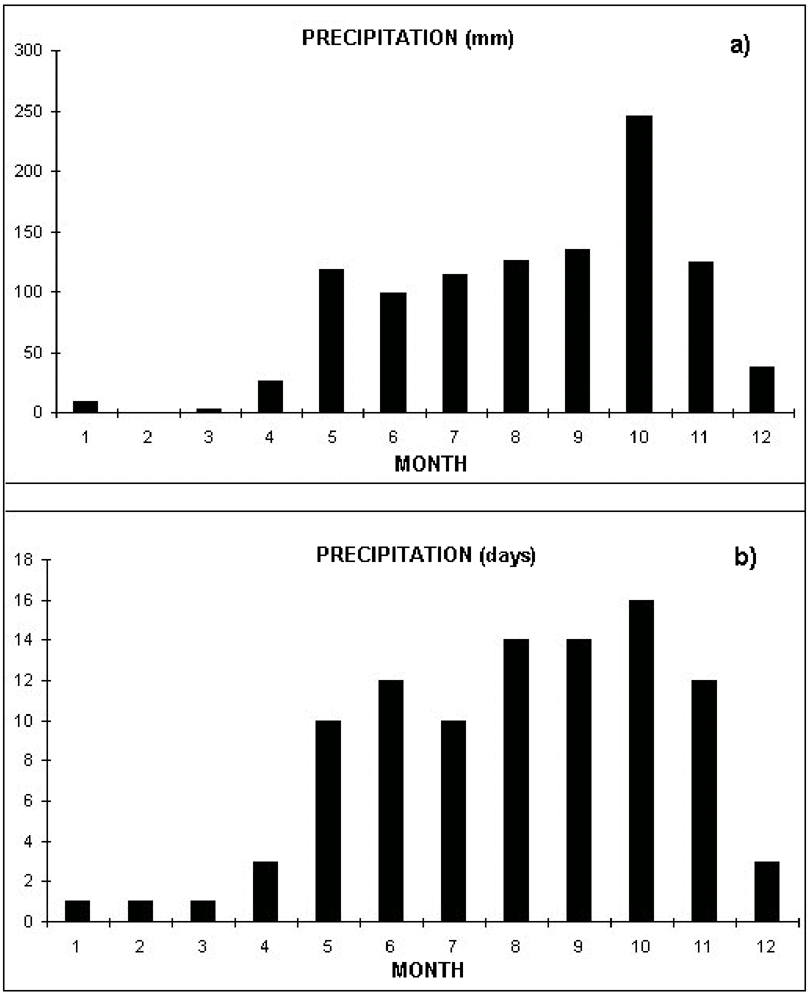

Figure 12. Precipitation. a) Monthly average precipitation (mm) in Cartagena for the period 1971 – 2000. a) Average days of precipitation per month in Cartagena for the period 1971-2000. Source: Colombian national meteorological agency (IDEAM) in: http://institucional.ideam.gov.co/jsp/loader.jsf?lServicio=Publicaciones&lTipo=publicaciones&lFuncion=loadContenidoPublicacion&id=882 (09/03/2011).

2.1.2 Wind Regime

According to the position of the ITCZ the stronger winds can be found from the beginning of December to the end of April. During March – November the wind is weaker. In figure 13 the monthly mean wind speed recorded at the Rafael Nuñez airport is shown. The wind direction corresponds mainly to the N-NE Trade Winds; during 50% of the time the wind blows from the N and NE (fig. 14).

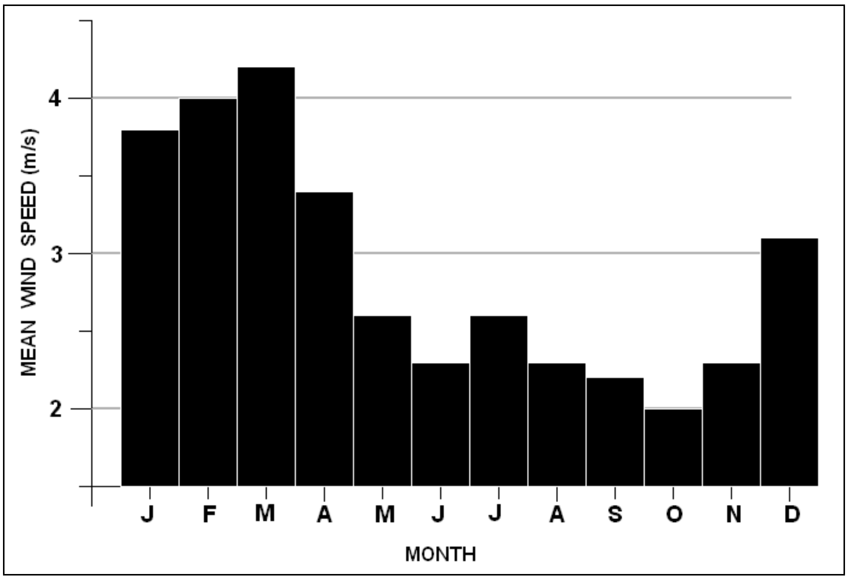

Figure 13. Monthly mean wind speed in Cartagena (1961 – 1990). The data was obtained from IDEAM, 1995

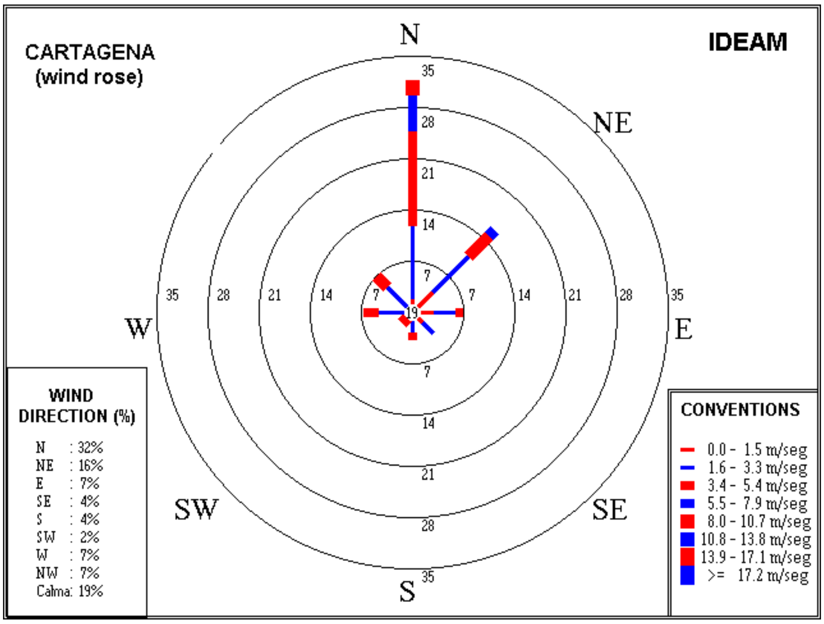

Figure 14. The wind rose was constructed by IDEAM using 19 years of wind records. Adapted from: http://institucional.ideam.gov.co/jsp/loader.jsf?lServicio=Publicaciones&lTipo=publicaciones&lFuncion=loadContenidoPublicacion&id=882 (09/03/2011).

The marine breeze can be found over the sea in a zone as wide as 25 km bordering the coastline between Punta Coralito and Barbacoas (fig. 15). The maximum values are not higher than 1,5 m/s. The zonal component of the breeze suffers important changes between Barbacoas and Punta Canoas (Cartagena Bay is in between). In figure 16 a weakening of the breeze can be found in the area between Baru Island and Cartagena reflecting the possible existence of a screen effect due to Bocagrande and Tierrabomba Island reducing the wind speeds in the bay (*Kazakov et al., 1996*).

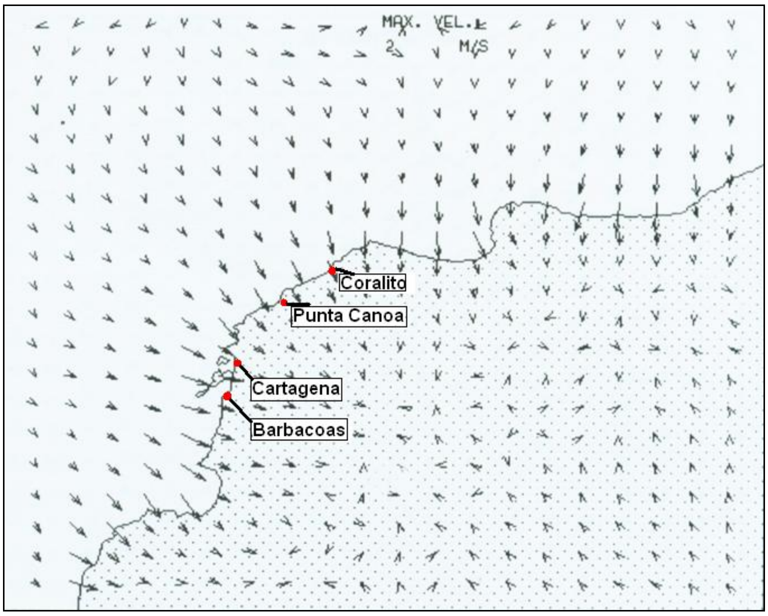

Figure 15. Breeze surface behaviour in the Colombian north coast. Adapted from Kazakov et al. (1996).

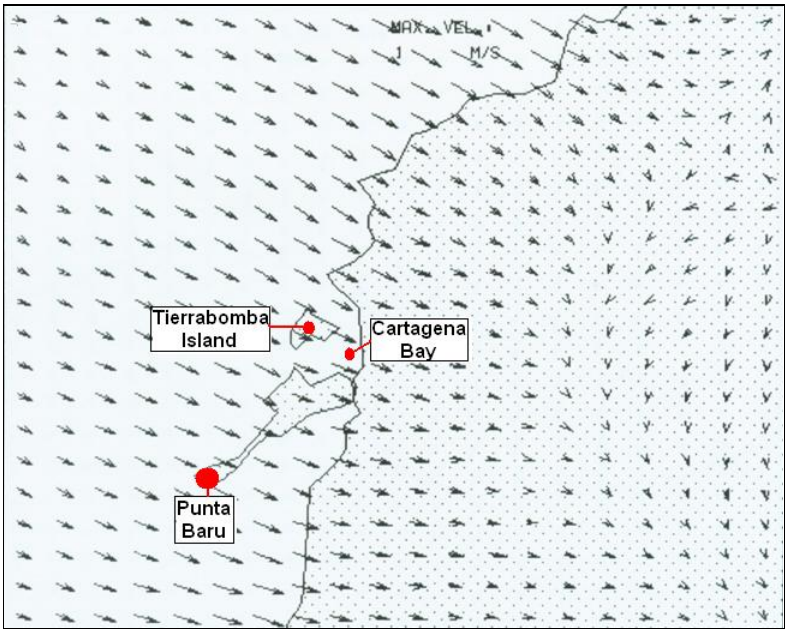

Figure 16. Breeze surface behaviour around Cartagena. Adapted from Kazakov et al. (1996).

Studying the Cartagena Bay water circulation, Lonin and Giraldo (1995) found a strong influence on the wind by the buildings along the north-eastern part of the bay, weakening the wind.

2.1.3 Easterly Tropical Waves

As explained before, the tropical waves are present during the rainy season. During the passing of the tropical wave the cloudiness increases and the wind changes direction, from the northeast to the east.

A review of the Monthly Meteomarine Weather Report (2004/2010) shows that the Colombian Caribbean coast is affected by these atmospheric disturbances from May to November, with an approximated interval of six to eight days, but they are more intense during July-August, when 10 to 9 waves can be expected.

2.1.4 Hurricanes

In 2004 the Colombian Oceanographic and Hydrographic Research Center (CIOH) carried out a review of the NOAA hurricane records from 1964 to 2004 in order to estimate the likelihood of a hurricane affecting the Colombian Caribbean coast. For this, the minimum distance at which at which a hurricane can affect the coast (swell – rain), was defined to be of 300 km.

According to that review, 32% of the hurricanes (13 hurricanes) originated in the Atlantic between 1961 – 2004 went into the Caribbean, but from those just 17% affected the Colombian coast. That means that from all the hurricanes developed in the Atlantic during 1961 – 2004 only 5.4% (2 hurricanes) was close enough to affect the oceanographic and meteorological conditions at the coast (CIOH, 2005).

2.2 The Dique Channel

The eco-region of the Dique Channel (fig. 17) in northern Colombia has an area around 4400 km^2 and is located in the western part of the delta of the Magdalena River. The Magdalena river is the largest in Colombia, with an average discharge of some 8000 m^3/s at the mouth. It is conformed by lowlands, mangrove swamps and salt marshes of riparian vegetation, more than 213 km^2 of water surfaces and wetlands of great ecological significance, and some 870 km^2 of deltaic wetlands (*Ordoñez et a.l, 2007*).

The water level in the Dique Channel depends on the water level in the Magdalena River and on the water level in the Cartagena and Barbacoas bays. The yearly averaged flow rate in the Magdalena River is around 7163 m^3/s; around 8% of that (540 m^3/s) is diverted to the Dique Channel. In extreme conditions, from the maximum flow rate in the Magdalena river (16000 m^3/s) 9% is derived to the Dique Channel (1,200 m^3/s). In low flow rate conditions, the relation between the channel and the river is in the order of 4%. On average, Cartagena Bay is receiving a flow rate of 130 m^3/s (*Ordoñez et al., 2007*).

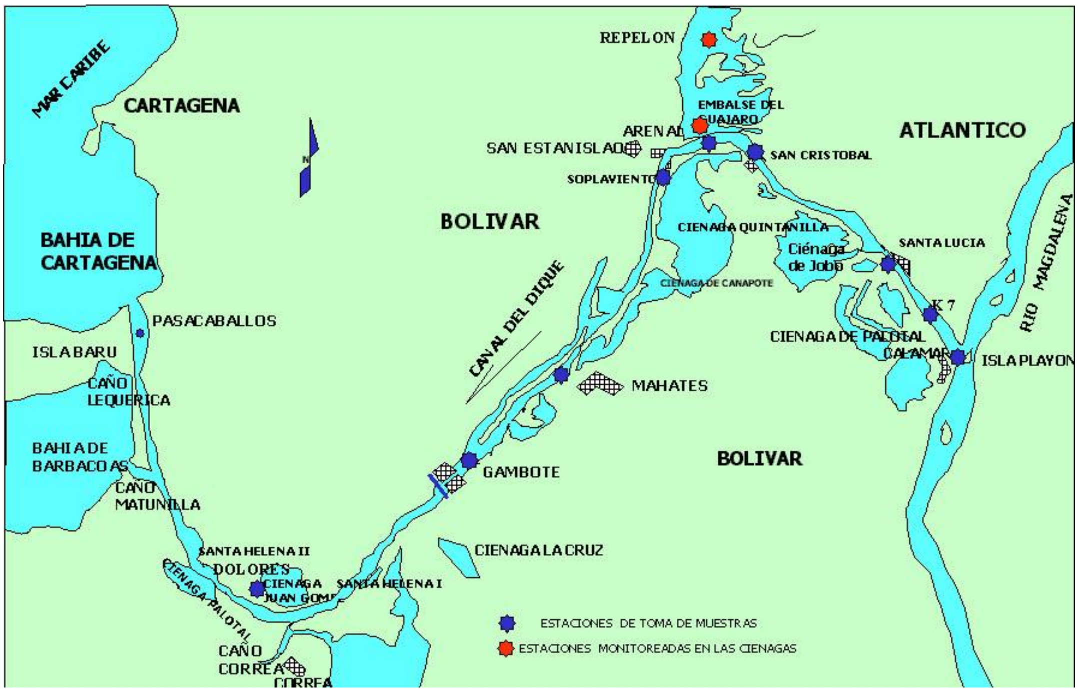

Figure 17. The Dique Channel basin connects the Cartagena Bay to the Magdalena River through different lagoons. Source: CIOH, 1999.

Taking into consideration the flow rate of solids, from the total (151 MTon/year) which is actually transported by the Magdalena River, it is estimated that a 10% is diverted to the Dique Channel. The sedimentological effects in Cartagena Bay are just perceived close to the mouth as far (into the bay) as 1,5 to 2 km. The deposited volume of sediments is around 1 mm^3. The progradation into the bay is in the order of 50 m/year, mostly due to the placement of dredged material at the edges of the Channel (*Ordoñez et al., 2007*).

Probably the main impact of the Dique Channel in the bay of Cartagena is its role in the hydro-chemical regime of the bay, as was identified by Tuchkovenko et al. (2002). The channel represents a strong supplier of nitrogen, phosphorous and sediments determining the transparency of the waters in the bay. On the other hand, a strong superficial pycnocline (0 - 4 m) is formed in the bay preventing the vertical exchange of the superficial and deeper waters. As a result, the polluted substances travelling in the Channel propagate along the bay in the limits of the superficial fresh water layer which at the same time is the photic layer.

The flow rate variation during the year can be seen in figure 18. The flow rate starts a steady increase in March till June when the flow rates have a small decrease until September. From that month on, a steady increase develops till November. Then the flow rates decrease again. This behaviour is closely related to the precipitation rates.

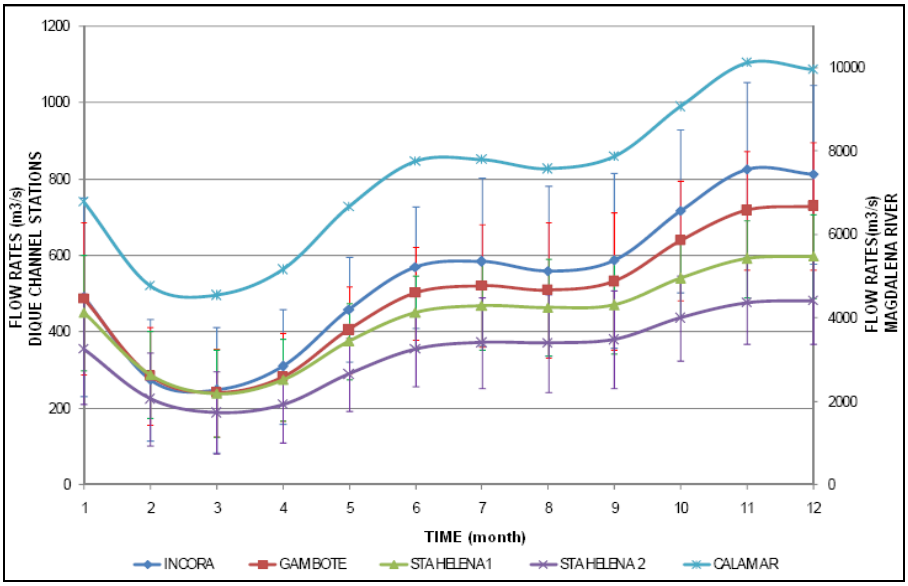

Figure 18. Monthly variation of the average flow rate (1984-2000) at four stations along the Dique Channel. Santa Helena 2 is the closest to the Dique Channel mouth. Adapted from UNAL, 2008.

The intra-annual variability of the flow rate in the Dique Channel basin associated to the ENSO events has been identified by various authors (*Mesa et al., 1997; Poveda, 2004*). In figure 19, using data from 1984 to 2000, the annual mean flow rate histogram is shown for the four stations in the Dique Channel. A close view shows that in 1984, 1996 and 1999 (la Niña years) the flow rates were above the multiyear average and the opposite in 1991, 1992 and 1997 (El Niño years).

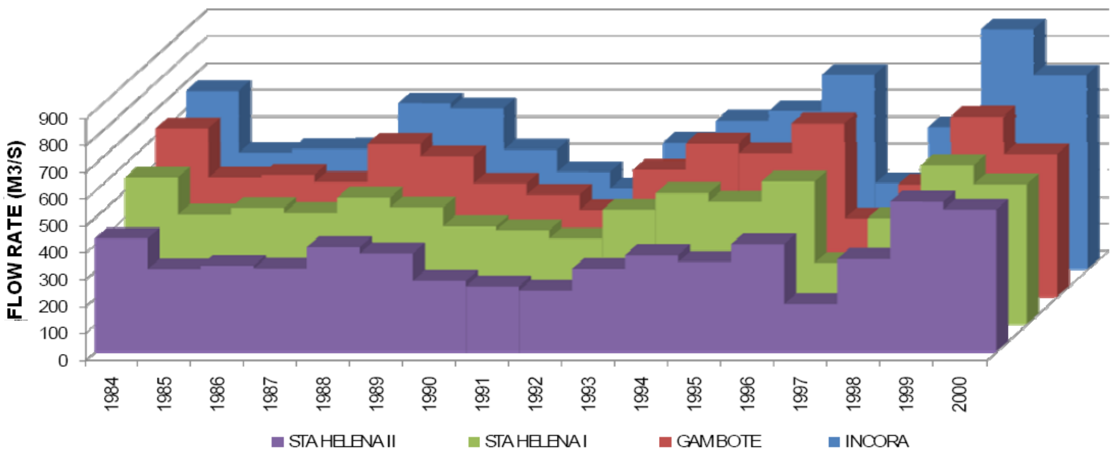

Figure 19. Mean yearly flow rate histogram for the hydrometric stations in the Dique Channel. Adapted from UNAL, 2008.

Using the flow rate data (1984 – 2000) of different stations along the Dique Channel, UNAL (2007) during the project "*Study and Research about the Works for Environmental and Navigational Restoration for the Dique Channel*", derived the curves of flow rate duration as is presented in figure 20.

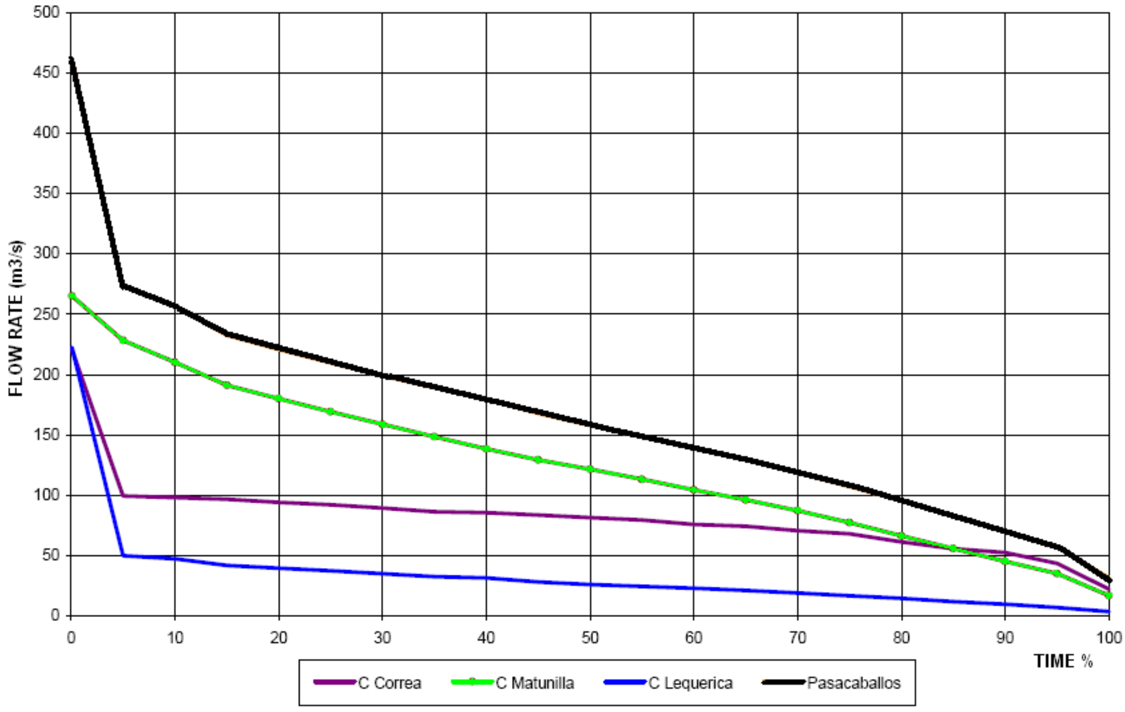

Figure 20. Curves of flow rate duration (period 1984 – 2000). The curves correspond to different station along the Dique Channel. The black line corresponds to Pasacaballos measuring station, the closest to the Dique Channel mouth. Adapted from UNAL, 2007.

2.3 Sea Level Variability in Cartagena Bay

In this section the classical and specific components of the sea level variability in Cartagena Bay will be examined in general, including tides, sea level rise, subsidence, the fluctuation of the sea level during the year, the ENSO implications, the water level differences due to the Dique Channel discharge and the possible implications of the Caribbean mesoscale eddies circulation in the sea level variability in Cartagena.

2.3.1 Astronomical Tide

In the previous chapter the Caribbean tides where classified (*Kjerfve, 1981*) and, according to that, in Cartagena Bay microtidal tides are expected, but mixed mainly diurnal. This classification of tides was done taking into consideration a time series of water level in Cartagena of 365 days (*Kjerfve, 1981).* A longer time series was used by Molares (2004), reaching the same classification. Applying spectral analysis and Matlab routines developed by Foreman (1996) for tidal analysis, the author found the tidal components in the Bay of Cartagena (table 5).

Table 5. Tidal components in Cartagena Bay.

TIDAL COMPONENT	AMPLITUDE (cm)	FREQUENCY Cycles/hr	PHASE (degrees)	PERIOD (hours)
*K1	8.6829	0.0418	146.2800	23.9349
*M2	7.1923	0.0805	154.6000	12.4208
*O1	4.8631	0.0387	354.4600	25.8198
*P1	3.1462	0.0416	153.7100	24.0674
*SSA	2.9493	0.0002	64.6300	4347.8261
*N2	2.3890	0.0790	226.3800	12.6582
*S2	1.6539	0.0833	240.0200	12.0005
*MF	1.1555	0.0031	128.3200	327.8689
*MSM	0.8421	0.0013	326.6000	763.3588
*Q1	0.7627	0.0372	82.3000	26.8673
*MM	0.7452	0.0015	264.1400	662.2517
*NO1	0.5450	0.0403	260.2300	24.8324
*MKS2	0.5341	0.0807	162.0000	12.3854
*K2	0.5004	0.0836	245.5300	11.9674
*NU2	0.4757	0.0792	211.8800	12.6263
*2N2	0.4296	0.0775	304.9200	12.9049
*J1	0.3696	0.0433	50.3000	23.1000
*PHI1	0.3660	0.0420	184.0500	23.8039
*L2	0.2667	0.0820	65.0500	12.1921
*RHO1	0.2595	0.0374	74.7600	26.7237
*TAU1	0.1880	0.0390	197.7400	25.6674
*MSF	0.1778	0.0028	56.5700	354.6099
*SIG1	0.1708	0.0359	221.4200	27.8474
*OO1	0.1708	0.0448	297.0100	22.3065
*M3	0.1562	0.1208	311.4800	8.2802
*MO3	0.1248	0.1192	53.0900	8.3864
*M4	0.1137	0.1610	155.0800	6.2104
*UPS1	0.1133	0.0463	301.0000	21.5796
*SO1	0.1101	0.0446	346.6600	22.4215
*SK3	0.1090	0.1251	180.8300	7.9930
*CHI1	0.1054	0.0405	235.1900	24.7097
*MSN2	0.0967	0.0849	351.1100	11.7855
*MK3	0.0752	0.1223	239.1300	8.1773
*2SK5	0.0678	0.2085	26.4000	4.7973
*BET1	0.0622	0.0400	342.0900	24.9750
*MS4	0.0597	0.1638	30.5600	6.1035
*LDA2	0.0566	0.0818	13.8800	12.2220
*OQ2	0.0564	0.0760	357.4800	13.1631
*2Q1	0.0553	0.0357	206.0200	28.0034
*EPS2	0.0513	0.0762	124.9500	13.1268

2.3.2 Storm Surge

Using water level data from Cartagena Bay measured by the tide gauge in the bay and meteorological data (wind and atmospheric pressure) Alexandre et al. (2008) found no significative correlation between the sea level rise due to storms (RSLST) and the local and semi-local meteorological data. They observed that the sea level increment (RSLST) was not coincident with the flooding events at the coast in the outer part of the bay (facing the open sea). For these authors, the rising of the sea level in the bay must be related to the flow rate variation of the Dique Channel discharge. The analysis at the local scale revealed, due to the lack of correlation with the local meteorological forcing and to the observation of the phenomena (storm surge), that the RSLST is due to the swell generated by cold fronts in the Caribbean. According to 28 swell events evaluated by the authors, the sea level can rise in average up to 50 cm, but in recorded extreme events, such as the swell generated by the hurricane Joan (1988), the water level can increase up to 1 m.

2.3.3 Sea Level Rise

According to Sutherland et al. (2008) using Cartagena's tide gauge data from 1951 – 1993 (88%) and 1994-2000 (79%), a 5.6 +/- 0.008 mm/yr sea level change rate was found. They do not define a relative sea level rise apparently because the GPS data available are unreliable (taking into consideration the data is intermittent since February 1996). On the other hand and according to their data in table 6, the GPS data is from Bogota and not from Cartagena. The first one is at 2500 meters above mean sea level (in the center of the country) and the other is at sea level at the coast.

Table 6. Motions at GPS stations, from Sutherland et al. (2008).

Site Location (State)	Site ID (GPS)	Data availability	Vertical Motion (mm/yr) SOPAC (2006)	IERS (2006)
Costa Rica	MOIN	Intermittent data over 31 months 1995 to 1998	-4.5±1.5	-3.1±9.8
Nicaragua	MANA	Near continuous data since may 2000, operational	1.3±1.2	-
El Salvador	SSIA	63 months between 2000 and 2005	3.5±1.2	-
Guatamala	ELEN	Intermittent data since Jan 2002, operational	2.6±2.7	-
Jamaica	JAMA	41 months between 1999 and 2003	2.3±1.7	1.4±121.3
Cuba	SCUB	Intermittent data since March 2002, operational	-5.4±3.0	-
Puerto Rico	PUR2	9 months between 2003 and 2004	-9.5±6.8	-
Puerto Rico	PUR3	From mid 1997 continuous	-	5.3±6.7
St Croix	CRO1	Continuous from 1995 on, except for 9 month in 2005	-0.8±0.7	0.9±0.5
Barbados	BARB	26 months between 1998 and 2001	0.8±1.7	3.0±2.6
Colombia	**BOGT**	**Intermittent data since February 1996, operational**	**-27.6±2.3**	**-27.2±2.6**

Restrepo and Lopez (2008) estimated a relative sea level rise by least squares linear regression from the Cartagena 1952–2000 tide gauge time series in 5.98 mm/yr (fig. 21).

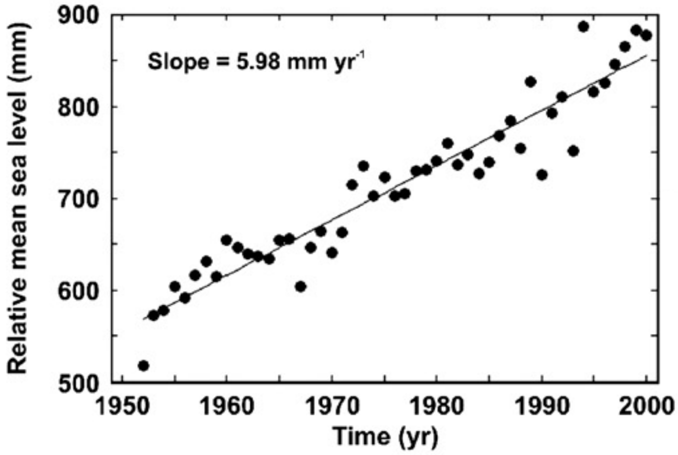

Figure 21. Relative mean sea level rise for Cartagena. Source: Restrepo and Lopez (2008).

2.3.4 Local Subsidence

During the last years, Colombia decided to qualify its national reference network by installing continuously operating GNSS stations (Global Navigational Satellite Systems), which have to be integrated into the SIRGAS (Geocentric Reference System for the Americas) continental network to guarantee the consistency of the regional reference frame with the global reference frame in which the GNSS orbits are computed.

According to the last report *(Seemüller et al., 2009)* the GPS station in Cartagena has measured a vertical velocity in the order of 1.4 mm/yr. In figure 22 the vertical component from 2000 to 2008 is shown.

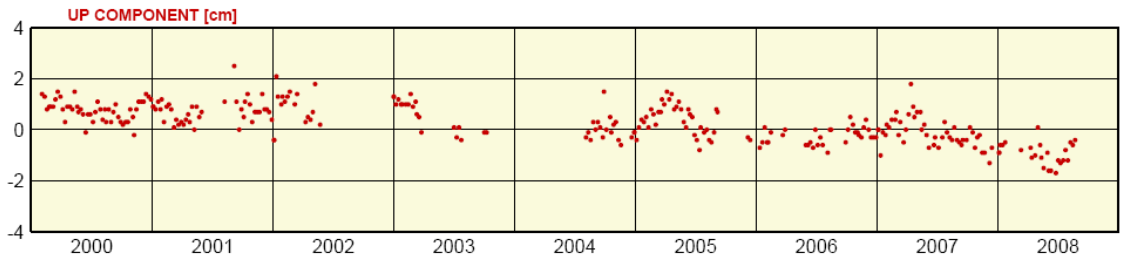

Figure 22. Vertical displacement measured in Cartagena (10° 23' 28.80" N - 75° 32' 1.87" W) according to Seemüller et al. (2009). Source: DGFI Report No. 85.

2.3.5 Caribbean Mesoscale Eddie Circulation

Cyclonic or anticyclonic circulation of surface water close to the coast may lower or rise the sea water level due to the converge or divergence of water off or to the center of rotation. Since there is a mesoscale variability in the Caribbean related to eddies travelling close to the coast (*Nystuen and Andrade, 1993; Andrade and Barton, 2000; Jouanno et al., 2008; Jouanno et al., 2009*) as was explained in section 1.1, a sea level variability in the coast is expected, as was introduced by Andrade, 2000. No further attempt to demonstrate and link this concept to the sea level variability in Cartagena Bay has been done.

2.3.6 Yearly Fluctuation of the Sea Level

Plotting the 1991-1992 monthly mean storm surge filtered sea level calculated by the PSMSL (Permanent Service for Mean Sea Level) and the 1991 – 1992 monthly mean water level without filtering the storm surge (fig. 23), as is expected the second one shows higher values (around 5 cm higher). In order to appreciate the influence of the different causes other than the astronomical tides, the time series were fitted at the lower water level by subtracting the water level difference in December, taking into consideration that at that time of the year the wind (causing water level to increase) is just beginning to increase, so that meteorological effects are unlikely.

From the figure, there can be seen a fluctuation during the year, apparently related to the tide itself (SSA – Solar Semianual component – Period 181 days), but SSA, SA and MF are strongly affected by variations of meteorological conditions and river discharges (*Cheng and Gardner, 1985; Arabelos et al., 1997; Hu et al., 2007*) and in many coastal areas, a large fraction of the seasonal cycle is steric, that is, due to density changes as a consequence of temperature and salinity variations (*Zerbini et al., 1996*).

In figure 23 (1991) no big difference is evident between the time series, but in 1992 and during the first half of the year, the tide gauge in Cartagena (no meteorological effects removed) shows higher values than the PSMSL data (met effect removed). Taking into consideration the fact that 1991 was El Niño year (low Dique Channel flow rate) it could play a role in the sense that the effects on the sea level are more pronounced in the normal year (1992) than in the dry one; but at the same time and during these first months of the year the trade winds are present, so they could increase the water level at the coast. However, Alexandre et al. (2008) found no significance correlation between the sea level rise and the local and semi-local meteorological data

Another feature that can be seen is in the second half of both years. In this case the water level measured by the tide gauge (no meteorological effects removed –CTG TG) shows a slightly faster increase (blue area) than the PSMSL data. That fits with the rainy season when the Dique Channel discharge in the bay is increasing and weaker winds are present.

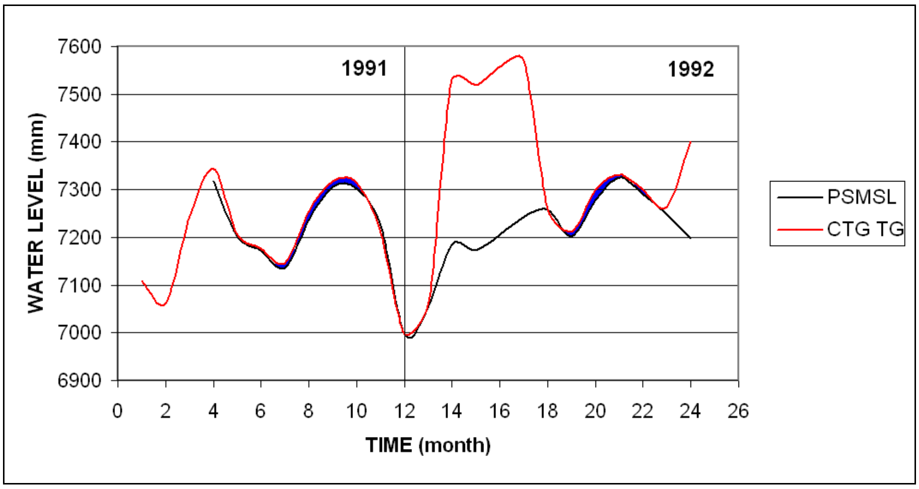

Figure 23. Monthly mean water level during 1991 – 1992. The red line corresponds to the mean sea water level once the meteorological component has been filtered by

PSMSL. The black line corresponds to the monthly mean water level recorded by the tide gauge in the Bay of Cartagena (1991-1992). The blue area shows a difference between both time series. Data source: Black line: Permanent Service for Mean Sea Level – PSMSL - http://www.psmsl.org/data/obtaining/. Red line: records from the tide gauge – CIOH.

In figure 24 the monthly mean (1995 – 2001) sea water level in Cartagena and the monthly mean (1984-2000) Dique Channel flow rate are plotted. The steady increase of the sea water level is coherent with the yearly Dique Channel flow rate behaviour.

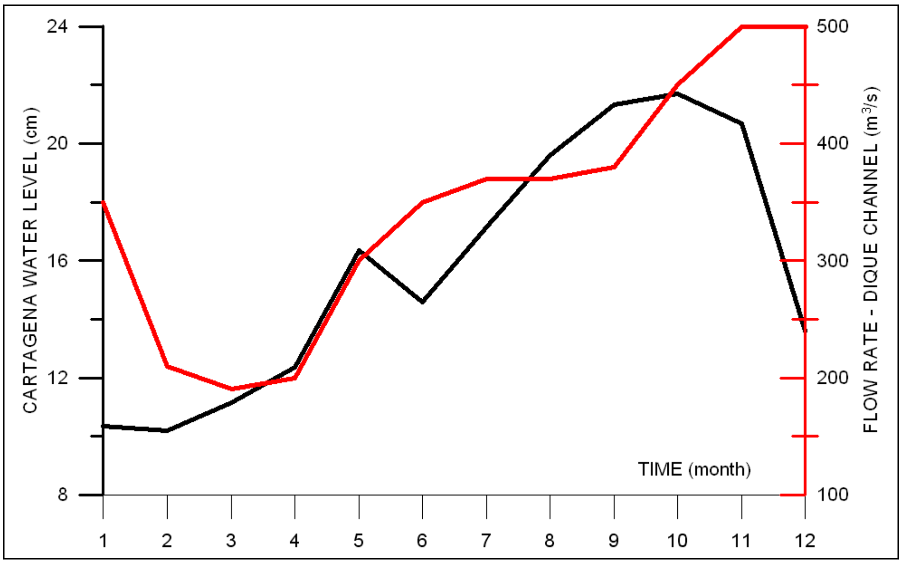

Figure 24. Monthly mean (1995 – 2001) sea water level in Cartagena (black line) vs monthly mean (1984-2000) Dique Channel flow rate (red line – Sta. Helena 2 station). In the water level data the sea level rise was removed.

According to Alexandre et al. (2008) the seasonal rising of the sea level in Cartagena Bay has a yearly frequency and they suggest that it is originated by the increase of the Dique Channel flow rate during the rainy season, and that the morphology of the Cartagena Bay in which the communication with the open sea is limited, leads to an accumulation of water in the bay with a progressive evacuation of the water keeping high water levels for weeks.

2.3.7 Sea Water Level, Dique Channel and ENSO

Taking into consideration the strong correlation found between the Dique Channel flow rate and the intrannual oscillations (ENSO) (*Mesa et al., 1997; Poveda, 2004*), using sea water level data between 1995 and 2002 (this period was chosen because the hourly water level data was with no gaps) in Cartagena Bay, in figure 25 the Niño (red) and Niña (blue) events are shown. The monthly increase of sea level due to climate change (5.98 mm/yr according to Restrepo and Lopez, 2008) had been removed in order to compare the monthly mean water level differences. Even though there is no clear image about the differences between the intrannual oscillations and the water level, it can be said that between 1998 – 2001 the water levels were higher when la Niña was present. However, checking the mean yearly Magdalena river flow rate (fig. 19) there is a clear increase in flow rate from 1997 to 2000. The same behaviour is present in the Cartagena Bay water level.

A better coincidence can be established comparing the 1991-1992 sea water levels in the bay of Cartagena (fig. 23) with the flow rate of the Dique Channel according to figure 26. The 1991 (El Niño year) flow rates in the Dique Channel were considerably lower than the ones in the previous years (no ENSO events). The same can be seen in the sea water level in Cartagena Bay where during the rainy season of 1991 the water level was lower than the sea water level during the 1992 rainy season.

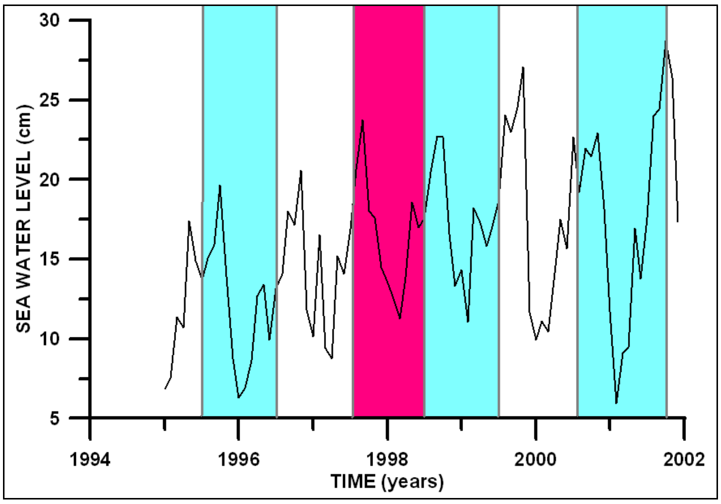

Figure 25. The sea water level in the bay of Cartagena is shown after removing sea level rise due to climate change. Blue, red and white areas indicate La Niña, El Niño and normal years respectively. The difference in the magnitude of the sea water level with figure 23 is because in that one the PSMSL added 7000 mm to the revised local reference (RLR) in order to avoid negative numbers.

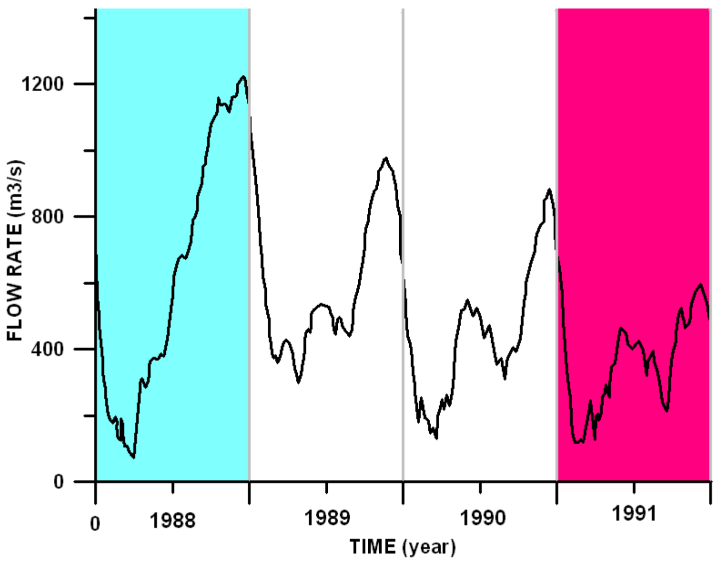

Figure 26. Dique Channel flow rates (station: Incora K7). Blue, white and red areas represents El Niño, normal and La Niña years. Source: the data was digitized from CNR, 2007.

2.3.8 Water Level Differences in the Bay of Cartagena

The role of the Dique Channel in the water quality of Cartagena Bay due to the sediment load input was studied during the project "*Preliminary design for a 2D-3D numerical model for the Dique Channel and its water bodies*". Using the theoretical basis of the hydrodynamic Model of Estuarine and Coastal Circulation Assessment (*Hess, 1985*), modified by Lonin (1997) to the CODEGO model (*Tuchkovenko and Lonin, 2003*), numerical experiments were undertaken in which barotropic fluxes were detected due to different water levels along the bay.

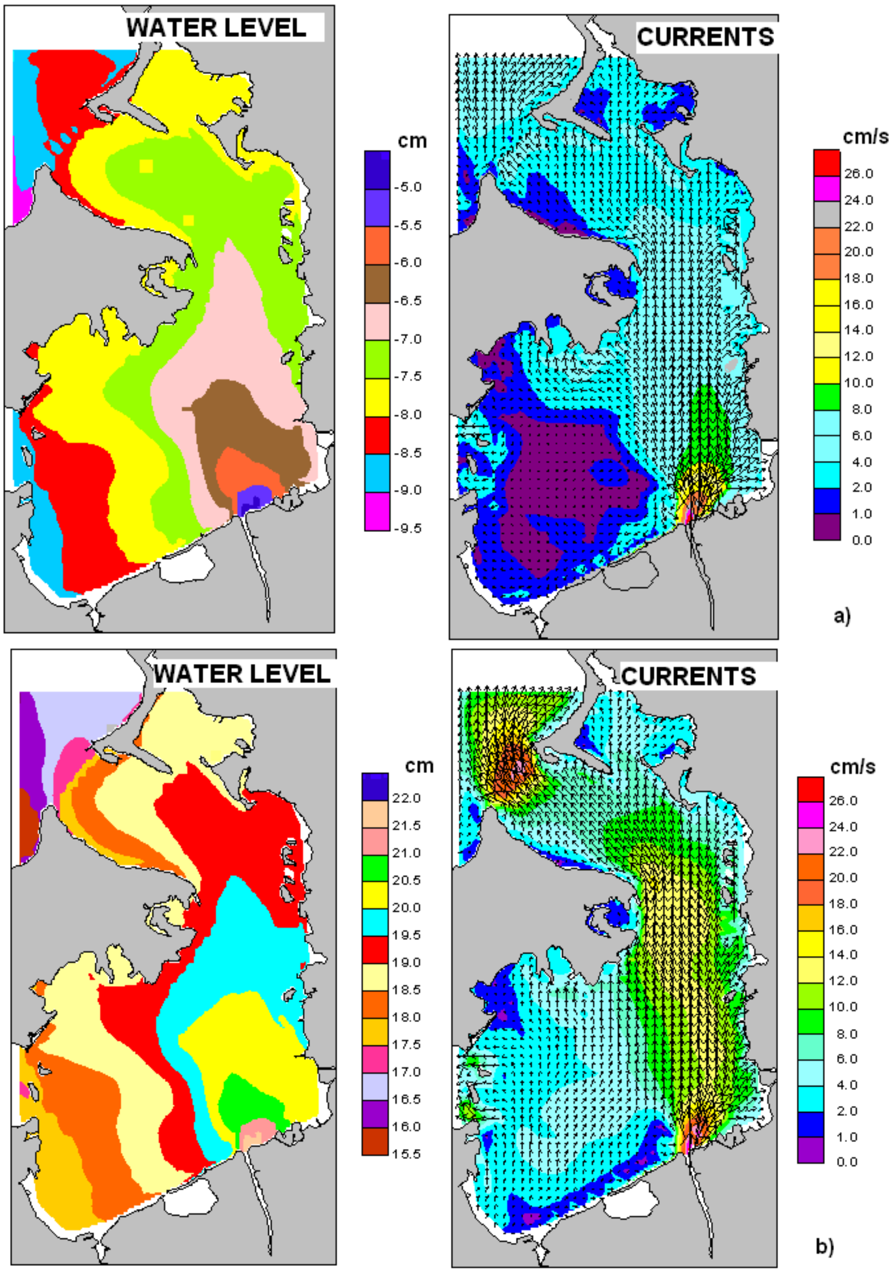

Figure 27. Calculated water level and currents using characteristic data for the rainy season (weak wind and Dique Channel high rate discharge). a) Ebb tide. b) Flood tide (CIOH, 1999).

The Dique Channel was found to produce a 4 to 7 cm water level difference between the Channel mouth and the open boundaries (Bocagrande). Contrary to previous results using the model in the internal bay, during the experiments (rainy season-high flow rate of the Dique Channel-weak winds) the wind was no longer the main forcing of the currents, but the tide and the Dique Channel load to the bay (*CIOH, 1999*). In figure 27 these preliminary results are shown.

2.4 Previous Works to Model Cartagena Bay's Circulation

During 1996-1998 using the Princeton Ocean Model (*Blumberg and Mellor, 1987*) coupled to a mesoscale atmospheric model *(Kazakov et al., 1996)* in the framework of the project *"Numerical Modelling of the Coastal Circulation and itsr Application in the Study of the Processes of the Transport of substances and Contaminated Particulates in the Colombian Caribbean Coastal Zone"*, the Colombian Oceanographic and Hydrographic Research Center modelled the Caribbean Sea circulation to get the boundary conditions for smaller areas of interest. One of these areas was Cartagena Bay. To model the Cartagena Bay hydrodynamic field the CODEGO model *(Lonin, 1997)* was built based on the MECCA (Model of Estuarine and Coastal Circulation Assessment – *Hess, 1985*).

At the same time (1998 – 2002) and for different projects, a mathematical model of eutrophication / oxygen regime for the most populated areas in the Colombian Caribbean coast, including the bay of Cartagena, was done. These projects were undertaken by the CIOH with other institutions. The model consists of hydrodynamic and biogeochemical blocks to assess engineering alternatives for improving the water quality and oxygen regime in the bay. The hydrodynamic block of the model is based on the primitive three-dimensional equations for estuarine and coastal dynamics. The biogeochemical block includes the balance equations for the following components of the ecosystem: phytoplankton, bacteria, detritus, dissolved organic matter (DOM), phosphate, ammonium, nitrite, nitrate and dissolved oxygen (*Tuchkovenko and Lonin, 2003).*

These experiences lead to an important knowledge of the characteristics of the bay and their modelling as it follows:

- Lonin and Giraldo (1995:a) in a preliminary application of numerical modelling in the bay of Cartagena, described the forcings and main processes that originate the currents in the internal bay. The authors established that the wind forcing is more important than the tides, and the circulation depends on the direction of the wind and its variations. An important unresolved question was how the buildings affect the wind around the internal bay.

- Lonin and Giraldo (1995:b) studied the bottom boundary conditions in order to take into consideration the heat exchange between the bottom and the water column, required by MECCA (Model Estuarine Coastal and Circulation Model, Hess, 1989) to be used in the bay of Cartagena. They checked three different conditions: T=Const; $\delta T/\delta z = 0$; $T(z)=\theta(z')$.

The third condition characterized the continuity of the water temperature profile T(z) and the sediment temperature profile θ (z') as well as the corresponding heat fluxes. As a result they found a very strong heat exchange between the water and the sediment at the bottom in shallow waters. On the one side that does not allow the use of the second condition and on the other it requires a solution of the problem related with the heat exchange between the superficial sediment and the water column, but due to the results the third condition was equivalent to the first condition. So the first condition (constant temperature at the bottom) was good enough to use in the Cartagena Bay (*Lonin and Giraldo, 1995:b*).

- Following the studies to implement MECCA in Cartagena Bay, Lonin and Giraldo (1996) noted that the accuracy in the calculation of the hydrodynamic field is closely related to different factors such as:
    - The correct formulation of the boundary conditions at the liquid boundary and the thermal condition at the bottom.
    - The variation in time of the cloudiness and the relative humidity.
    - The distribution of the transparency of the water has to be taken into consideration.
- The forcing of the bay circulation are mainly the tides, the wind, the thermal and saline stratification produced by the exchange with the atmosphere and the fresh water discharged by the Dique Channel *(CIOH, 1997)*.
- In the south sector (Bocachica) of the bay a difference in the water level with the northern sector (Bocagrande) is present due to the local effects of the tide and the influence of the Dique Channel. This produces a general circulation of water from the south to the north *(CIOH, 1997)*
- The bay has two entrances (Bocachica – Bocagrande). The amplitude of the tide in Bocachica (south) is a little bit larger than in Bocagrande (north), due to the bathymetry close to the Bay. The depth close to Bocachica is larger than the depth close to Bocagrande. In shallow water (as is the case around Bocagrande) the tide energy dissipation is greater, then the tide amplitude is lower. The main characteristic of that is a steady increase of the water level at the Dique Channel discharge sector and a slope to the north of the bay. For that reason the barotropic circulation is always directed to the north of the bay *(CIOH, 1997).*
- The currents in the bay have differences in their behaviour depending on the dynamic regime of the dry and rainy season *(CIOH, 1997).*

2.5 Preliminary Conclusions

According to the previous sections the following conclusions can be established:

The sea water level in the bay of Cartagena shows a steady increase with a fluctuation during the year, apparently related to the tide itself (SSA – Solar Semianual component

– Period 181 days), but SSA, SA and MF are strongly affected by variations of meteorological conditions and river discharges (*Cheng and Gardner*, *1985; Arabelos et al., 1997; Hu et al., 2007*) and, in many coastal areas, a large fraction of the seasonal cycle is steric, that is due to density changes as a consequence of temperature and salinity variations (*Zerbini et al., 1996*). Therefore this fluctuation could be related to the Dique Channel discharge which shows the same steady flow rate increment during the year with a fluctuation related to the climatic season.

The increase of the sea water level may be explained by the presence of the trade winds during January - April, but Tierrabomba Island (with hills up to 80 m) may produce a shadow effect in the bay. On the other hand, the trade winds are not present during August – November when the higher water level occurs. According to Lonin and Giraldo (1995), even the high buildings in the north-eastern part of the bay weaken the winds.

The hurricane season is between June and November. Taking into consideration that the higher water levels in the bay occur during October and November, it may be argued that this can produce an increment of the water levels, but these are specifics events and historically Cartagena Bay has not been affected by hurricanes.

Previous numerical experiments in the bay show differences in the water level related to the Dique Channel discharge in Cartagena Bay *(CIOH, 1999)*

The precipitation in the area is strongly affected by ENOS phenomena, as is the Dique Channel flow rate. That situation could lead to variations in the sea water level of the bay.

3 MODEL AND TOOLS DESCRIPTION

3.1 Model Description

To study the Cartagena Bay circulation and water level behaviour the ROMS_AGRIF V.2.1 was chosen. This version of ROMS (Regional Ocean Model System) was developed by IRD (Institut de Recherche pour le Développement) and makes use of the AGRIF grid refinement procedure developed at the LJK-IMAG (Laboratoire Jean Kuntzmann).

The Regional Oceanic Modeling System (ROMS; *Shchepetkin and McWilliams, 2005*) is an evolutionary descendent from the S-Coordinate Rutgers University Model (SCRUM: *Song and Haidvogel, 1994*). ROMS solves the primitive equations in an earth-centered rotating environment, based on the Boussinesq approximation and hydrostatic vertical momentum balance. ROMS is discretized in coastline and terrain following curvilinear coordinates. ROMS is a split explicit, free-surface ocean model, where short time steps are used to advance the surface elevation and barotropic momentum, with a much larger time step used for temperature, salinity, and baroclinic momentum (ROMS employs a special 2-way time-averaging procedure for the barotropic mode, which satisfies the 3D continuity equation (*Shchepetkin and McWilliams, 2005*). The specially designed predictor-corrector time step algorithm used in ROMS allows a substantial increase in the permissible time-step size.

Most of the information related in the present chapter has been taken from Hedström (2009) and the available information in the Wiki ROMS web page (https://www.myroms.org/wiki/index.php/Documentation_Portal).

For a particular case some of the characteristics of the model can be chosen defining it in the configuration. The main characteristic of the model are as follows:

General

- Primitive equations with potential temperature, salinity, and an equation of state.
- Hydrostatic and Boussinesq approximations.
- Optional third-order upwind advection scheme.
- Optional Smolarkiewicz advection scheme for tracers (potential temperature, salinity, etc.).
- Point sources and sinks.

Horizontal

- Orthogonal-curvilinear coordinates.
- Arakawa C grid.
- Closed basin, periodic, prescribed, radiation, and gradient open boundary conditions.
- Horizontal free-slip or no-slip boundaries.
- Masking of land areas.

Vertical

- Terrain following coordinate.
- Free surface.
- Tridiagonal solve with implicit treatment of vertical viscosity and diffusivity.

Mixing Options

- Horizontal Laplacian and biharmonic diffusion along constant s, z or density surfaces.
- Horizontal Laplacian and biharmonic viscosity along constant s or z surfaces.
- Optional Smagorinsky horizontal viscosity and diffusion (but not recommended for diffusion).
- Vertical harmonic viscosity and diffusion with a spatially variable coefficient, with options to compute the coefficients with Large et al. (1994), Mellor and Yamada (1974), or generic length scale (GLS) Umlauf and Burchard (2001) mixing schemes.

3.1.1 Ocean Model Formulation

3.1.1.1 Equations of Motion

ROMS is a member of a general class of three-dimensional, free-surface, terrain-following numerical models that solves the Reynolds-averaged Navier-Stokes equations using the hydrostatic and Boussinesq assumptions. The governing equations in Cartesian coordinates can be written:

$$\frac{\partial u}{\partial t} + \vec{v}\cdot\nabla u - fv = -\frac{\partial \phi}{\partial x} - \frac{\partial}{\partial z}\left(\overline{u'w'} - \nu\frac{\partial u}{\partial z}\right) + F_u + D_u \tag{1}$$

$$\frac{\partial v}{\partial t} + \vec{v}\cdot\nabla v + fu = -\frac{\partial \phi}{\partial y} - \frac{\partial}{\partial z}\left(\overline{v'w'} - \nu\frac{\partial v}{\partial z}\right) + F_v + D_v \tag{2}$$

In the momentum balance equations (eq. 1, 2) u and v are the (x, y) components of vector velocity $\vec{v}$; x, y denotes horizontal coordinates, and z the vertical coordinate; ; $f(x, y)$ represents the coriolis parameter; $\phi(x, y)$ corresponds to the dynamic pressure. The effects of forcing and horizontal dissipation are represented by the schematic terms F and D.

In the Boussinesq approximation, density variations are neglected in the momentum equations except in their contribution to the buoyancy force in the vertical momentum equation (3). Under the hydrostatic approximation, it is further assumed that the vertical pressure gradient balances the buoyancy force.

$$\frac{\partial \phi}{\partial z} = \frac{-\rho g}{\rho_o} \tag{3}$$

Where $\phi(z)$ corresponds to the dynamic pressure; g is acceleration of gravity, and ρ is the density.

Equation (4) expresses the continuity equation for an incompressible fluid.

$$\frac{\partial u}{\partial x}+\frac{\partial v}{\partial y}+\frac{\partial w}{\partial z}=0 \tag{4}$$

The time evolution of all scalar concentration fields $\left(\frac{\partial C}{\partial t}\right)$, including those for temperature ($T(x,\ y,\ z,\ t)$) and salinity ($S(x,\ y,\ z,\ t)$), are governed by the advective-diffusive equation (5).

$$\frac{\partial C}{\partial t}+\vec{v}\cdot\nabla C=-\frac{\partial}{\partial z}\left(\overline{C'w'}-v_{\theta}\frac{\partial C}{\partial z}\right)+F_C+D_C \tag{5}$$

The equation of state is given by equation

$$\rho=\rho(T,S,P) \tag{6}$$

3.1.1.2 Vertical Boundary Conditions

The vertical boundary conditions can be prescribed as follows:

Top:

$$z=\zeta(x,y,t) \tag{7}$$

$$K_m\frac{\partial u}{\partial z}=\tau_s^x(x,y,t) \tag{8}$$

$$K_m\frac{\partial v}{\partial z}=\tau_s^y(x,y,t) \tag{9}$$

$$K_C\frac{\partial C}{\partial z}=\frac{Q_C}{\rho_o cp} \tag{10}$$

$$w=\frac{\partial \zeta}{\partial t} \tag{11}$$

Bottom:

$$z=-h(x,y) \tag{12}$$

$$K_m \frac{\partial u}{\partial z} = \tau_b^x(x, y, t) \tag{13}$$

$$K_m \frac{\partial v}{\partial z} = \tau_b^y(x, y, t) \tag{14}$$

$$K_C \frac{\partial C}{\partial z} = 0 \tag{15}$$

$$-w + \vec{v} \cdot \nabla h = 0 \tag{16}$$

Where $\zeta(x, y, t)$ corresponds to the surface elevation; K_m, K_c denotes the vertical eddy viscosity and diffusivity; $h(x, y)$ represents the depth of sea floor below mean sea level; Qc is the surface concentration flux; τ_s^x , τ_s^y are the surface wind stress and τ_b^x , τ_b^y are the bottom stress in *x* and *y* coordinates.

On the variable bottom (eq.12), the bottom stress is prescribed by either a linear, quadratic, or logarithmic expression.

3.1.1.3 Horizontal Boundary Conditions

The model can easily be configured for a periodic channel, a doubly periodic domain, or a closed basin. Code is also included for open boundaries which are the one used in the present study.

3.1.1.4 Terrain-Following Coordinate System

The model is terrain following, what means that the vertical coordinate is stretched and "flattens out" the variable bottom at $z = -h(x, y)$.

In the stretched system, the vertical coordinate σ spans the range $-1 \le \sigma \le 0$. In this case, $H_z = \partial z / \partial \sigma$; where $H_z=H_z(x, y, \sigma, t)$ are the vertical layer thicknesses and H_z is computed as $\Delta z / \Delta \sigma$, since this leads to the vertical sum of Hz being exactly the total water column depth D .

The transformation used for the vertical coordinate is:

$$z(x, y, \sigma, t) = \zeta(x, y, t) + S(x, y, \sigma) \;\; \zeta(x, y, t) + h(x, y) \tag{17}$$

$$S(x, y, \sigma) = \frac{h_c \sigma + h(x, y) C(\sigma)}{h_c + h(x, y)} \tag{18}$$

Where $S(x, y, \sigma)$ is a nonlinear vertical transformation functional, $\zeta(x, y, t)$ is the time-varying free-surface, $h(x, y)$ is the unperturbed water column depth and $z = -h(x, y)$ corresponds to the ocean bottom, σ is a fractional vertical stretching coordinate, $C(\sigma)$ is a nondimensional, monotonic, vertical stretching function ranging from $-1 \le C(\sigma) \le 0$, and h_c is a positive thickness controlling the stretching.

The stretching function used is Song and Haidvogel's (1994):

$$C(\sigma) = (1-\phi_B)\frac{\sinh(\phi_S\sigma)}{\sinh\phi_S} + \phi_B\left[\frac{\tanh\left[\phi_S\left(\phi+\frac{1}{2}\right)\right]}{2\tanh\left(\frac{1}{2}\phi_S\right)} - \frac{1}{2}\right] \tag{19}$$

Where ϕ_S and ϕ_B are the surface and bottom control parameters. Their ranges are $0 < \phi_S \leq 20$ and $0 \leq \phi_B \leq 1$, respectively.

3.1.2 Nesting Capabilities

The model has a nesting capability in which AGRIF (Adaptive Grid Refinement in Fortran) is the chosen method. One of the major advantages of AGRIF in static-grid embedding is the ability to manage an arbitrary number of fixed grids and an arbitrary number of embedding levels.

A recursive integration procedure manages the time evolution for the child grids during the time step of the parent grids. In order to preserve the CFL criterion, for a typical coefficient of refinement, for each parent time step the child grid must be advanced using a time step divided by the coefficient of refinement as many time as necessary to reach the time of the parent. The procedure for 2-level embedding, which is the one used in the present study, is as follows and in that order:

- Advance the parent grid by one parent time step.

- Interpolate the relevant parent variables in space and time to get the boundary conditions for the child grid.

- Advance the child grid by as much child time steps as necessary to reach the new parent model time.

- Update point by point the parent model by averaging the more accurate values of the child model (in the case of 2-way embedding).

3.2 ROMSTOOLS

ROMSTOOLS is a collection of global data sets and Matlab programs for processing data and visualising model results in an integrated toolbox. ROMSTOLS simplifies the building of the initial files containing the necessary input data for the model (horizontal and vertical grids, bottom topography, surface forcing, initial conditions and boundary conditions).

3.2.1 Grid Generation

ROMSTOOLS generates rectangular Mercator grids. The bathymetry is derived from ETOPO2 (global topography of 2 minutes resolution derived from depth soundings and satellite gravity observations - Smith and Sandwell, 1997). An iterative averaging procedure is applied to prevent under-sampling. To prevent pressure gradient errors, h (depth) is smoothed to reduce a ‘‘slope parameter’’: $r = \left|h_{+1/2} - h_{-1/2}\right| / \left|h_{+1/2} + h_{-1/2}\right|$. Since $r \sim \Delta h / h$, a modified Shapiro smoother is applied iteratively on $\log(h)$ where r is above the required value, generally 0.25 (*Penven et al., 2008*).

3.2.2 Surface Forcing

Surface forcing is derived from COADS (monthly climatology with a 0.5^{o} and 1º resolution) of air and sea parameters derived from individual observations - *Da Silva et al., 1994*). Missing values are replaced by objective analysis. The resulting matrices are interpolated using a cubic method (*Penven et al., 2008*).

3.2.3 Initialization

Model initialization uses WOA05 (World Ocean Atlas 2005 - set of objectively analyzed (1° grid) climatological fields of *in situ* temperature, salinity at standard depth levels for annual, seasonal, and monthly compositing periods for the world ocean – *Locarnini et al., 2006; Antonov et al., 2006*) hydrography and no flow. For each WOA z-level missing values are replaced by objective analysis. The resulting matrices are horizontally, and subsequently vertically, interpolated on the ROMS terrain-following grid (*Penven et al., 2008*).

3.2.4 Tide Forcing

Tidal constituents are interpolated from TPXO6 (global tidal model of 0.25^{o} resolution of ocean tides assimilating satellite altimetry - *Egbert and Erofeeva, 2002*) and high frequency currents and elevations are added to the low frequency boundary conditions condition (*Penven et al., 2008*).

4 INPUT FILES AND MODEL CONFIGURATION

In this chapter the model configuration and the climatological and forcing data used for the simulations is explained.

4.1 Input Files

In this chapter the input data necessary to run the model is presented.

4.1.1 The Domain

Taking advance of the characteristics of the ROMS_AGRIF model it was decided to run the model using nested grids in order to take into consideration the oceanographic characteristics of the region outside the area of interest (Cartagena Bay). In that sense the grids was created. The parent grid area covers $1^o \times 1^o$, in a 1×1 km resolution, while the child grid covers the Cartagena Bay in 300×300 m resolution (1/3 the parent grid).

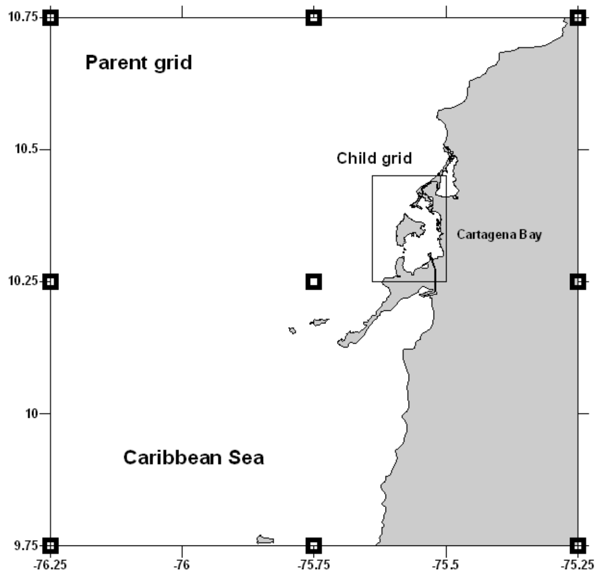

Figure 28. The domain. The black squares show the position of the forcing parameters in the COADS data base.

The size of the parent grid is defined considering:

- The COADS (forcing parameters) data base is 30’ resolution. Having $1^o \times 1^o$ parent grid, interpolation of the forcing parameters can be done for the area (fig. 28).

- A parent grid of 1×1 km resolution allows a child grid of 300×300 m resolution. Bocagrande and Bocachica, the entrances to the bay, are 2 km wide corresponding to 6 nodes in the grid, considered enough for the calculation. In the previous modelling of the bay undertaken by the CIOH using CODEGO model, 250 m resolution grid was used (*Tuchkovenko and Lonin, 2003*).

4.1.2 Bathymetry Grid

Taking into consideration the relative small area of the bay (8’ X 12’) and the resolution of the available bathymetry in the ROMSTOOLS (ETOPO5 - 5' resolution) it is necessary to get a higher resolution bathymetry. In order to do that, different hydrographic surveys undertaken by the CIOH, for nautical charts purposes, are used. In figure 29 the available bathymetric point’s positions are plotted. In table 7 a relation of the nautical charts related to these bathymetric points is listed. In general, the resolution of the bathymetric data is 50 m (Cartagena bay) and 300 m (from 50 to 200 m depth).

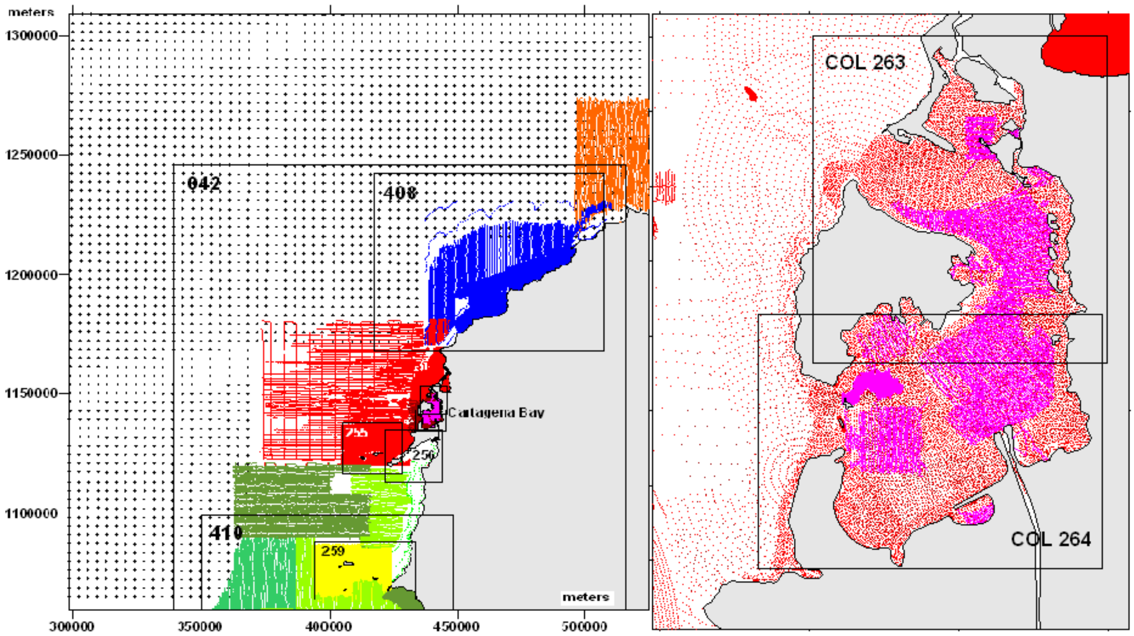

Figure 29. Bathymetric data points. Left: Green colours: Nautical chart COL 410; Yellow: COL 259; red colours: COL 255 – 256 – 263- 264 – 042; blue: COL 408; orange: COL 407; black points: ETOPO5. The square identifies different nautical charts of the area. UTM coordinates – DATUM Bogotá. Right: Cartagena Bay. The square identifies different nautical charts of the area.

Table 7. Nautical charts based on surveys.

Nautical chart	Coverage	Edition
COL – 410	Isla Fuerte – Punta Comisario	
COL – 259	Archipielago de San Bernardo	1999
COL – 255	Archipielago Islas del Rosario	2010
COL – 256	Bahia Barbacoas	1999
COL – 263	Bahia Interna Cartagena	2009
COL - 264	Entrada a la Bahia de Cartagena	2006
COL – 042	Isla Fuerte – B/quilla	2004
COL – 408	Pta Canoas – Pto Colombia	1999

Using the kriging interpolation method, the bathymetric data is interpolated onto a 75×75 m bathymetry grid covering the parent grid. In figures 30 and 31 the resulting bathymetry is shown. The most important characteristic regarding the modelling in the bay is the shallow water in the entrances of the Cartagena Bay. In Bocagrande it is an artificial submerged wall, built to prevent the invasion of pirates in the 15^{th} century (section 2). In Bocachica, the navigational channel is the deepest feature along that entrance (fig. 31).

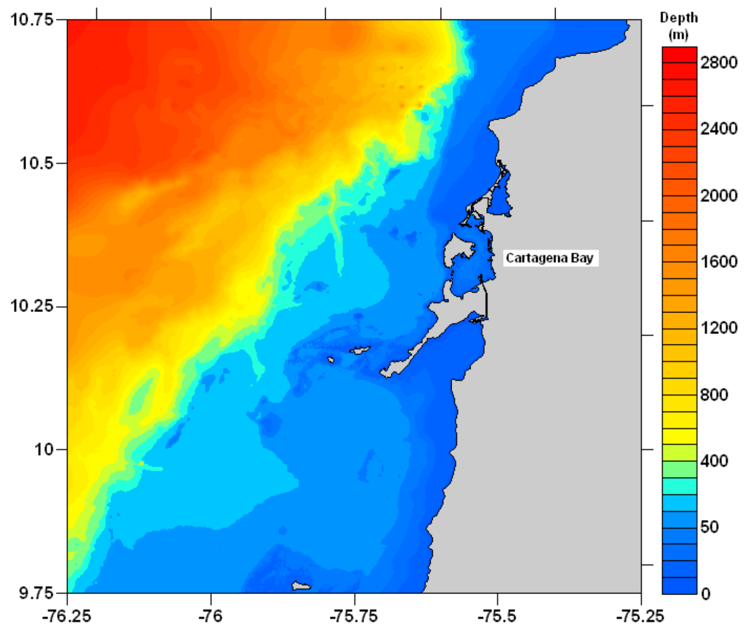

Figure 30. Bathymetry grid contour (resolution 75×75 m) covering the parent grid area.

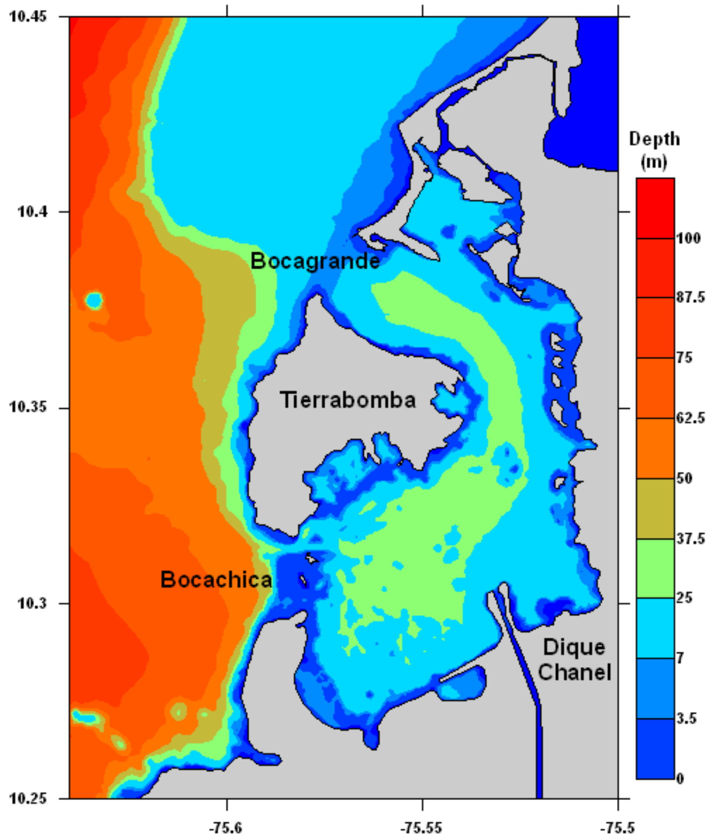

Figure 31. Bathymetry grid contour (resolution 75×75 m) covering the child grid area (Cartagena Bay).

The combination of steep topography and strong stratification, as is the case in Cartagena Bay, can cause errors in numerical simulation (*Haney, 1991*). This error is minimized by smoothing the bathymetry using the available method in ROMSTOOLS. Additionally, a number of passes of a Hanning filter to prevent the occurrence of noise and isolated seamount on deep regions is also applied (*Penven et al., 2010*).

Having created the bathymetry data base, ROOMSTOOLS was used to create the parent and grid bathymetry files for the modelling (Shapiro smoother - slope parameter r=0.25 - two passes of Hanning filter to reduce isolated seamounts on deep water and two passes of Hanning filter at the end of the smoothing procedure to ensure no noise in the bathymetry) . The smoothing process reduced too much the depth at the entrances, making it necessary to reshape those areas to get a realistic bathymetry. The resulting bathymetry grid specifications are related in table 8 and shown in figure 32.

Table 8. Bathymetry grid main characteristics.

Grid	Latitude (north)		Longitude (west)		Resolution (m)	Size (nodes)
	Max	Min	Max	Min		
Parent	9,75 °	10.75 °	75.25 °	76.25 °	1000×1000	120×123
Child	10.25 °	10.41 °	75.63 °	75.30 °	300×300	52×76

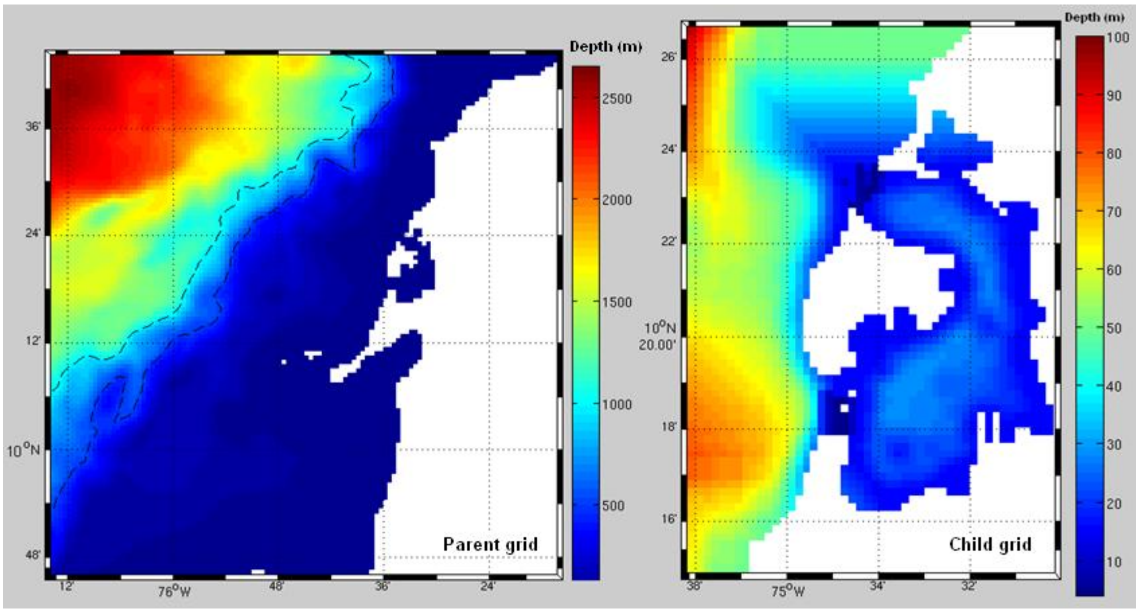

Figure 32. Bathymetric parent and child grid contours using ROMSTOOLS.

4.1.3 Forcing Parameters

The forcing parameters needed to run ROMS are the following:

- Surface u-momentum stress
- Surface v-momentum stress
- Surface net heat flux
- Surface freshwater flux (E-P)
- Sea surface temperature (SST)

- Sea surface salinity
- Surface net heat flux sensivity to SST
- Solar shortwave radiation
- Tide elevation phase angle
- Tidal elevation amplitude
- Tidal current inclination angle
- Tidal current phase angle

For each parameter, except the tidal parameters, the monthly climatologic data is required. This data were obtained using COADS data base and interpolated for the grids using ROMSTOOLS.

4.1.3.1 Wind Stress

In order to define the monthly wind stress for the domain, a statistical analysis of the wind is presented in appendix A.

Using the monthly wind data values described in appendix A, in table 9 the surface *u* and *v* – momentum stress is calculated for each month according to equations 20 and 21. In the entire domain the forcing parameters are assumed equal in space but not in time.

$$\tau_x = \rho_a C_d U_{10}^2 sin\phi \tag{20}$$

$$\tau_y = \rho_a C_d U_{10}^2 \cos\phi \tag{21}$$

Where, ρ_a =1.2 kg/m^3; C_d = 0.0013.

Table 9. Monthly predominant wind (direction and speed) in Cartagena Bay.

MONTH	DIRECTION (degrees)		SPEED (m/s)	τ_x (N/m^2)	τ_y (N/m^2)
January	N	0	3.06	0	-0.0149
February	N	0	3.82	0	-0.0225
March	N	0	3.43	0	-0.0180
April	NNE	11	3.41	-0.0034	-0.0177
May	NW	318	2.98	0.0093	-0.0104
June	W	262	2.84	0.0129	0.0018
July	WSW	242	2.97	0.0123	0.0065
August	W	260	2.85	0.0129	0.0022
September	SW	228	3.23	0.0118	0.0106
October	SW	227	2.84	0.0089	0.0083
November	W	271	2.93	0.0140	0
December	N	354	2.72	0.0014	-0.0139

4.1.3.2 Tide

The tidal parameters were calculated using ROMSTOOLS making use of the TPX06 model output, and interpolated for the parent and child grid. In order to check the TPX06 tide data, these data were compared with the Cartagena's tide gauge data (TPX06 sea level data was obtained for the Cartagena's tide gauge location). The hourly time series data correspond to January 2001. In figure 33 both time series are plotted. The time series were manipulated to have a common mean sea level, reducing the TPX06 data by 80 cm. This reduction corresponds to the difference between the averages of both time series.

Small differences were found; the tide signals are five hours out of phase, the daily maxima of both series have an average difference of 2.59 cm and the average differences between the daily minima is 6.37 cm. The phase difference is due to the reference time used in ROMSTOOLS (Greenwich Meridian Time); Cartagena local time is -5 hours. The Cartagena tide signal (figures 33 and 34) has a 5 hours delay if compared with TPX06 data, what is expected to be.

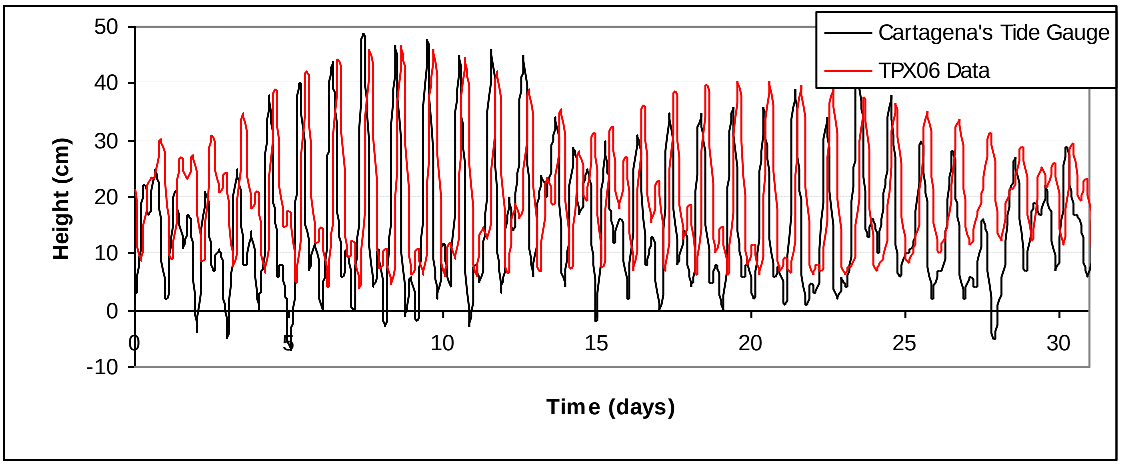

Figure 33. TPX06 tide data and Cartagena's tide gauge data series corresponding to January 2001.

The same analysis is applied to the time series for October, considering the yearly fluctuation of the sea level in Cartagena Bay described in section 2.3.6 (fig. 24). The difference in the mean sea level between the time series was found to be 67.67 cm, 12.33 cm less than the January's tide data. In figure 34, the time series are plotted, reducing the mean sea level of the TPX06 sea level data by 67.67 cm. As in the previous analysis, the signals are 5 hours out of phase. The daily maxima of both series have 3.5 cm average difference for the period. In the case of the minimal, the average difference is 0.14 cm.

According to these results, the TPX06 data are considered as an adequate forcing parameter for the modelling in Cartagena Bay, since these data are an accurate representation of the tide in the bay.

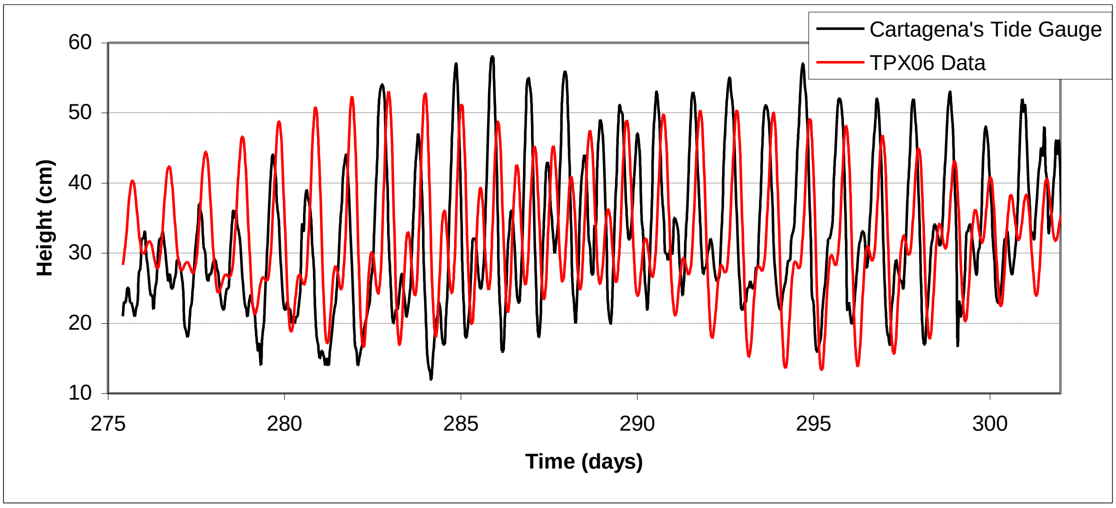

Figure 34. TPX06 tide data and Cartagena's tide gauge data series corresponding to October 2001.

4.1.3.3 Dique Channel Discharge

According to UNAL (2007), the Dique Channel flow rate discharge in Cartagena Bay is calculated based on the Incora Station (7 km from Magdalena River – fig. 17). The discharge in Cartagena Bay is 30.5% of the measured flow rate in Incora station. In table 10, the 1988 (Niña year) flow rates recorded by Incora station (CNR, 2007) and the corresponding values in Pasacaballos, are presented. In figure 35 the data is plotted.

Considering increases in flow rates during La Niña years, the 1988 (Niña year) flow rate record was chosen in order to compare the results of the simulation, using these data, with the 2001 (1999 / 2001 Niña year) Cartagena Bay water level data form the CIOH tide gauge. No data of 2001 Dique Channel flow rate or 1988 Cartagena Bay water level were available for this study.

Table 10. Measured 1988 flow rates of the Dique Channel in Incora station, and the calculated for Pasacaballos (Cartagena Bay). J.D (julian day); F.R (flow rate); D.I (day interval); Av.FR (average flow rate every 15 days – black line in figure 35).

DIQUE CHANNEL FLOW RATE - FIRST SEMESTER												
J.D	**0**	**15**	**30**	**45**	**60**	**75**	**90**	**105**	**120**	**135**	**150**	**165**
F.R	213	114	67	56	51	32	23	76	87	111	111	118
D.I	0 15	15 30	30 45	45 60	60 75	75 90	90 105	105 120	120 135	135 150	150 165	165 180
Av.FR	163	90	61	54	42	27	49	81	99	111	115	138
DIQUE CHANNEL FLOW RATE - SECOND SEMESTER												
J.D	**180**	**195**	**210**	**225**	**240**	**255**	**270**	**285**	**300**	**315**	**330**	**345**
F.R	159	198	205	215	250	284	316	335	344	342	352	367
D.I	180 195	195 210	210 225	225 240	240 255	255 270	270 285	285 300	300 315	315 330	330 345	345 360
Av.FR	179	201	210	233	267	300	325	340	343	347	360	360

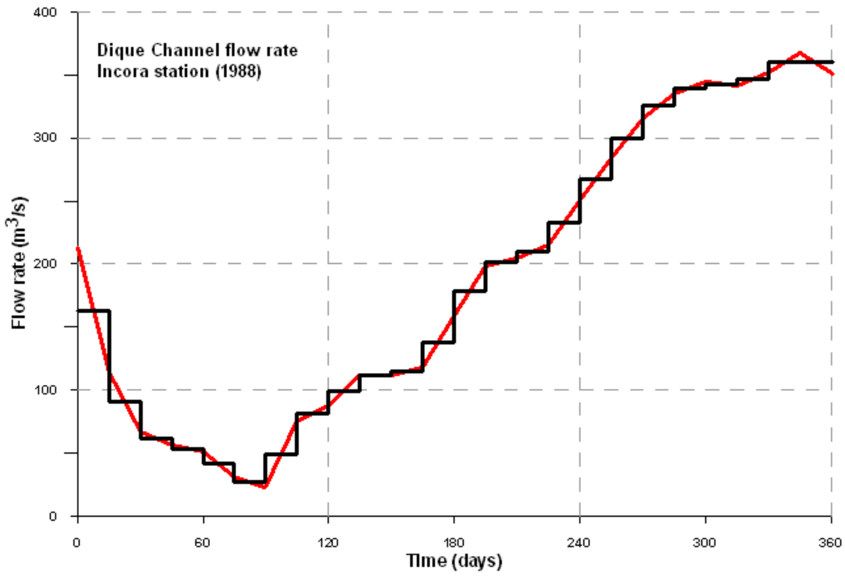

Figure 35. Dique channel flow rate at Pasacaballos (Cartagena Bay) calculation based on Incora station data (red curve). Black line indicates values taken for the simulation.

4.2 Model Configuration

In the following, the configuration of the model is described. These options were chosen for the ROMS model in the CPP_Key file. The information described was obtained from Hedström (2009) and Penven et al. (2010).

Nesting

AGRIF: The Adaptive Grid Refinement in Fortran method for nesting a parent and child grid is used. In the previous section these grids are shown.

Open Boundary Conditions

TIDES: Defined on the open boundaries.
OBC_EAST: Open boundary on the east is defined.
OBC_WEST: Open boundary on the west is defined.
OBC_NORTH: Open boundary on the north is defined.
OBC_SOUTH: Open boundary on the south is defined.

Model dynamics

SOLVE3D: ROMS solves 3D (baroclinic and barotropic) primitive equations.
UV_COR: Coriolis term is activated.
UV_ADV: Horizontal and vertical advection is defined. This is an important characteristic to describe the buoyancy due to high stratification, taking into consideration the water discharge in the bay.
SSH_TIDES: Tidal elevation is imposed for tidal forcing at the open boundaries using TPX06 data.
UV_TIDES: Tidal currents are reconstructed at the open boundaries.
TIDERAMP: A ramping of the tidal current is applied in for an initial swiftly process.

SPHERICAL: Latitude and longitude grid positioning is activated.
MASKING: The land in the domain is masked out.

Lateral momentum mixing

UV_VIS2: Laplacian horizontal mixing of momentum is activated.
MIX_GP_UV: The mixing is activated on geopotential (constant Z) surfaces.

Vertical mixing

LMD_MIXING: The Large, McWilliams and Doney scheme (LMD) matches separate parameterizations for vertical mixing of the surface boundary layer and the ocean interior.
LMD_SKPP: : To add a bottom boundary layer from a local K-Profile Parameterization (KPP), this key is activated.
LMD_BKPP: To add a bottom boundary layer from a local K-Profile Parameterization (KPP), this key is activated.
LMD_RIMIX: Is defined to add diffusivity due to shear instabilities.
LMD_NONLOCAL: Defined to add convective nonlocal transport.

Equation of state

NONLIN_EOS: The nonlinear equation of state is activated. The density is obtained from the temperature and salinity.
SALINITY: Needed for nonlinear equation of state.
SPLIT_EOS: Activate the split of the nonlinear equation of state in an adiabatic part and a compressible part for the reduction of pressure gradient errors. For reasons of efficiency, is chosen to use a split-explicit time step, integrating the depth integrated equations with a shorter time step than the full 3-D equations.

Surface forcing

QCORRECTION: Defined to use the net heat flux correction.
SFLX_CORR: Defined to activate freshwater flux correction.
DIURNAL_SRFLUX: Defined to impose the local diurnal cycle onto the shortwave.

Lateral forcing

SPONGE: Activate areas of enhanced viscosity/diffusion close to the lateral open boundaries.
CLIMATOLOGY: Activate processing of climatology data.
ZCLIMATOLOGY: Activate processing of sea surface height climatology.
M2CLIMATOLOGY: Activate processing of barotropic velocities climatology.
M3CLIMATOLOGY: Activate processing of baroclinic velocities climatology.
TCLIMATOLOGY: Activate processing of tracer climatology (salinity).
ZNUDGING: Activate nudging layer for zeta.
M2NUDGING: Activate nudging layer for barotropic velocities.
M3NUDGING: Activate nudging layer for baroclinic velocities.
TNUDGING: Activate nudging layer for tracer.

Bottom forcing

The surface and bottom fluxes are either defined analytically, read from a forcing file, or computed inside ROMS using a bulk flux formula from the appropriate atmospheric fields (air temperature and winds, for instance). In this case the bottom fluxes are defined analytically.

ANA_BSFLUX: Defined to use analytical bottom salinity flux.
ANA_BTFLUX: Defined to use analytical bottom temperature flux.

Rivers

PSOURCE: Is used to provide river inflow to the model (the Dique Channel discharge).

Open boundary condition

OBC_M2FLATHER: The tidal constituents is propagated from the lateral boundaries using Flather open boundary radiation scheme.
OBC_M2CHARACT: Activate open boundary conditions based on characteristic methods for u and v.
OBC_M3ORLANSKI: Activate 2D radiation open boundary conditions for u and v.
OBC TORLANSKI: Activate 2D radiation open boundary conditions for tracers.
OBC M3SPECIFIED: Activate specified open boundary conditions for u and v.

Time interval

The time interval of the parent and child grids are defined according to the CFL criteria (eq. 22),

$$dt < \sqrt{\frac{dx^2 + dy^2}{g(h(x,y)}} \qquad (22)$$

where *g* is gravity; *h(x,y)* is maximum depth in *x,y* coordinates; *dx* and *dy* are grid size in *x* and *y* respectively. For the parent grid a 60 seconds time step was found. The child grid is 1/3 the parent grid, allowing a 20 seconds time steep.

5 ROMS VERIFICATION

The lack of hydrodynamic measurements in the bay makes the proper calibration of the model imposible; however, it is possible to compare the results of the ROMS model with another model previously used for modelling the bay.

The CODEGO model was implemented by the CIOH in three different Colombian bays (Cartagena, Santa Marta and Morrosquillo) as part of a project with the objective to assess engineering alternatives for improving the water quality and oxygen regime in these bays. CODEGO was calibrated using data of ecological monitoring at Cartagena Bay, measured since 1996 by the CIOH. The monitoring included from two to five seasonal measurements at 23 sites in the bay. The measured parameters were temperature and salinity, transparency, nutrient and oxygen contents, BOD and chlorophyll “a”. Some samples were obtained for phytoplankton primary production, bacterioplankton biomass and bottom demand of oxygen. (*Tuchkovenko et al., 2002*).

In this chapter, a description of the CODEGO model is presented, and the analysis of the comparison between CODEGO and ROMS results in a specific scenario are shown.

5.1 CODEGO Model

The theoretical basis of the CODEGO hydrodynamic model is the three-dimensional Model of Estuarine and Coastal Circulation Assessment (MECCA - Hess, 1985), modified by Lonin (1997). It incorporates river plume dynamics into the model’s governing 3-dimensional equations. The model was designed to predict tidal, wind and density driven flows in bays, and the basic equations are as follows:

(23)

$$\frac{\partial u}{\partial t}+\frac{\partial u^2}{\partial x}+\frac{\partial uv}{\partial x}+\frac{\partial vw}{\partial z}=-\alpha_0\frac{\partial P}{\partial x}+fv+\frac{\partial}{\partial x}\left(2A_h\frac{\partial u}{\partial x}\right)+\frac{\partial}{\partial y}\left(A_h\left[\frac{\partial v}{\partial x}+\frac{\partial u}{\partial y}\right]\right)+\frac{\partial}{\partial z}\left(A_v\frac{\partial u}{\partial z}\right)$$

(24)

$$\frac{\partial v}{\partial t}+\frac{\partial v^2}{\partial y}+\frac{\partial uv}{\partial x}+\frac{\partial vw}{\partial z}=-\alpha_0\frac{\partial P}{\partial y}-fu+\frac{\partial}{\partial y}\left(2A_h\frac{\partial v}{\partial x}\right)+\frac{\partial}{\partial x}\left(A_h\left[\frac{\partial v}{\partial x}+\frac{\partial u}{\partial y}\right]\right)+\frac{\partial}{\partial z}\left(A_v\frac{\partial v}{\partial z}\right)$$

$$\frac{\partial P}{\partial z}=-\rho g \tag{25}$$

$$\frac{\partial u}{\partial x}+\frac{\partial v}{\partial y}+\frac{\partial w}{\partial z}=0 \tag{26}$$

$$\rho=\rho_0\left[1+F_\rho\quad S,T\quad\right] \tag{27}$$

$$\frac{\partial S}{\partial t}+\frac{\partial uS}{\partial x}+\frac{\partial vS}{\partial y}+\frac{\partial wS}{\partial z}=\frac{\partial}{\partial x}\left(D_h\frac{\partial S}{\partial x}\right)+\frac{\partial}{\partial y}\left(D_h\frac{\partial S}{\partial y}\right)+\frac{\partial}{\partial w}\left(D_v\frac{\partial S}{\partial z}\right) \tag{28}$$

$$\frac{\partial T}{\partial t}+\frac{\partial uT}{\partial x}+\frac{\partial vT}{\partial y}+\frac{\partial wT}{\partial z}=\frac{\partial}{\partial x}\left(D_h\frac{\partial T}{\partial x}\right)+\frac{\partial}{\partial y}\left(D_h\frac{\partial T}{\partial y}\right)+\frac{\partial}{\partial w}\left(D_v\frac{\partial T}{\partial z}\right)+R \tag{29}$$

where u, v and w, are velocity components for x, y and z (vertical), respectively; t, time; f, Coriolis parameter; P, pressure; g, gravity; ρ, water density; α_0, specific volume; A_h and A_v, eddy viscosity in horizontal and vertical directions; and D_h, Dv , turbulent diffusion on these directions; T, temperature; S, salinity; R, internal heat sources.

The boundary conditions at the sea surface (z = 0) for (20)–(26) are defined as follows: dynamic conditions for the wind stresses (τ_{sx}, τ_{sy}) and the atmospheric pressure P_a, heat Q_T and salinity Q_S fluxes and the kinematic condition for the free surface h, i.e.

$$\tau_{sx},\tau_{sy} \;\; =\rho A_V\left(\frac{\partial u}{\partial z},\frac{\partial v}{\partial z}\right) \tag{30}$$

$$D_V\left(\frac{\partial T}{\partial Z},\frac{\partial S}{\partial Z}\right)=\left(\frac{Q_T}{\rho C_W},Q_S\right) \tag{31}$$

where C_W, specific heat capacity of water.

For the bottom (z = H), the drag law parameterization and zero-flux conditions for (25) and (26) are:

$$\tau_{bx},\tau_{by} \;\; =\rho A_V\left(\frac{\partial u}{\partial z},\frac{\partial v}{\partial z}\right) \tag{32}$$

$$D_V\left(\frac{\partial T}{\partial Z},\frac{\partial S}{\partial Z}\right)= \;\; 0,0 \tag{33}$$

More information regarding the model equations can be found in Lonin (1997) and Tuchkovenko et al. (2002).

5.2 ROMS and CODEGO Comparison Experiment

5.2.1 General Conditions

A scenario, simulating the Cartagena bay circulation, is implemented in order to verify the ROMS model configuration and results. These results are compared with the results obtained using the CODEGO model.

The bay circulation is simulated considering no wind and a low flow rate (10 m^3/s) of the Dique Channel discharge; the TPX06 tide data was used for both cases.

For CODEGO, the time step interval is 12 s; for ROMS the time interval was chosen to be 20 seconds taking into consideration DX and DY of the grid. The grids have small differences since the CODEGO's grid is 250 X 250 m; the grid used in ROMS is 300 X

300 m. The ROMS's vertical resolution is 10 levels while CODEGO's is 9 levels. The ROMS configuration is described in section 4.2.

For the experiment, the scenario is simulated for eight days, and the last 3 days results at 3 different points (stations in figure 36) every 3 hrs are shown in figures 37 - 45. This simulation time is chosen considering that the stabilization of the results is achieved after two days of simulation.

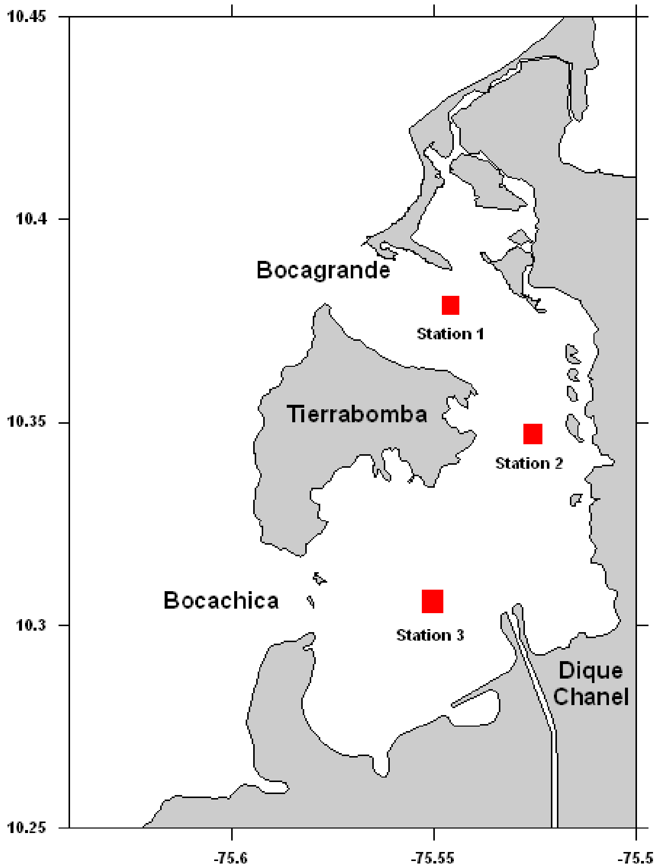

Figure 36. Control points (stations – red squares) at which u and v current velocity components and water level are obtained and compared using ROMS and CODEGO.

5.2.2 Results

In stations 1 and 3, the *u*-component is negative, however the rising and falling periods of the tide (fig. 39 and 45) can be appreciated in the oscillation of the *u*-component (fig. 37 and 43). This result is consistent with the fact that the superficial water (lower density water due to the fresh water discharge of the Dique Channel) is pushed out of the bay by the superficial currents generated by the discharge.

The superficial current *v*- component in these stations (1 and 3) is very small and directed mainly to the north in station 1 and to the south in station 3 (fig. 38 and 44). These results are consistent in both models; however in station 1, ROMS shows a decreasing current (in Y direction) and current reversal during the tide rising period, while CODEGO's results only shows decreasing velocities (only at the end of the simulation this reversal can be appreciate in CODEGO's results – fig. 38); this can be explained considering the differences in the amplitude of the tides in the stations (fig. 39 and 45); ROMS tidal amplitude is higher than CODEGO's.

The main flow in station 2 is north directed considering the Dique Channel flow discharge in which the superficial *v* – current component, for both model results, is positive in Y direction (fig. 41). The results using both models show a very small superficial *u*-component in both models (fig. 40).

The *u* and *v* current velocity components at the stations, comparing both model results, show a very similar oscillatory behaviour considering the forcings used for the experiment (low Dique Channel flow rate and tide). Small differences can be appreciated; however the directions are consistent in both cases and for both parameters.

In order to have an insight of the precision of the results comparing both models, the root mean-square error (RMSE) is considered a good measure of precision. According to equation 34 the RMSE is calculated and the results are listed in table 11.

$$RMSE = \sqrt{\frac{\sum_{i=1}^{n} X_{R,i} - X_{C,i}{}^{2}}{n}} \qquad (34)$$

Where *X* represents the variable to be compared (*u-component*, *v-component*, *water level-*ζ); sub-indices *R* and *C* corresponds to ROMS and CODEGO; *n* denotes the number of data (every 3 hours) obtained during the time of the simulation (72 hours).

Table 11. RMSE calculated for *u-component*, *v-component* and water level (ζ) obtained during 72 hours simulation using ROMS and CODEGO.

STATION	u_{rmse} (cm/s)	v_{rmse} (cm/s)	ζ_{rmse} (m)
1	1.523	0.794	0.052
2	0.530	2.393	0.049
3	0.597	0.503	0.053

Even though the RMSE for the currents (*u* and *v*) was found to be small, if these are compared with the magnitude of the parameters, the error has to be considered. The water level RMSE (ζ_{rmse}) for the 3 stations shows better results. These errors may be explained if the following aspects are considered:

- Even though the models basic equations are the same, the models have different configuration.

- The differences in the time and spatial resolution of the models make it difficult to compare results in the same points and at the same time (timing).

- Even though both models were configured with the same tide forcing data, differences in the water level can be appreciated at each station (fig. 39, 42, 45).

These differences produce differences among the *u* and *v* values of the models results.

- The differences of the water level can be produced by the differences of the bathymetry data, due to the grid resolution.

- The compared currents are the superficial for both cases. However, considering the vertical resolution differs, small differences are likely to occur.

- The magnitude of the currents modelled with both models is very small (0 – 6 cm/s). Small differences due to numerical causes are likely to stand out.

- The vertical resolution of both models differs (ROMS – 10 levels, CODEGO – 9 levels). Considering the *u* and *v* components are the obtained values in the superficial level for both models, and that the distances between the levels have differences, some differences in the results is likely.

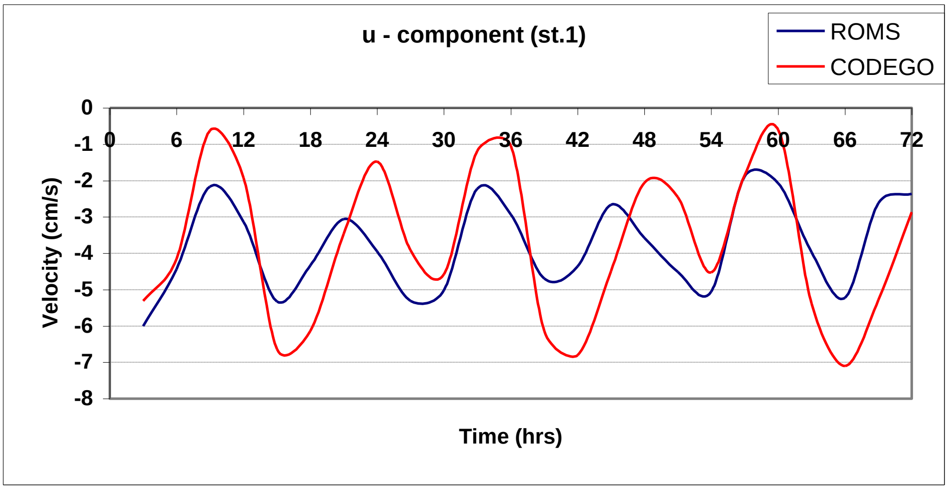

Figure 37. *u* -current component parameter calculated in station 1.

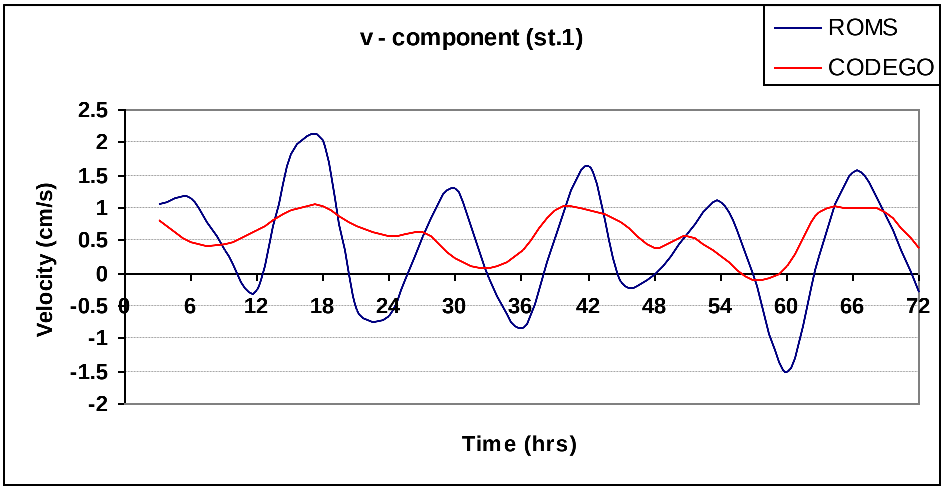

Figure 38. *v* -current component parameter calculated in station 1.

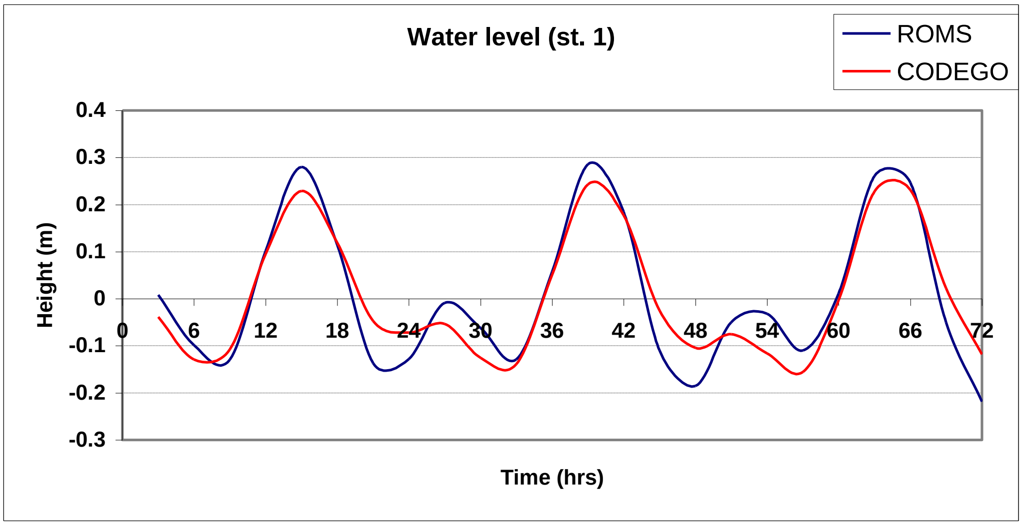

Figure 39. Water level height calculated in station 1.

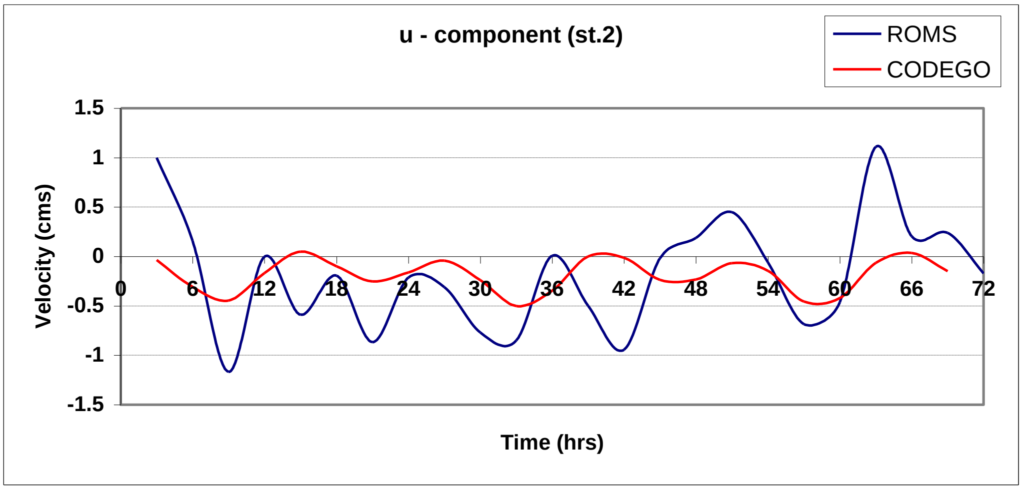

Figure 40. *u* -current component parameter calculated in station 2.

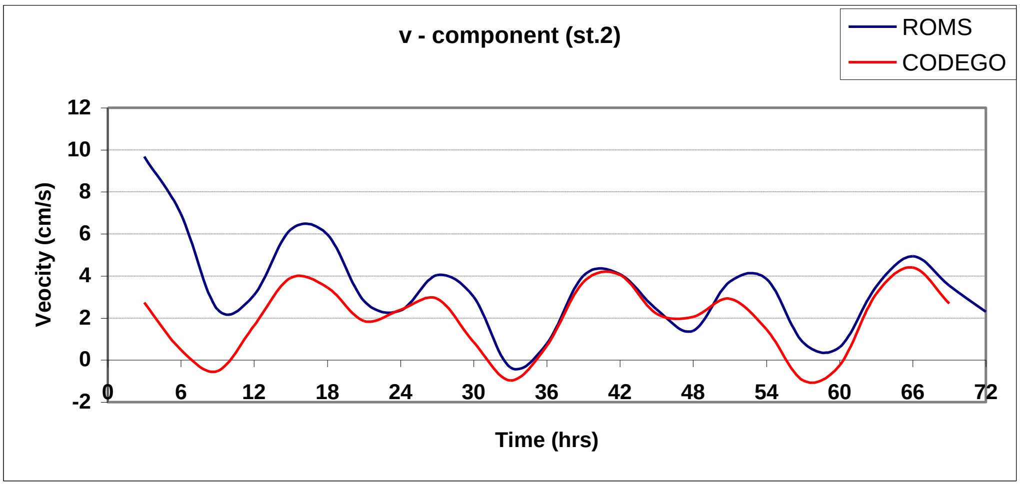

Figure 41. *v* -current component parameter calculated in station 2.

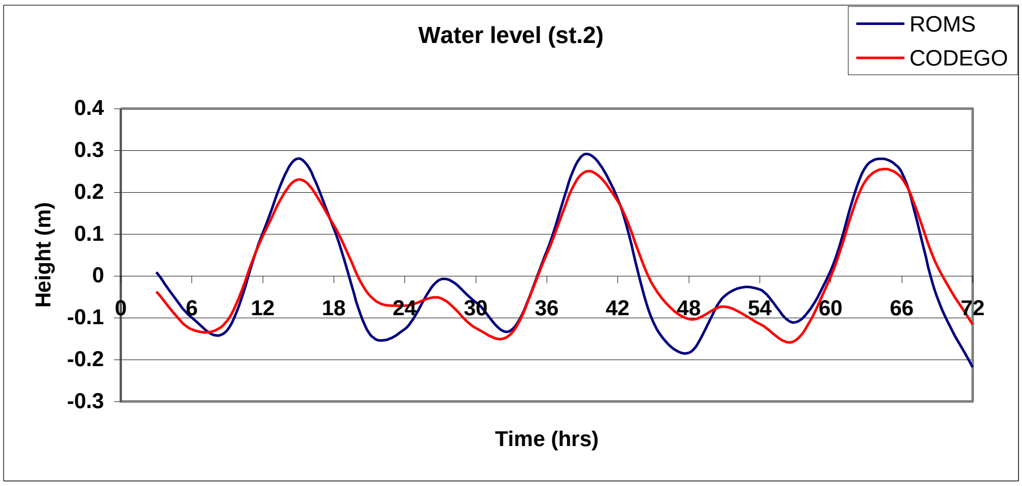

Figure 42. Water level height calculated in station 2.

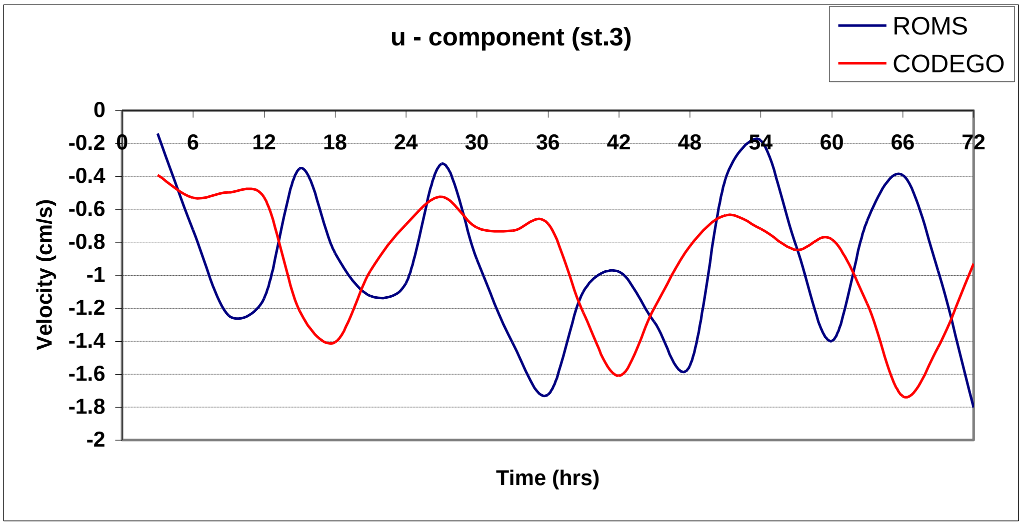

Figure 43. *u* -current component parameter calculated in station 3.

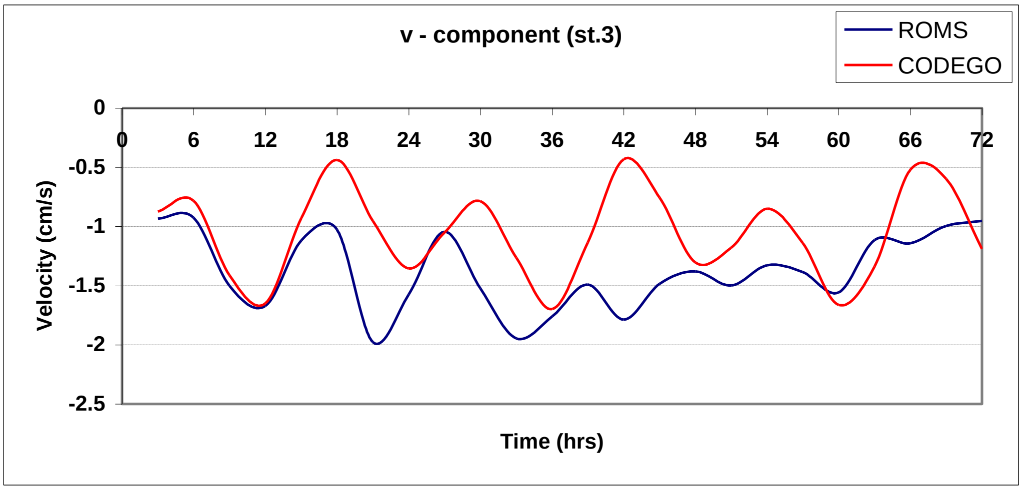

Figure 44. *v* -current component parameter calculated in station 3.

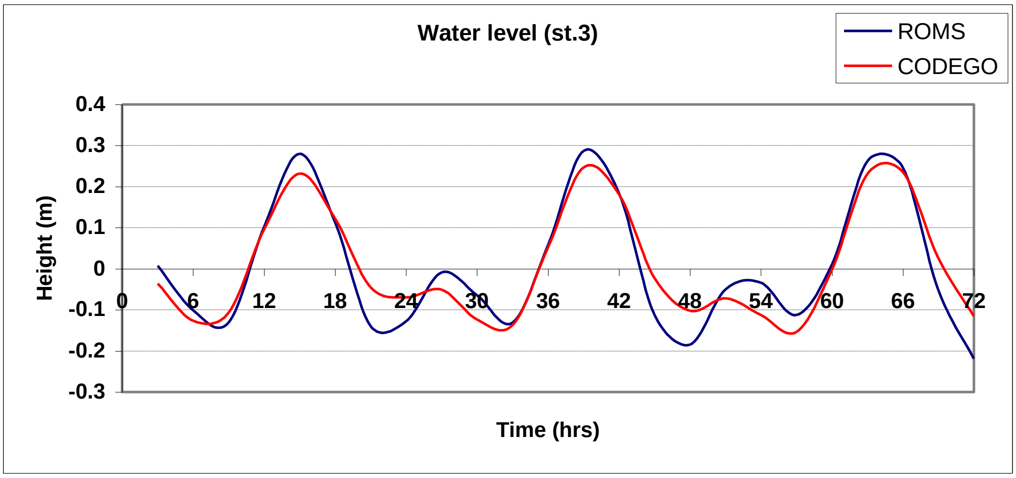

Figure 45. Water level height calculated in station 3.

No further experiments to compare the models results were done because only the executable of the CODEGO model was available for this study. This limitation makes it not possible to obtain results of other parameters as temperature, salinity or density. Current velocity (u – v components) vertical profile can not be obtained with the CODEGO model version used.

6 SIMULATION OF THE BAY DYNAMICS

To determine the effects of the Dique Channel discharge on the Cartagena Bay water level, a set of scenarios is required, in which the forcings have to be included and then isolated. This chapter presents the implementation of these scenarios and the results.

Five numerical experiments were designed. The first evaluates the effects of the wind and the Dique Channel discharge (using 1988 flow rate data – La Niña year); the second experiment simulates one year of the bay dynamics including as forcings the Dique Channel discharge and the wind in order to evaluate the water level throughout the year; the third experiment, similar to the second, does not consider the wind forcing, to confirm that the seasonal rising of the sea level in Cartagena bay may be caused by its limited communication with the open sea, which leads to an accumulation of water in the bay as proposed by Alexander et al. (2008). The forcing parameters, Dique Channel discharge and tide, are obtained from the 2001 measured discharge and TPX06 respectively, in order to compare the results with the measured water level data at the CIOH tide gauge. The fourth and fifth experiments were designed to understand the water exchange mechanism of the bay.

6.1 First Experiment

Even though this project is focused on the effects of the Dique Channel discharge on the Cartagena Bay water level, it is necessary to isolate it from the wind effects. In order to isolate the forcings, 3 different scenarios are proposed. The first scenario represents January conditions, in which the Dique Channel discharge is lower than in October; the wind is the strongest along the year, and opposite to the discharge flow. The second scenario represents October conditions, characterized by higher flow rate discharge and weak wind, in the direction of the discharge flow. The third scenario is designed to evaluate the effects on the water level due to an increment of the Dique Channel discharge using the October conditions, representing a stronger La Niña phenomenon (higher precipitation rates); the sub-scenarios 2.3 and 2.4 are considered for scenario 3; October was chosen taking into consideration that this month shows the highest water level along the year (fig. 24). In table 12 the scenarios are described.

As can be appreciated in table 12, the scenarios are divided in sub-scenarios. The results of the modelling for each one of the sub-scenarios are compared between them in the same scenario in order to find the effect of the forcing in 5 different points (stations) of the bay. The scenario 1.1 and 2.1 are the base line in which no forcing, different than the tide, is used. The positions of the stations are chosen in accordance with the extension of the bay and the importance of the area close to the points (table 13).

Table 12. Scenarios for the first experiment.

ID	Flow rate (m3/s)	Wind velocity (m/s)	Wind direction (comes from)	Month	Tide (source)
SCENARIO 1					
1.1	0	0		January	TPX06
1.2	213	0		January	TPX06
1.3	0	3.06	North	January	TPX06
1.4	213	3.06	North	January	TPX06
SCENARIO 2					
2.1	0	0		October	TPX06
2.2	344	0		October	TPX06
2.3	0	2.84	Southwest	October	TPX06
2.2	344	2.84	Southwest	October	TPX06
SCENARIO 3					
3.1	400	2.84	Southwest	October	TPX06
3.2	450	2.84	Southwest	October	TPX06

Table 13. Stations description in which the results are obtained.

Station	Latitude	Longitude	Description
A	10.3902º N	75.5583º W	Residential and touristic area (Castillogrande)
B	10.4119º N	75.5445º W	Touristic and military installations (Base Naval, Arsenal Pier; Manga Island)
C	10.3820º N	75.5362º W	Tide gauge site (CIOH)
D	10.3575º N	75.5141º W	Industrial area (Mamonal)
E	10.2731º N	75.5666º W	Left side of Dique Channel

6.1.1 First Experiment Results

In figures 47, 49, 51, 53, 55, 57, the water level effect at the chosen stations is revealed by plotting the daily averaged water level data (dt = 1.5 hours) obtained during the simulations. The water level anomaly is obtained subtracting the water level data of the sub-scenarios 1.2, 1.3, 1.4, from the base line water level data (scenario 1.1). Same is applied to scenario 2, using sub-scenario 2.1 as water level data base line.

Figures 46, 48, 50, 52, 54 and 56, show the distribution of the instantaneous water level along the bay during high tide.

In the description of the results, special interest is given to station C, considering the available water level data from the CIOH tide gauge, which is used to compare the results of the second experiment.

Scenario 1

Only considering the 1988 January Dique Channel discharge (scenario 1.2), it produces a water level elevation that is mostly concentrated on the east coast of the bay, decreasing from south to north (E station is not affected by the discharge). In average, the water level anomaly (WLA) in station C is +1.65 cm (fig. 46 and 47). However the water level difference between the northern (B) and southern (E) stations is very small (around 5mm), and is considered insignificant. If only the characteristic January north wind forcing is considered (scenario 1.3), it acts increasing the water level from north to south. In station E (south) the water is piled up against the shore, increasing the sea level up to 0.5 cm, while in station C the water level decrease (fig. 48 and 49). Like the scenario 1.2 results, the water level difference between stations B and C is very small (2.5 mm).

Wind and flow rate forcings (scenario 1.4) produce a water level increment mostly concentrated on the southeast of the bay; however +1.35 cm WLA is detected in station C (fig. 50 and 51). Both forcings acts increasing the water level from south to north. January conditions show a decreasing in the water level on station C; this trend is consistent with the water level measurements on station C (fig. 24).

Scenario 2

Considering the Dique Channel discharge of October (scenario 2.2), a steady increment of the water level is detected during the first half of the month in which +2.5 cm is the highest value for the WLA. On average, the discharge produces a water level increase of 2 cm in station C (fig. 53). As in scenario 1.1, the water elevation is mostly concentrated on the east coast of the bay, decreasing from south to north (fig. 52). Only considering the October characteristic southwest wind forcing (scenario 2.3), the water is piled up against the northeast part of the bay (stations A, B, C). In station C, an average WLA of +1 cm is detected (fig. 54 and 55).

The combination of both forcings (wind and flow rate) produce + 2.8 cm WLA in station C. The water level decrease from east to west (fig. 56 and 57). Considering station C, the forcings acts increasing the water level. This trend is consistent with the water level measurements on station C (fig. 24). However the magnitude is much lower (just 14% of the October water elevation).

Scenario 3

In the third scenario the effect of the Dique Channel discharge is evaluated using October wind conditions and a 50 m^3/s flow rate increment from the 1988 La Niña year flow rate, in order to evaluate the effect of stronger (than 2001) La Niña phenomenon in the bay. The result of the evaluation of the increment of the flow rate only gives 0.1 cm increment in the sea level at station C (fig. 58).

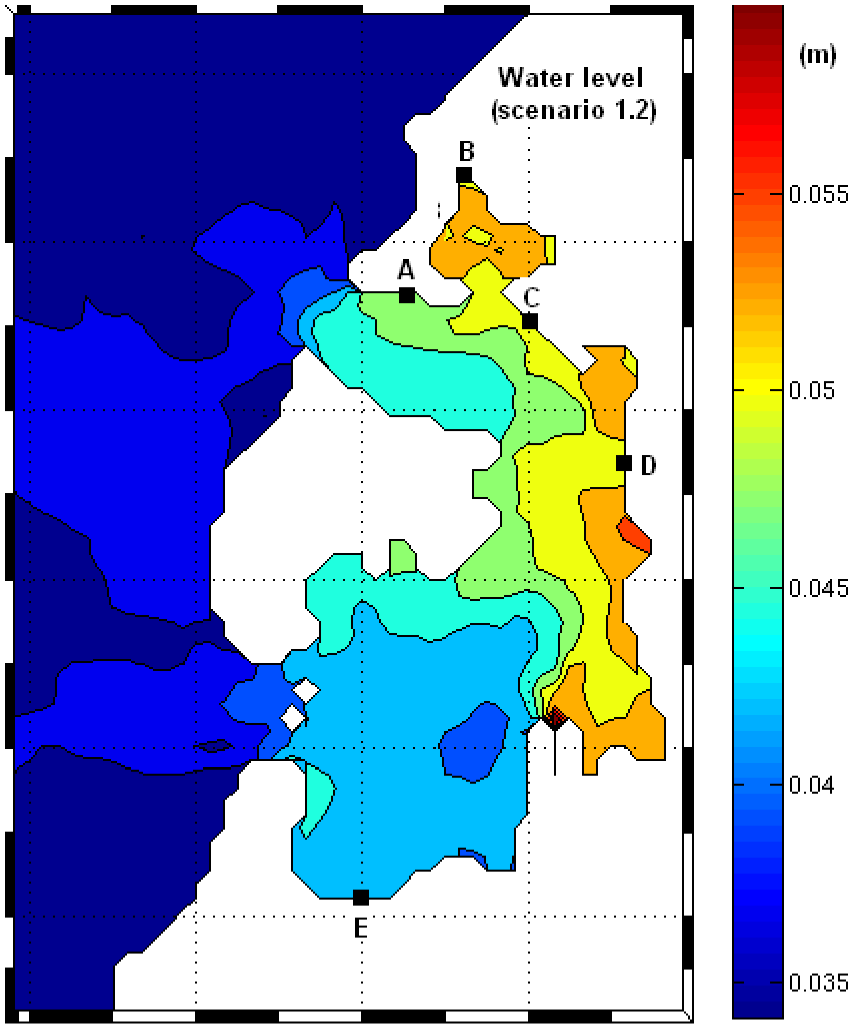

Figure 46. Water level distribution in the bay during high tide (day 27). Black squares indicate stations related in table 13. Experiment 1, scenario 1.2 (forcing: river discharge).

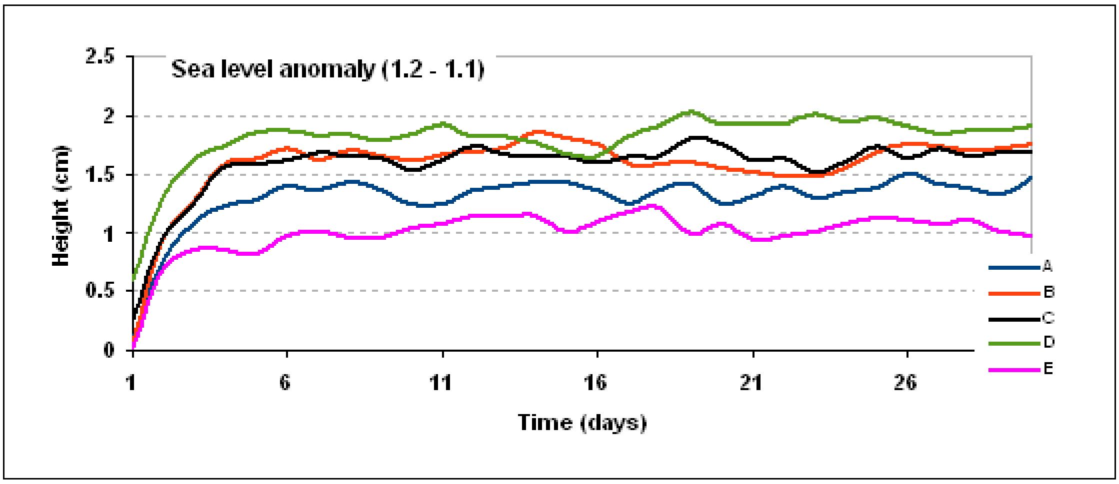

Figure 47. Water level effect in different stations, caused by the river discharge forcing. Experiment 1, scenario 1.2.

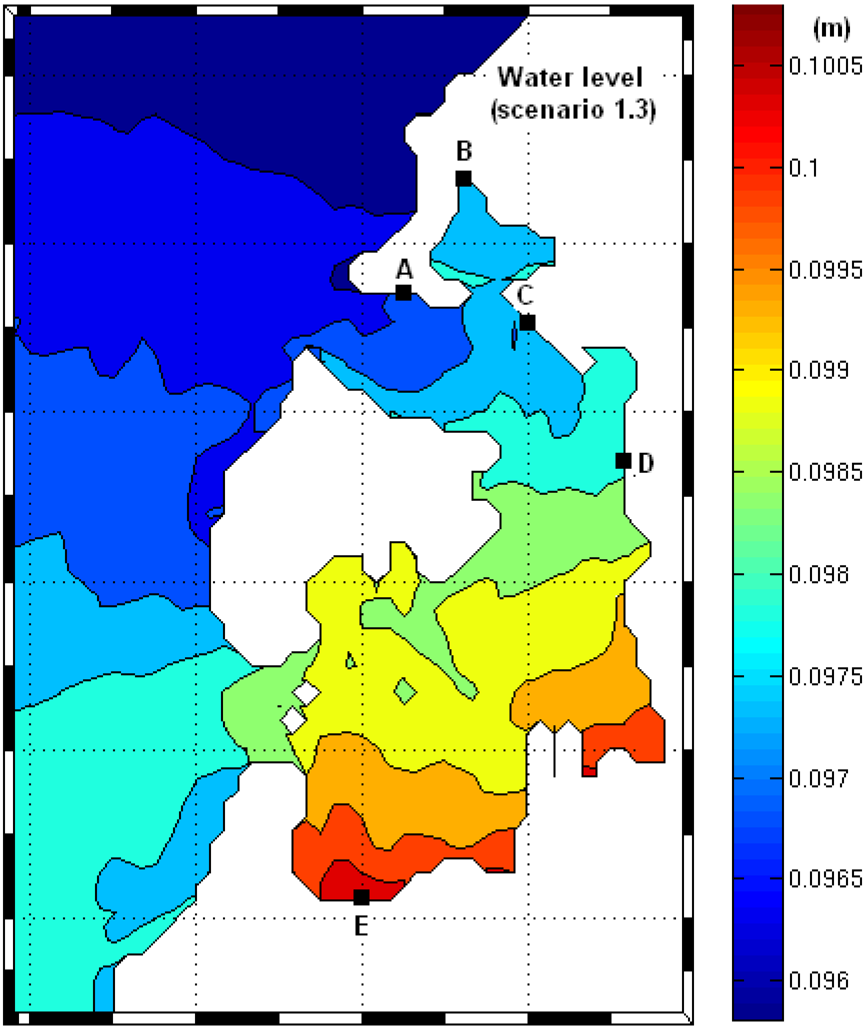

Figure 48. Water level distribution in the bay during high tide (day 27). Black squares indicate stations related in table 13. Experiment 1, scenario 1.3 (forcing: N wind).

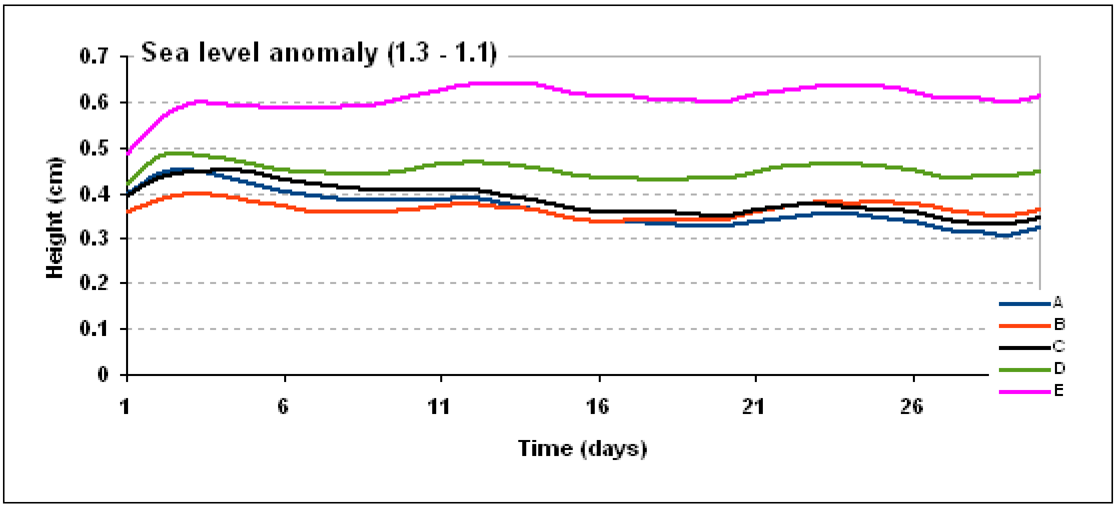

Figure 49. Water level anomaly in different stations, caused by the wind forcing (north). Experiment 1, scenario 1.3.

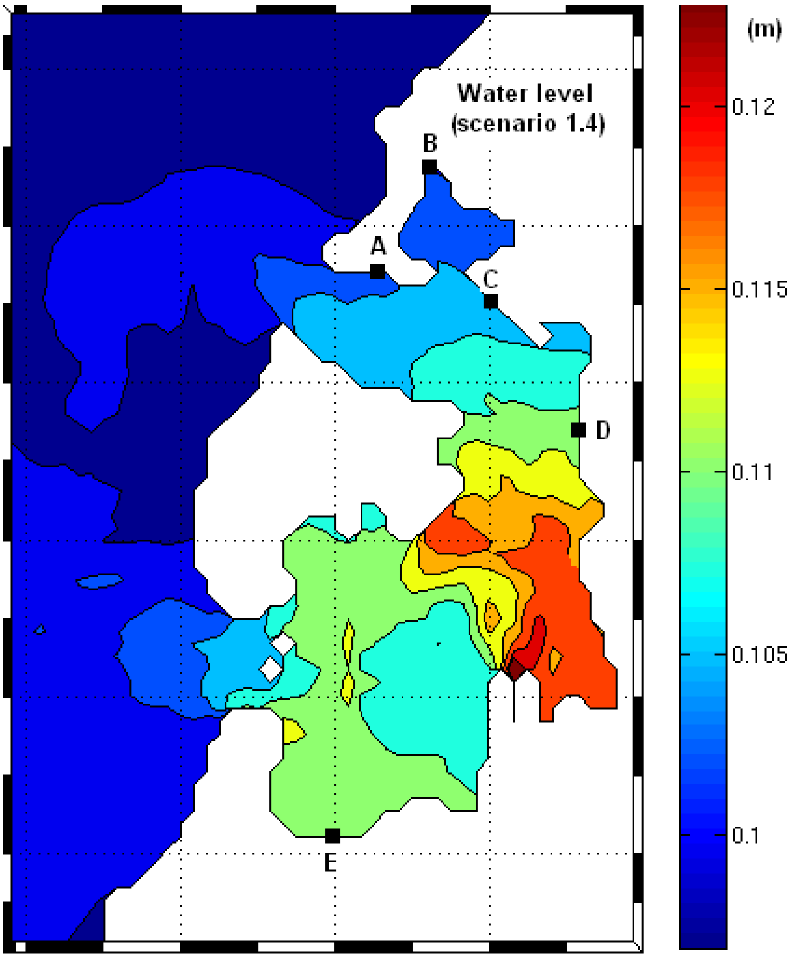

Figure 50. Water level distribution in the bay during high tide (day 27). Black squares indicate stations related in table 13. Experiment 1, scenario 1.4 (forcings: north wind – river discharge).

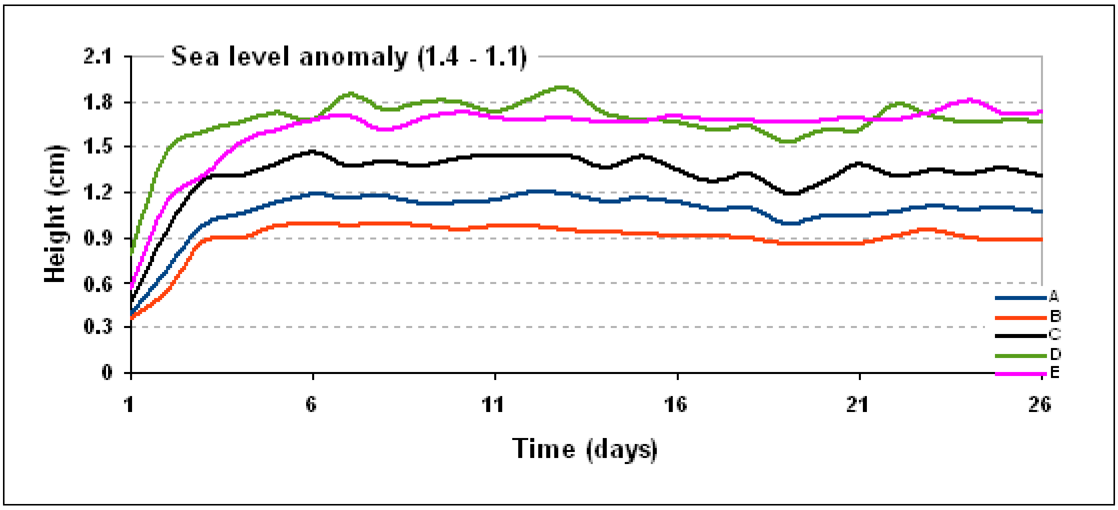

Figure 51. Water level effect in different stations, caused by combined river discharge and wind forcing (north). Experiment 1, scenario 1.4.

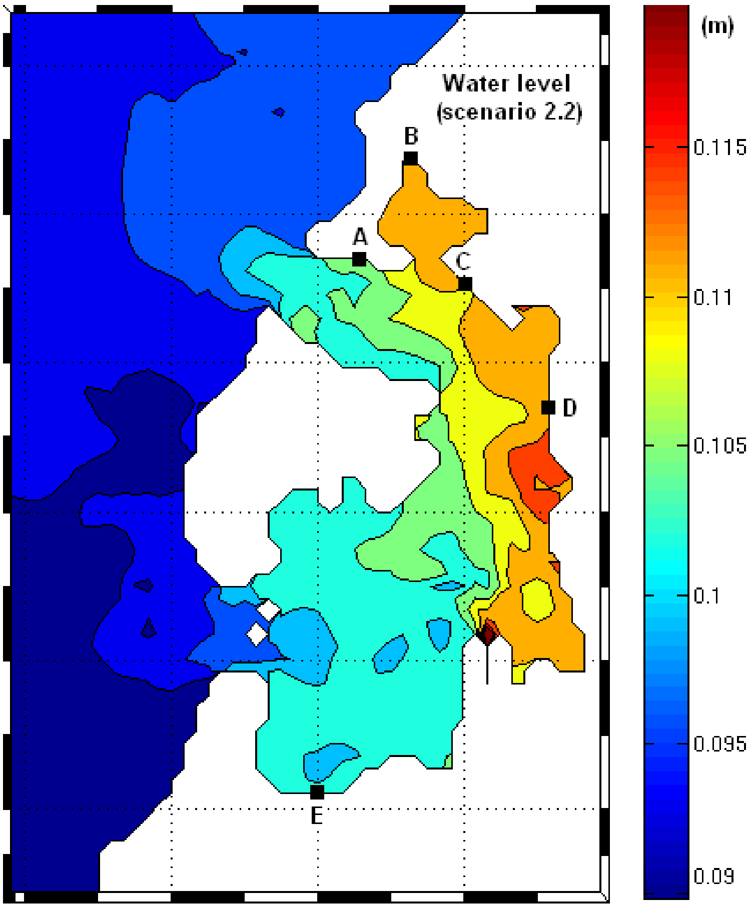

Figure 52. Water level distribution in the bay during high tide (day 297). Black squares indicate stations related in table 13. Experiment 1, scenario 2.2 (forcing: river discharge).

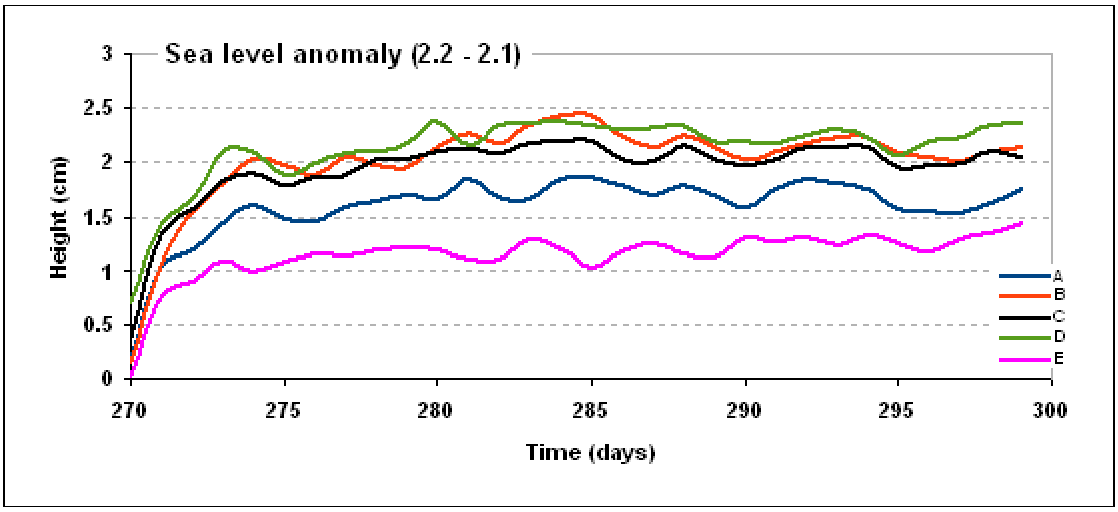

Figure 53. Water level effect in different stations, caused by the river discharge. Experiment 1, scenario 2.2.

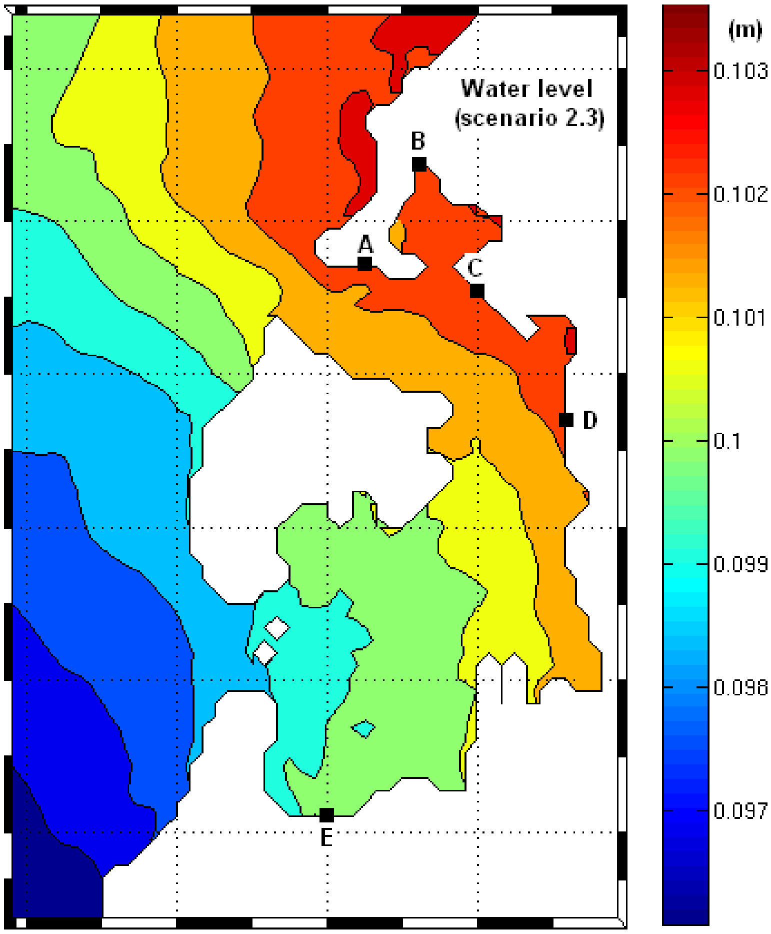

Figure 54. Water level distribution in the bay during high tide (day 297). Black squares indicate stations related in table 13. Experiment 1, scenario 2.3 (forcing: SW wind).

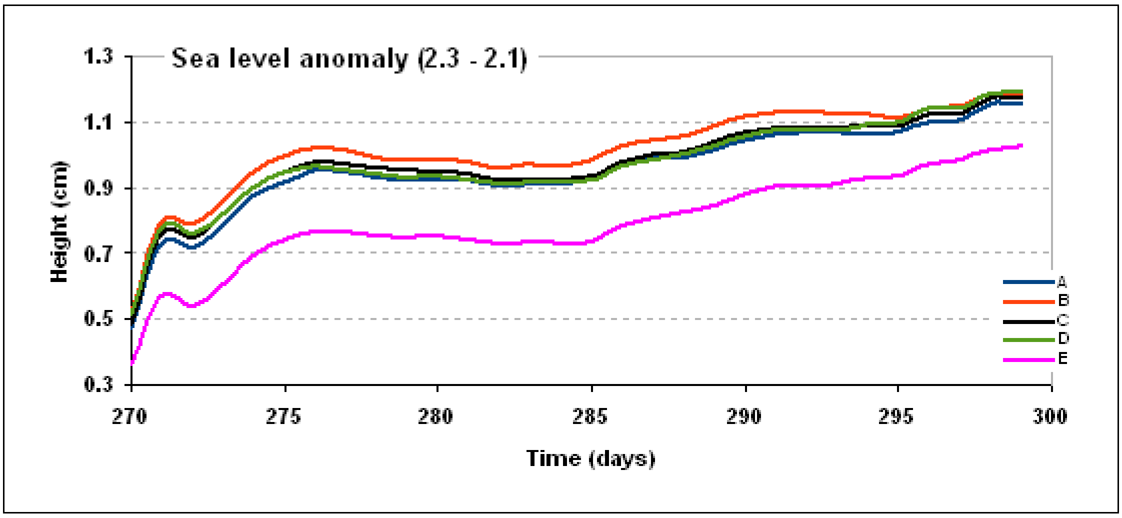

Figure 55. Water level effect in different stations, caused by the wind forcing (southwest).. Experiment 1, scenario 2.3.

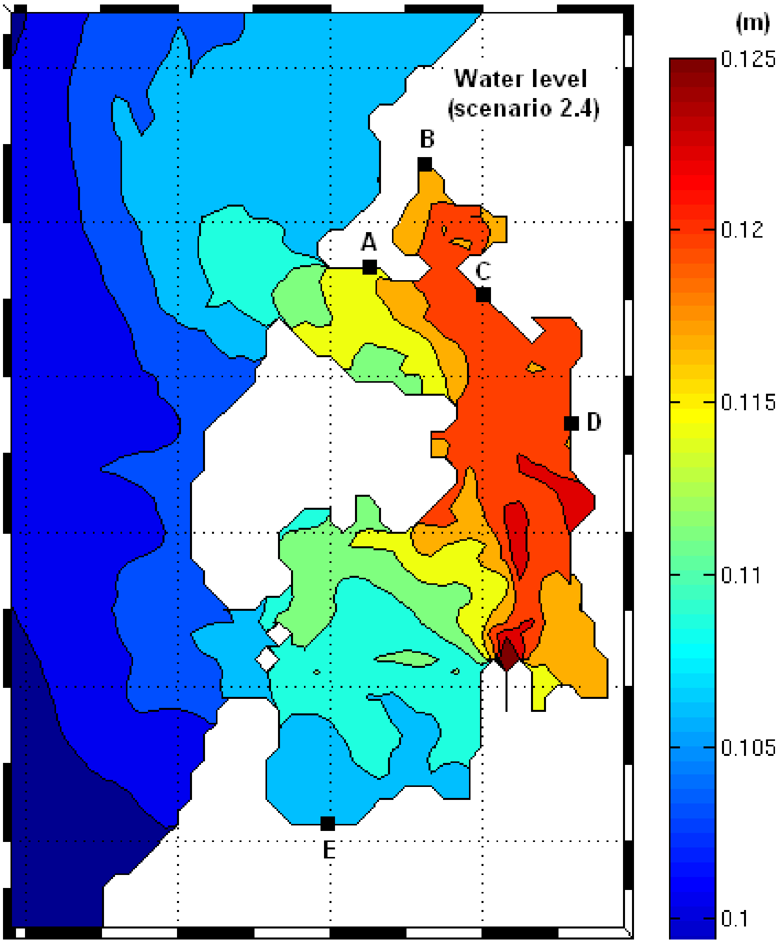

Figure 56. Water level distribution in the bay during high tide (day 297). Black squares indicate stations related in table 13. Experiment 1, scenario 2.4 (forcing: SW wind – river discharge).

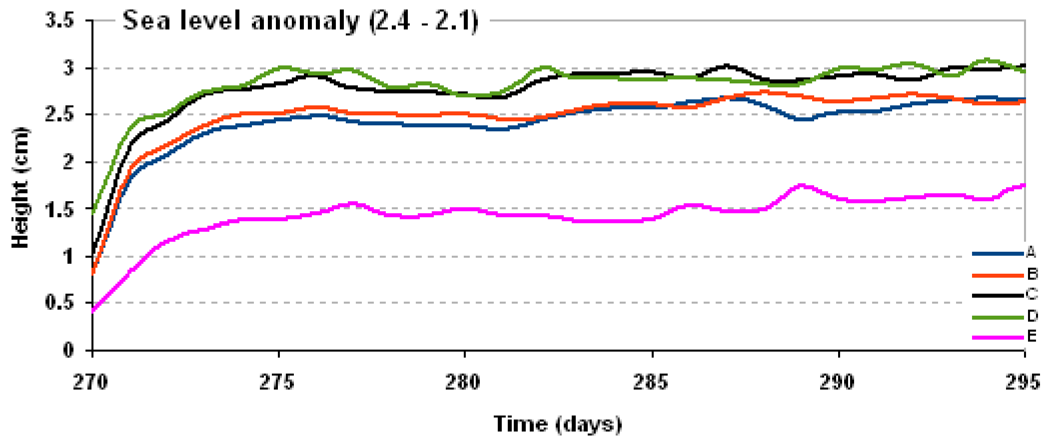

Figure 57. Water level effect in different stations, caused by combined river discharge and wind forcing (southwest). Experiment 1, scenario 2.4.

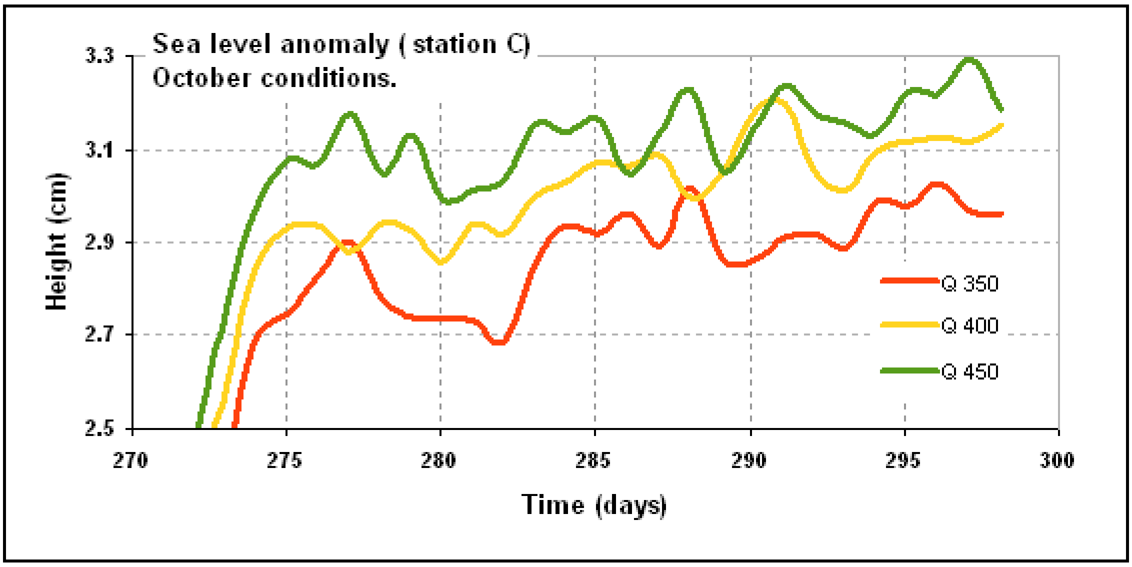

Figure 58. Sea level anomaly in station C, scenarios 2.3 (red), 3.1 (yellow), 3.2 (green). Q represents Dique Channel flow rate (m^3/s).

6.2 Second Experiment

The second experiment was implemented in order to analyse the Cartagena bay water level behaviour through the year. The forcings include the wind speed and direction according to section 4.1.3 and appendix A; the Dique Channel flow rate used is according to 1988 (La Niña year) data records (section 4.1.3.3) and the tide parameters according to TPX06 (section 4.1.3.2) 2001 data, in order to compare the results with the available water level records measured by the CIOH in the bay; no water level records were available for 1988. These years were chosen considering that 1988 and 2001 are classified as La Niña years, characterized by high precipitation rates and, consequently, high Dique Channel flow rates. In that way, the effect of the Dique Channel in Cartagena Bay is evaluated considering extreme values.

The other forcings (surface net heat flux, surface freshwater flux (E-P), sea surface temperature, sea surface salinity, surface net heat flux sensitivity to SST and solar shortwave radiation) used are from COADS data base.

The simulation was computed during 360 days, but restarted every 15 days in order to update the Dique Channel flow rate.

6.2.1 Second Experiment Results

Due to limitations of the model, the bathymetry at the bay's entrances had to be smoothed because strong currents were created by the high Dique Channel flow rate discharge and enhanced by the wind shear stress, leading to the model blow up. Even though a non-realistic bathymetry was used, the experiment was kept to get a general overview of the effect of the wind.

In figure 59 the calculated 15 days averaged water level at CIOH tide gauge station is plotted and compared with the 2001, 15 days averaged water level records measured at the same location; the Dique Channel flow rate is plotted to visualise the trend. The simulated water level shows the same trend as the Dique Channel flow rate and the measured water level, however the magnitudes between the simulated and averaged water level differs in about 80% (average value). Considering this result may be related to the unrealistic bathymetry used at the bay's entrances, which could lead to a higher water exchange, a third experiment is necessary.

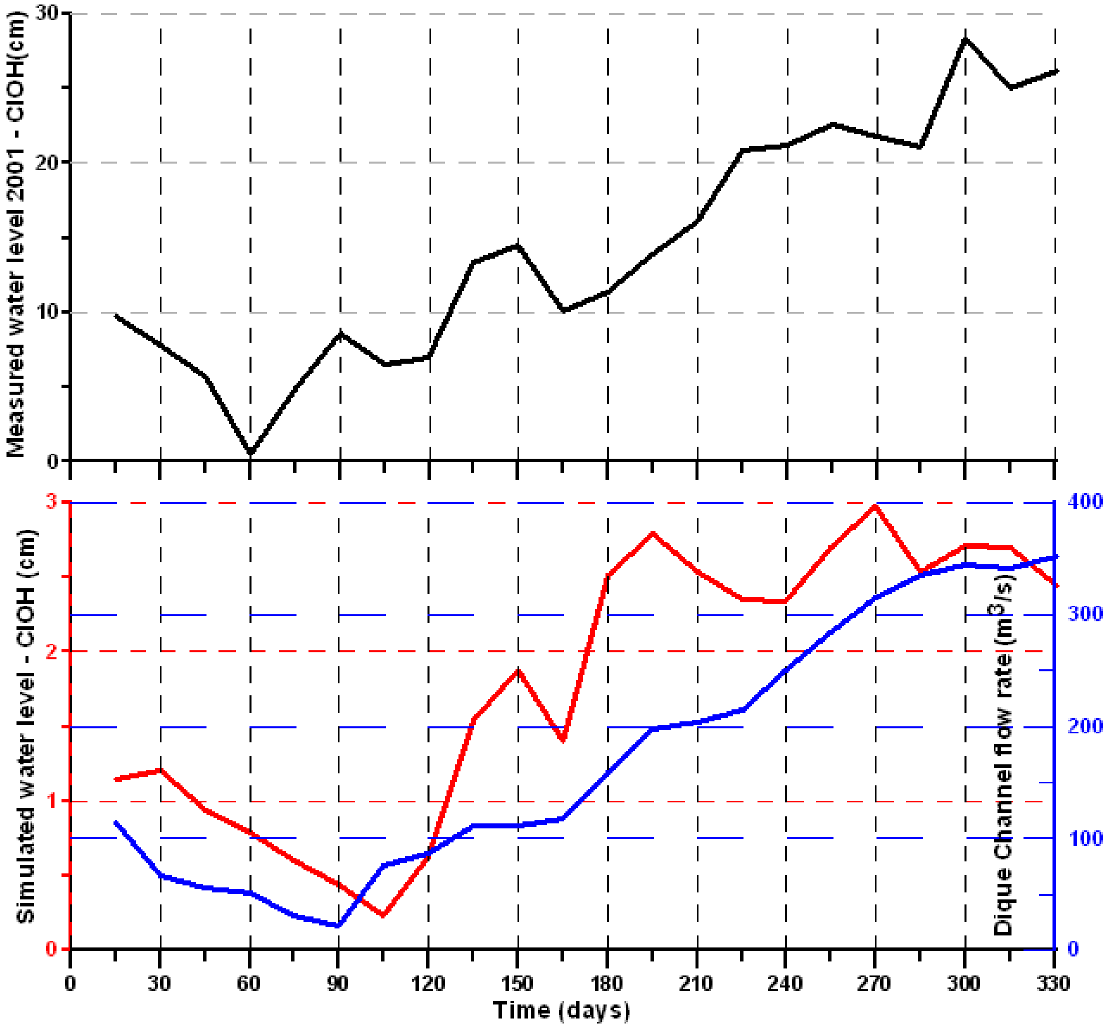

Figure 59. Water level results during the second experiment. Above: measured water level by the CIOH (records averaged every 15 days – black line); below: computed water level results (red line) – Dique Channel flow rate discharge (blue line).

6.3 Third Experiment

Bearing in mind the limitations faced in the second experiment, for the third experiment no wind was considered and the Dique Channel flow rate discharge used corresponds to 1990, considered a normal year (no Niño or Niña) (table 14 and figure 60).

The simulation was computed using realistic bathymetry (the entrance depths were not smoothed as in the second experiment), during 360 days, but restarted every 15 days in order to update the Dique Channel flow rate. The other forcings are as explained in section 6.2.

Table 14. Averaged flow rates at Pasacaballos (Cartagena Bay), calculated from the Incora station data - 1990). J.D (julian day); F.R (flow rate); D.I (day interval); Av.FR (average flow rate every 15 days – black line in figure 35).

DIQUE CHANNEL FLOW RATE - FIRST SEMESTER												
J.D	**0**	**15**	**30**	**45**	**60**	**75**	**90**	**105**	**120**	**135**	**150**	**165**
F.R	168	125	64	69	50	44	71	74	109	153	164	154
D.I	0 15	15 30	30 45	45 60	60 75	75 90	90 105	105 120	120 135	135 150	150 165	165 180
Av.FR	147	95	67	60	47	58	73	92	131	159	159	152
DIQUE CHANNEL FLOW RATE - SECOND SEMESTER												
J.D	**180**	**195**	**210**	**225**	**240**	**255**	**270**	**285**	**300**	**315**	**330**	**345**
F.R	150	136	126	110	99	120	123	163	200	227	250	266
D.I	180 195	195 210	210 225	225 240	240 255	255 270	270 285	285 300	300 315	315 330	330 345	345 360
Av.FR	143	131	118	105	109	121	143	182	214	239	250	217

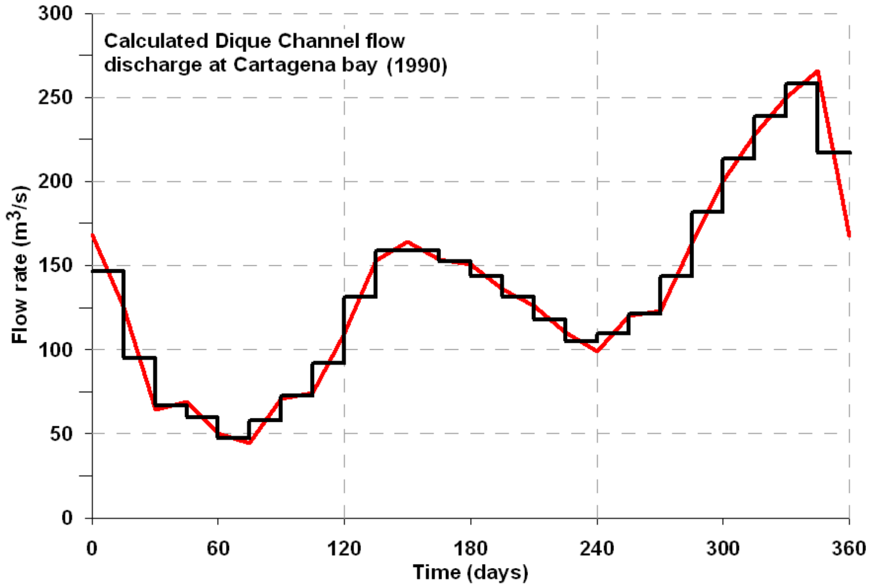

Figure 60. Dique channel flow rate (red line) at Pasacaballos (Cartagena Bay); calculation based on Incora station data. Black line indicates values taken for the simulation.

6.3.1 Third Experiment Results

In figure 61 the measured water level (averaged every 15 days) at the CIOH tide gauge station is plotted and compared with the water level (averaged every 15 days) obtained during the simulation at the same position. The trend of the simulated water level is consistent with the measurements. Comparing the simulated water level with the Dique Channel flow rate discharge, a 150 m^3/s increment of the flow rate reflects an increment in about 0.8 cm in the water level; however that behaviour may not be lineal as was found during the first experiment (scenario 3).

If the magnitudes of the measured and simulated water level are compared, is evident the presence of other forcing different than the Dique Channel or the wind (second experiment) responsible for the water level difference through all the year, even though the Dique Channel plays a small role (incrementing the water level in less than 2 cm during the rainy season).

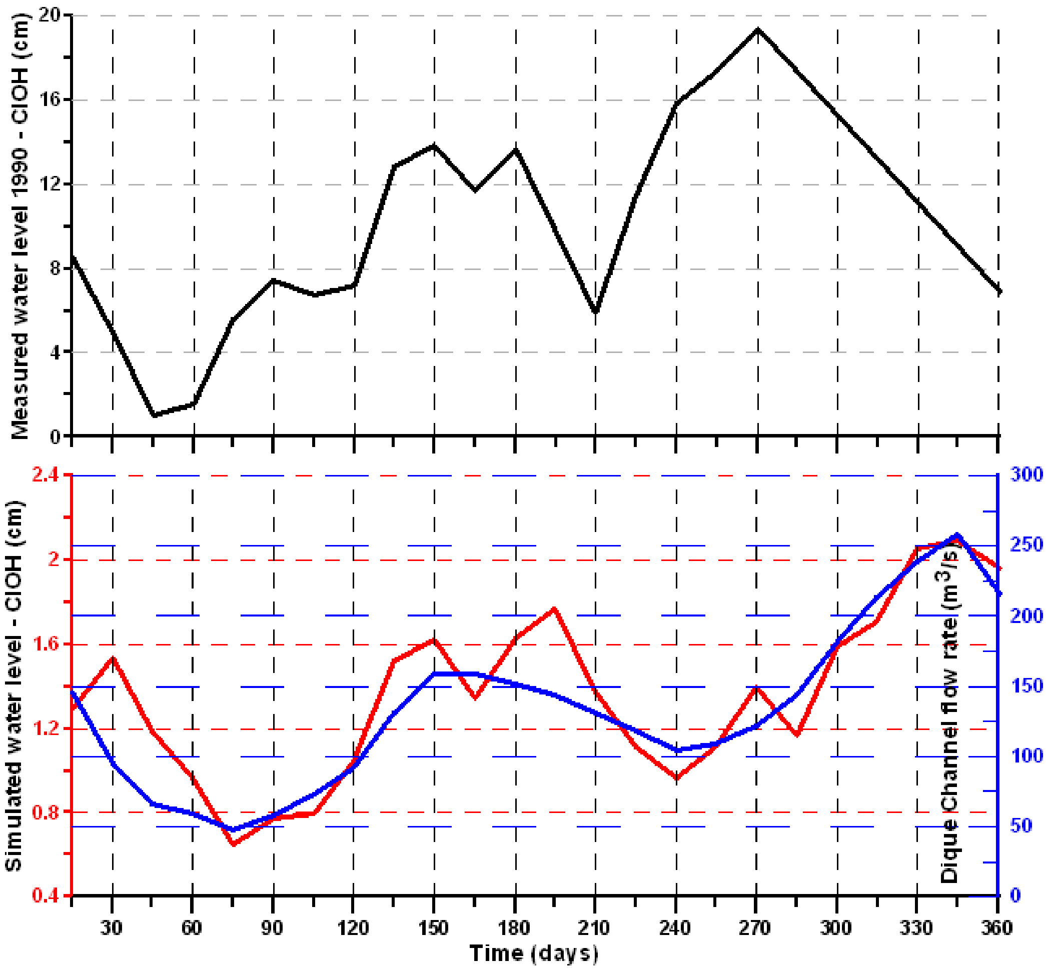

Figure 61. Water level results during the third experiment. Above: measured water level by the CIOH (records averaged every 15 days – black line); bellow: computed water level results (red line) – Dique Channel flow rate discharge (blue line).

6.4 Fourth Experiment

In order to understand the implications of the Dique Chanel discharge in the Cartagena bay hydrodynamics, vertical sections of the *u* and *v*- momentum components are obtained along three transects (figure 62) simulating the bay hydrodynamics during a tidal cycle, forcing the model with the average High Dique Channel flow rate Discharge (HDD – 150 m^3/s), and the average Low Dique Channel flow rate Discharge (LDD – 50 m^3/s).

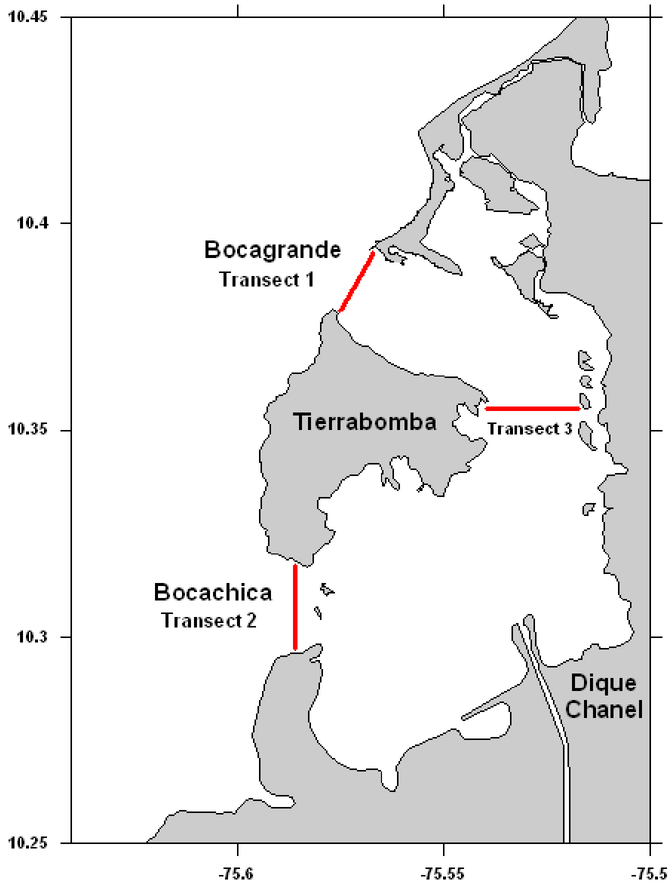

Figure 62. Transects (red lines) in which vertical sections of *u* and *v* currents components are calculated.

6.4.1 Fourth Experiment Results

During the entire tidal cycle, in Bocagrande (transect 1) the water flows mainly directed outside the bay, however during the rising period the currents decrease and oceanic denser water in the deeper layer can enter the bay passing over the Escollera sill (fig. 63)

In Bocachica (transect 2) the water exchange shows the same behaviour in the superficial layers (0 – 4 m) as in Bocagrande. However the existence of the navigational channel allows the entrance of oceanic water into the bay. On the surface, less dense mixed water flows outside of the bay, while denser oceanic water below the mixed water, enters to the bay. This dynamic is permanent during the tidal cycle (fig. 64).

In the middle of the bay (transect 3), the superficial water (0-5 m) flows north directed close to Tierrabomba, and south directed, but with lower velocity, close to the continent. In deeper layers the flow is slower and changes direction accordingly to the tide (fig. 65).

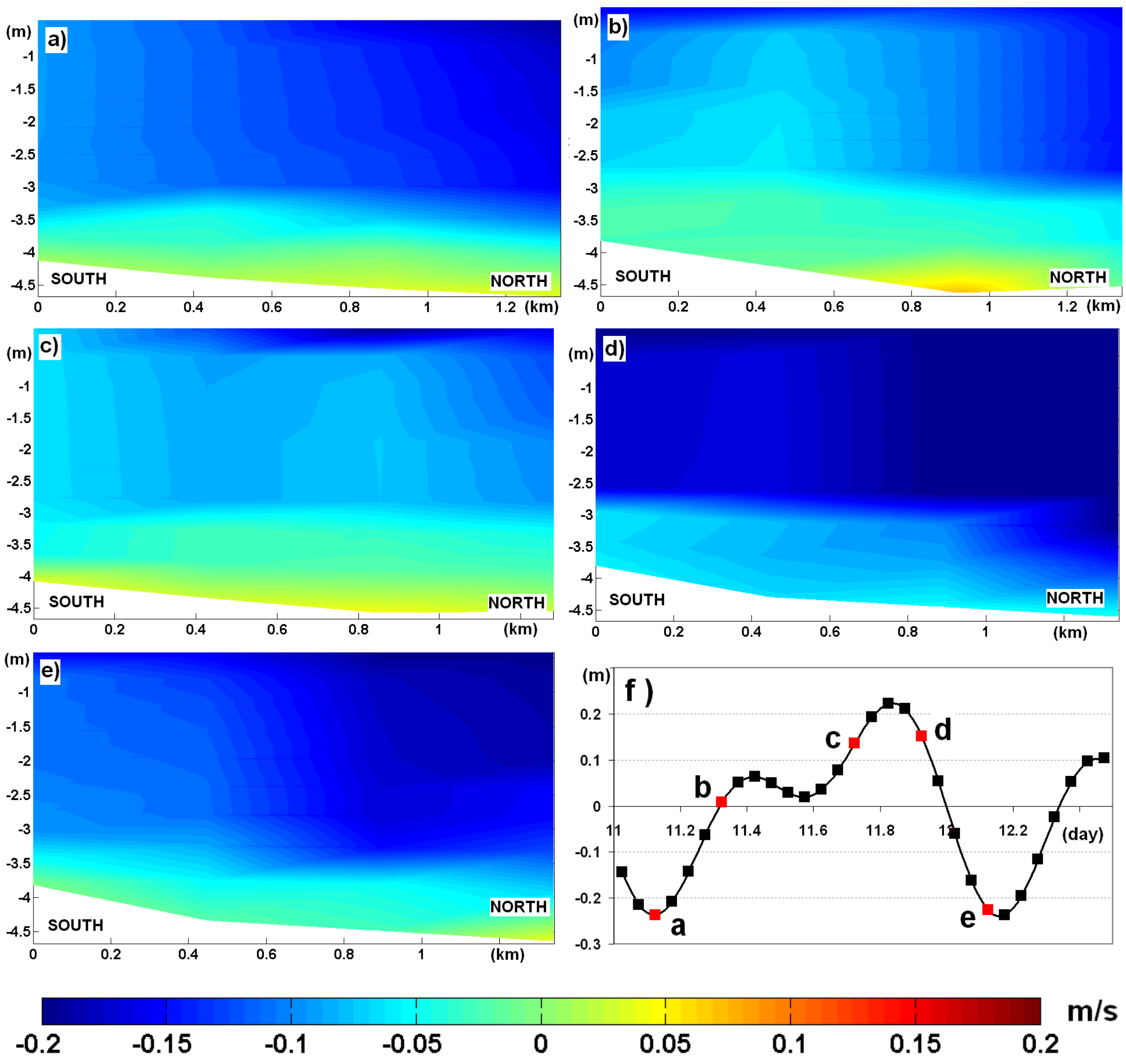

Figure 63. Vertical sections of current *u*-component in transect 1 (Bocagrande) during one tide cycle. The section starts (km. 0) in Tierrabomba Island. In f) the corresponding tidal cycle is plotted; red dots indicate the time in which the vertical sections were obtained. Blue colours represent the water flowing outside the bay.

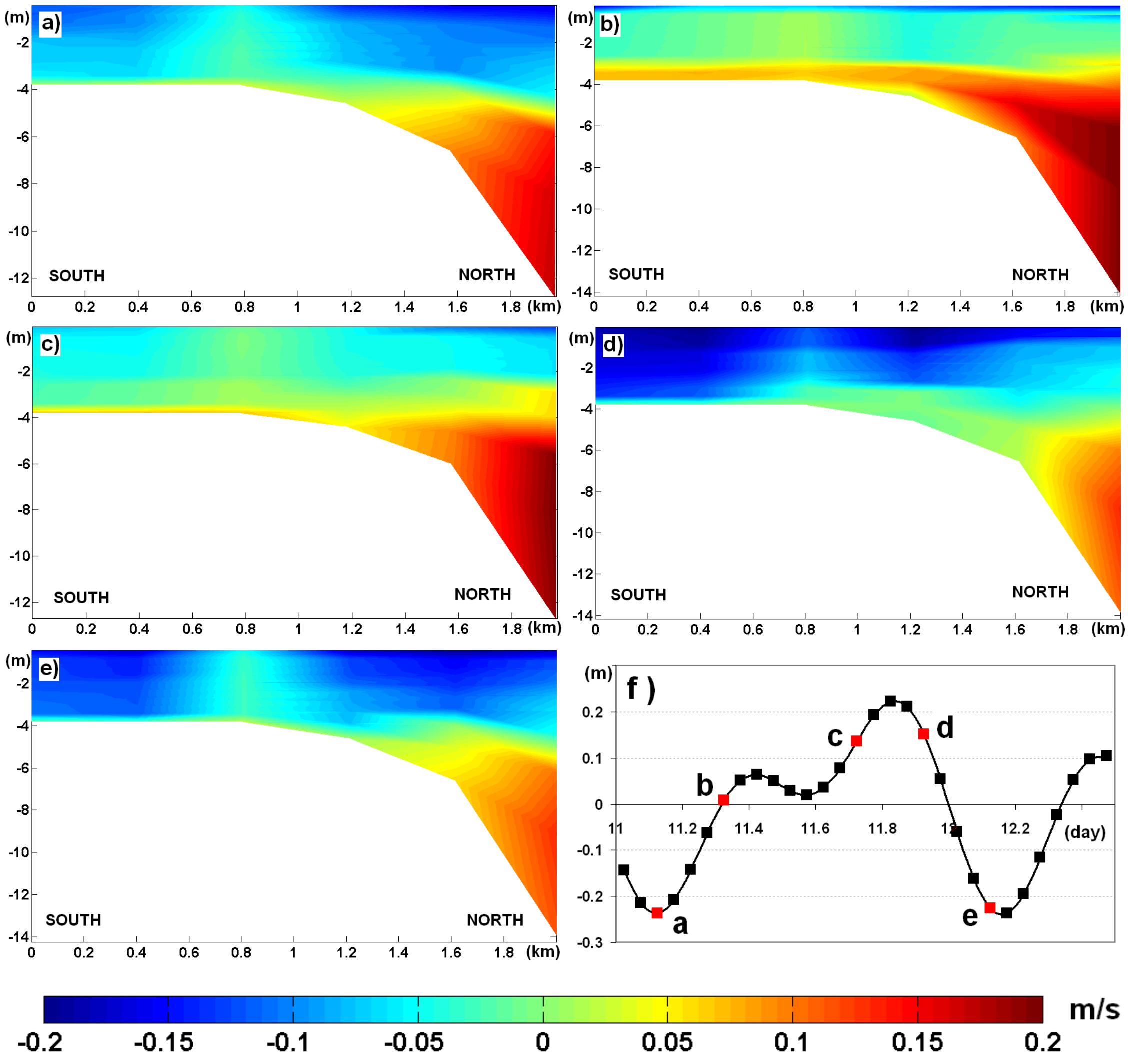

Figure 64. Vertical sections of current *u*-component in transect 2 (Bocachica) during one tide cycle. The section ends (km. 2) in Tierrabomba Island. In f) the corresponding tidal cycle is plotted; red dots indicate the time in which the vertical sections were obtained. Red colours represent the water flow entering the bay.

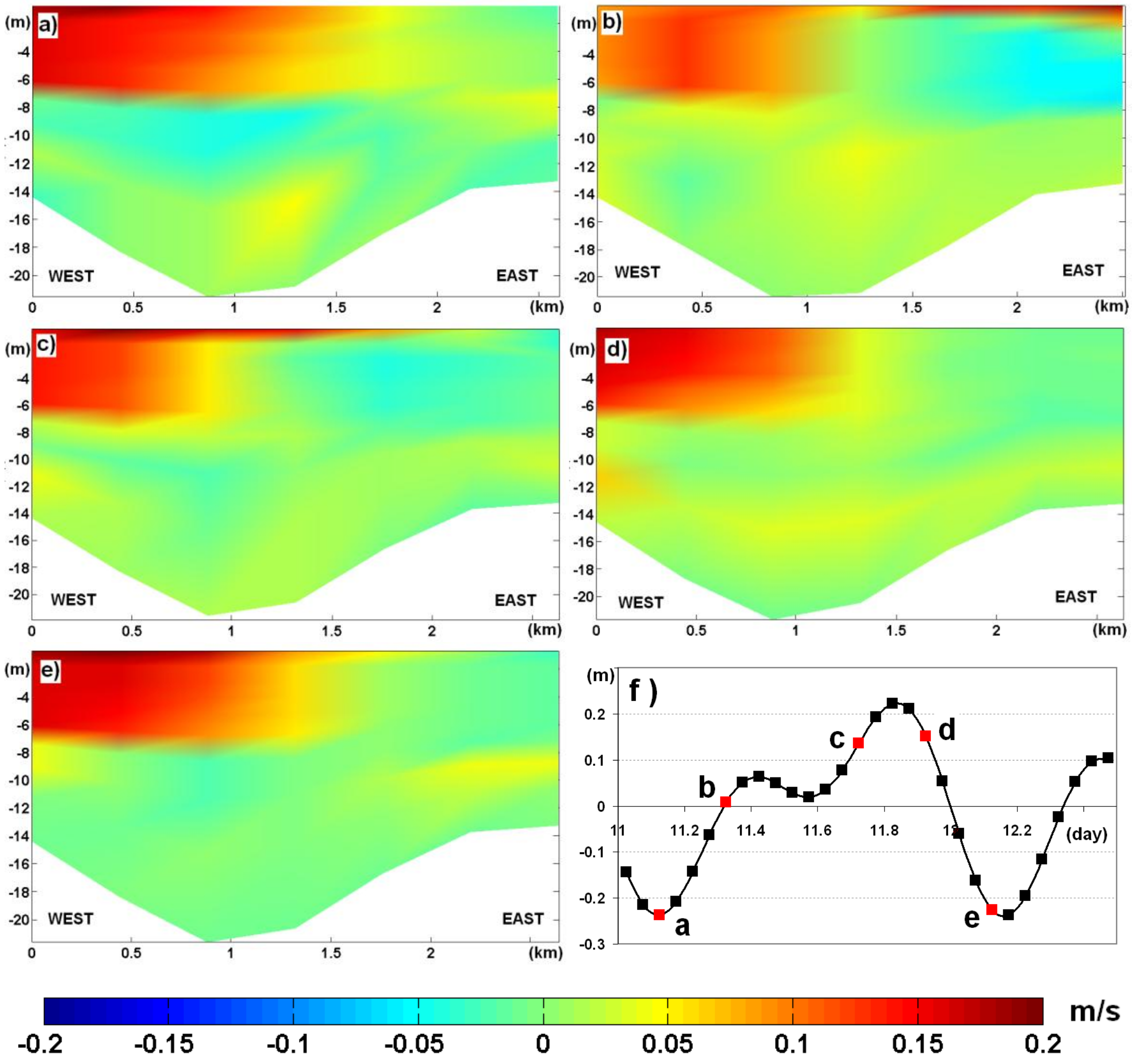

Figure 65. Vertical sections of current *v*-component in transect 3 (Bay) during one tide cycle. The section starts (km. 0) in Tierrabomba Island. In f) the corresponding tidal cycle is plotted; red dots indicate the time in which the vertical sections were obtained. Red colours represent the water flowing to the north.

The analysis of the averaged vertically integrated *u*-momentum component (fig. 66) reveals the water exchange mechanism of the bay. Through Bocagrande (transect 1) the water flows out of the bay; in Bocachica (transect 2), through the shallow water section of the transect (close to the continent), the water flows outside the bay, while along the deeper part (navigational channel), oceanic waters enters the bay.

The above water exchange mechanism depends on the tide and the Dique Channel flow rate. Comparing the vertically averaged *u*-momentum component obtained using LDD (50 m^3/s) in figure 67, with the one using higher flow rate (fig. 66), some differences are revealed. In Bocagrande (transect 1) the *u*-component weakens, and even positive values can be appreciated (fig. 67 – f) during the tide rising period. In Bocachica (transect 2), along the navigational channel, the *u*-momentum component weakens during the tide falling period and a change in direction is appreciated (fig. 67 – e). In the shallower section of Bocachica, higher current velocity in negative direction, during the rising tide period can be appreciated (fig. 67 – b, c, f)

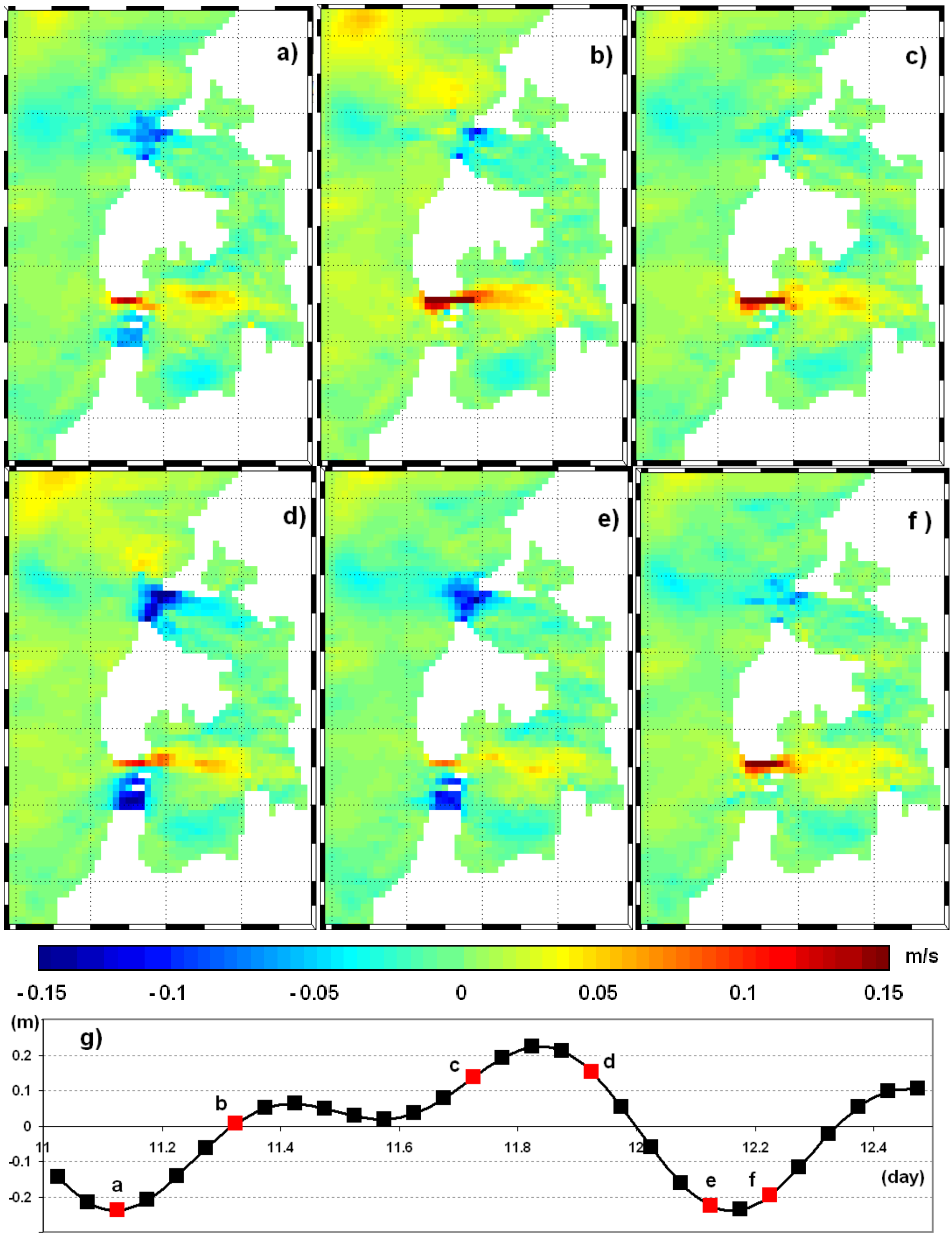

Figure 66. From a) to f) averaged vertically integrated *u*-momentum component on the basin using Dique Channel high rate discharge (150 m^3/s). In f) the corresponding tidal cycle is plotted; red dots indicate the time in which the vertically integrated *u*-momentum component was obtained.

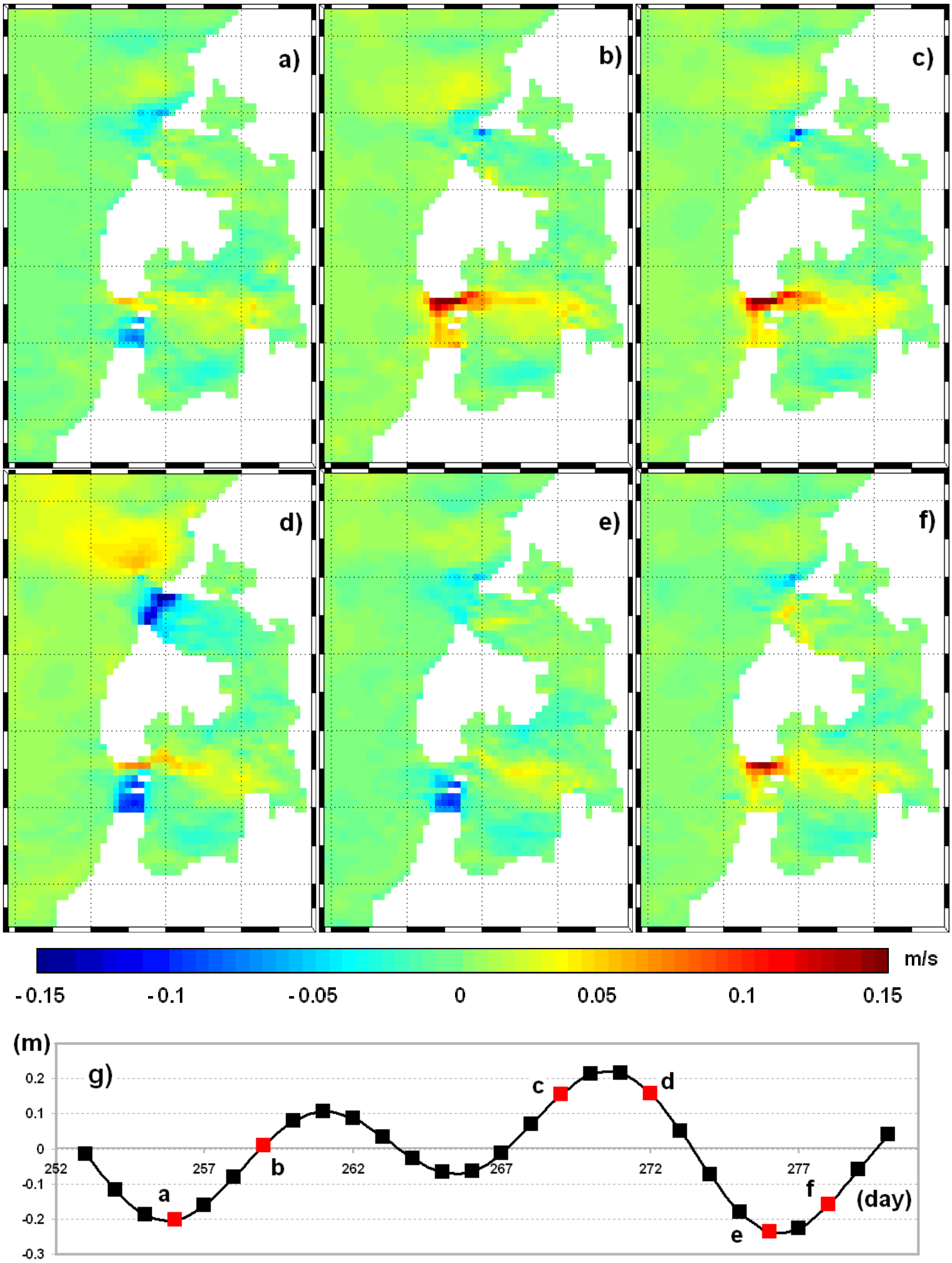

Figure 67. From a) to f) averaged vertically integrated *u*-momentum component on the basin using Dique Channel low rate discharge (50 m^3/s). In f) the corresponding tidal cycle is plotted; red dots indicate the time in which the vertically integrated *u*-momentum component was obtained.

6.5 Fifth Experiment

In order to clarify the findings in the fourth experiment, the vertically averaged *u* and *v* momentum in both entrances are used to find the resulting vertically averaged currents along Bocagrande and Bocachica during 15 days simulation using October 2001 forecasted tide, the HDD (150 m3/s) and the LDD (50 m3/s). No wind forcing is used.

In Bocagrande, to differentiate the vertically integrated inflow currents from the outflow currents, currents with directions (angles) higher than 53º and lesser than 233º are considered negative (outflow), while currents with directions lesser than 53º or higher than 233º are considered positive (inflow); this is according to the inclination angle of transect 1 (fig. 62).

In Bocachica (transect 2) currents with directions (angles) higher than 90º and lesser than 270º are considered negative (outflow currents), while currents with directions lesser than 90º or higher than 270º are considered positive, indicating inflow currents.

The distance between the nodes (transect 1: 430 m; transect 2: 302 m), the water level and the depth (of each node) along the transects were used to compute the water fluxes. The obtained vertically integrated currents in each node along the transects (transect 1 : 5 nodes; transect 2: 7 nodes) were averaged in order to obtain representative values of water fluxes for the transect.

6.5.1 Currents Through the Entrances

Considering HDD (150 m^3/s), the water flow mechanism in Bocagrande is mainly directed out of the bay; however, small differences exist along transect 1. In the center of the Bocagrande entrance, the current is weaker (in average -0.04 m/s) than at the edges (-0.08 m/s); along Bocagrande, the vertically integrated and averaged current was found to be -0.067 m/s (fig. 68).

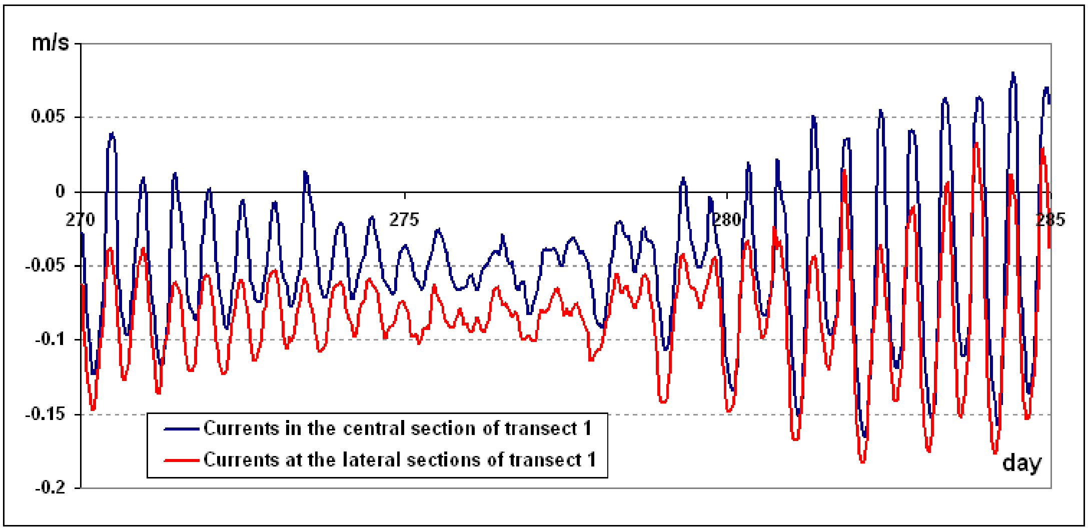

Figure 68. Vertically integrated and averaged currents along the Bocagrande entrance during HDD. Simulation time: 15 days. Blue: vertically integrated and averaged currents in the central section of the transect 1 (861 m long); red: vertically integrated and averaged current at the ends of the transect 1 (south-western section of the transect

1: 430 m long; north-eastern section of the transect 1: 860 m long). Negative values indicate flow exiting the bay.

The resulting vertically averaged currents along Bocachica are plotted in figure 69. According to the results, transect 2 can be divided in two sections. The first one extends from the south of the transect along 1500 m, and is characterized by -0.042 m/s vertically integrated and averaged outflow currents, while the northern section of the transect that extends along 906 m, is characterized by currents in opposite direction with the same magnitude (0.049 m/s).

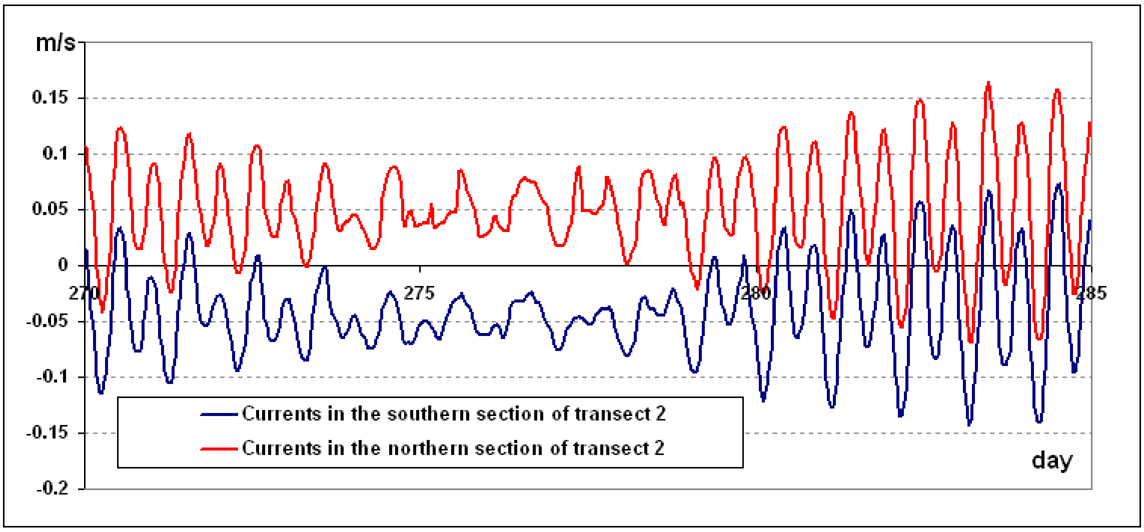

Figure 69. Vertically integrated and averaged currents along the Bocachica entrance during HDD. Simulation time: 15 days. Blue: vertically integrated and averaged current in the southern section of the transect 2 (1.500 m long); red: vertically integrated and averaged current in the northern section of transect 2 (906 m long). Negative values indicate flow exiting the bay.

Simulating the bay dynamics considering LDD (50 m^3/s), the results of the vertically integrated and averaged current along transects 1 and 2 are plotted in figures 70 and 71. In general, the currents behaviour is the same than during the HDD (fig. 68); however, the magnitudes are smaller; in the central section of transect 1 (Bocagrande) the vertically integrated and averaged current was found to be -0.027 m/s, while in the south-western and north-eastern the current was found to be -0.050 m/s.

In transect 2 (Bocachica), even though the results are very similar than those obtained considering HDD (fig. 69), the difference between the inflow and outflow currents is higher when LDD is considered. In this case a vertically integrated and averaged current of -0.033 m/s in the southern section of transect 2 was found, while in the northern section it was 0.0407 m/s (fig. 71).

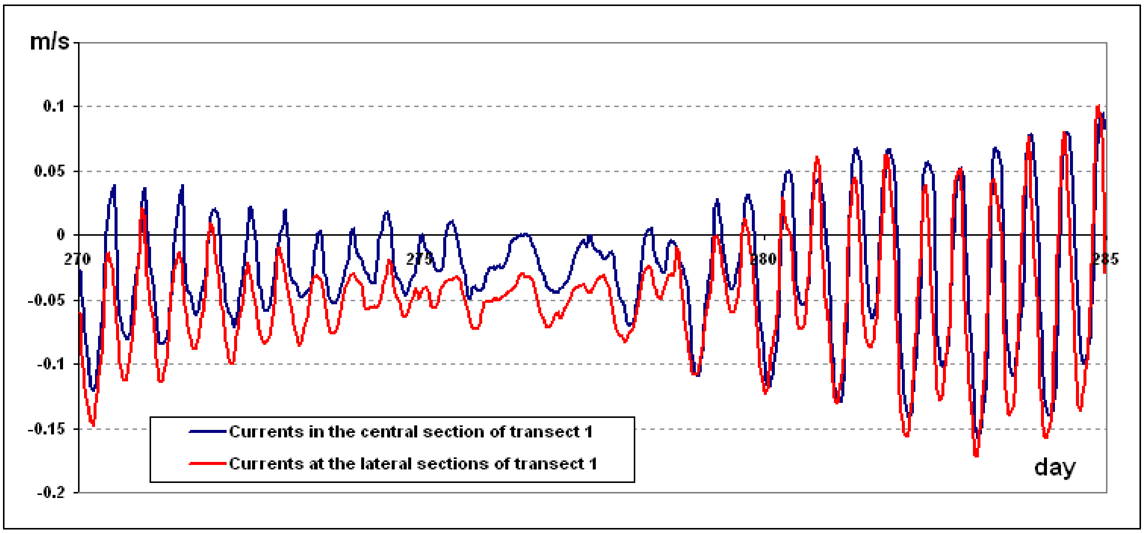

Figure 70. Vertically integrated and averaged currents along the Bocagrande entrance during LDD. Simulation time: 15 days. Blue: vertically integrated and averaged currents in the central section of the transect 1 (861m long); red: vertically integrated and averaged current at the extremes of the transect 1 (south-western section of the transect 1: 430 m long; north-eastern section of the transect 1: 860 m long). Negative values indicate flow exiting the bay.

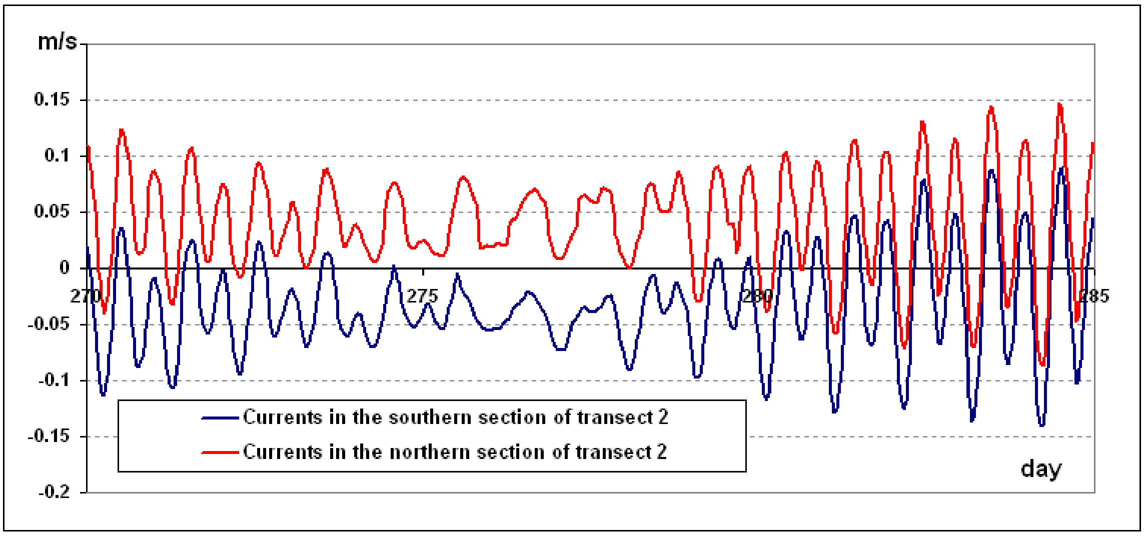

Figure 71. Vertically integrated and averaged currents along the Bocachica entrance during LDD. Simulation time: 15 days. Blue: vertically integrated and averaged current in the southern section of the transect 2 (1.500 m long); red: vertically integrated and averaged current in the northern section of transect 2 (906 m long). Negative values indicate flow exiting the bay.

6.5.2 Water Fluxes Through the Entrances

The water fluxes through the entrances of the bay during high and low Dique Channel flow rate discharge periods are calculated using the vertically integrated and averaged currents. In figure 72 and 73 these water fluxes are plotted.

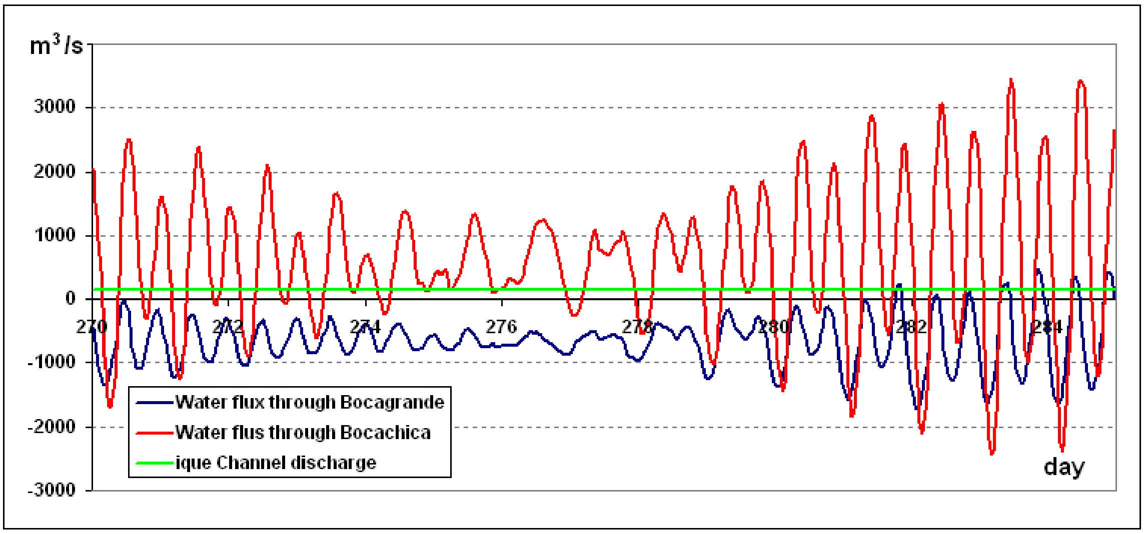

Figure 72. Vertically integrated and averaged water flux through Bocagrande (blue) and Bocachica (red), during 15 days simulation period considering HDD (green).

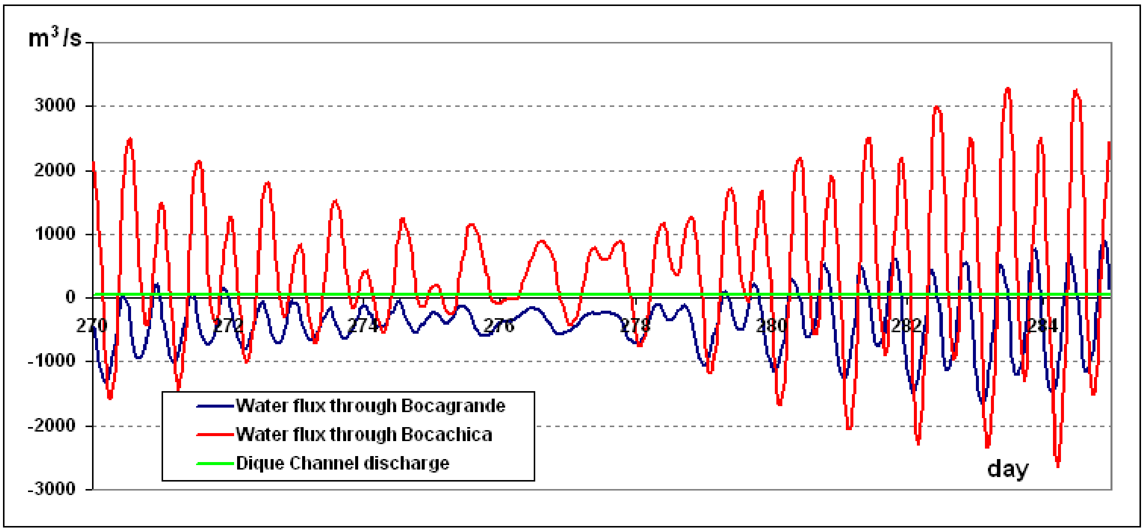

Figure 73. Vertically integrated and averaged water flux through Bocagrande (blue) and Bocachica (red), during 15 days simulation period considering LDD (green).

As was found previously, through Bocagrande the water flux is directed outside the bay in both cases (HDD and LDD – fig. 72, 73), while on average, through Bocachica the water flux is directed inside the bay; however, according to the results in table 15, through Bocagrande and during HDD, the water flux is higher than in Bocachica which results in a residual water outflow, but the water flux is positively balanced by the Dique Channel discharge.

During LDD, the water flux mechanisms works in on opposite way. The water inflow (through Bocachica) is higher than the outflow (through Bocagrande), which leads to a residual water inflow that is increased by the Dique Channel discharge. The total balance of water fluxes for both cases (HDD and LDD) including Bocagrande, Bocachica and the Dique Cannel is equal and positive.

Table 15. Vertically integrated and averaged water fluxes (m^3/s) through Cartagena Bay entrances during 15 days simulation, considering HDD and LDD.

Water fluxes (m^3/s)					
	Bocagrande (BG)	Bocachica (BCH)	Dique Chan.	BG - BCH	Total Balance
HDD	-664.25	585.49	150	-78.76	71.24
LDD	-390.97	414.53	50	23.55	73.55
Difference	-273.28	170.97	100	-102.31	-2.31

The fact that the total balance of water flux is positive and higher (73.55 m^3/s) for the LDD case than the Dique Channel discharge (50 m^3/s), may be explained due to the mixed character of the tide, in which two high tides are interrupted by one low tide higher than, or lower than but very close to, the mean sea level producing higher inflow water flux. Besides, the calculation was done during 15 days simulation period using the tide according to figure 74, and the water fluxes magnitudes may be different depending on the tides. These results just give an insight of the water exchange mechanism of the bay.

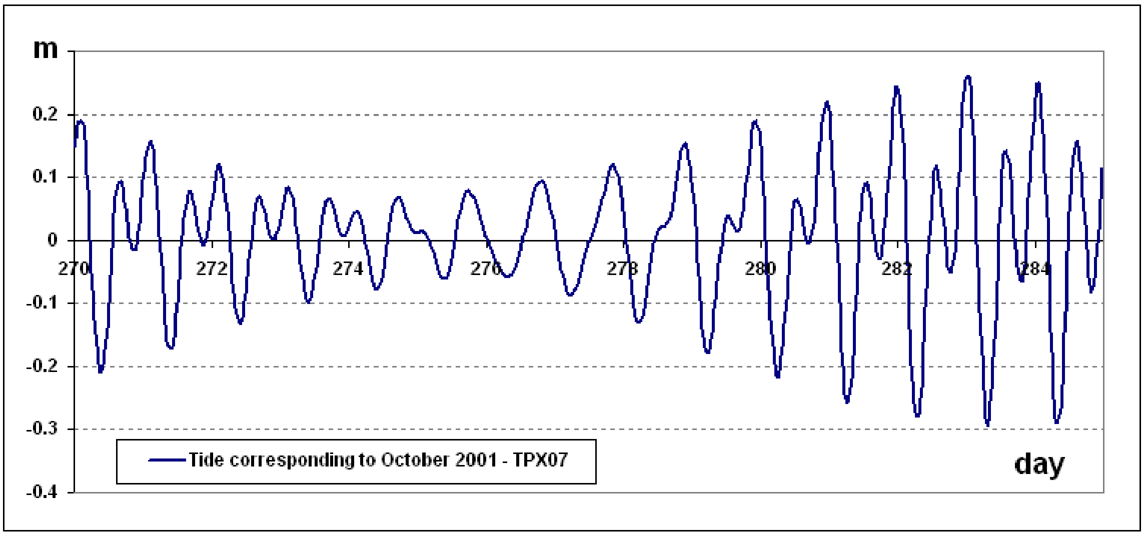

Figure 74. Tide forcing used for the calculation of the water fluxes through the entrances of the bay in the fifth experiment.

7 CONCLUSIONS AND RECOMENDATIONS

The water exchange mechanism of Cartagena Bay depends on the tides and the Dique Channel flow rate regime during the year. Through the Bocagrande entrance at the northwest of the bay, the water flux is directed outside the bay; at the center stronger currents can be found. The Escollera sill, between Tierrabomba Island and the continent, acts as a wall preventing the inflow of denser salty water, while the superficial and less dense mixed water, is pushed out of the bay by the currents generated by the Dique Channel discharge.

At the southwest of the bay, through the Bocachica entrance, two different water exchange regimes are detected. Close to the continent, in shallow waters, the water flux is directed outside the bay. Same characteristic is detected at the surface (0 – 4 m) over the navigational channel along the Bocachica entrance, but in deeper waters the water flux is directed into the bay (inflow).

During low Dique Channel flow rate discharge, that mechanism changes; in Bocagrande the *u*-current component weakens, and even positive values (inflow) can be obtained during the rising tide period. In Bocachica, along the navigational channel, the *u*-current momentum component weakens during the tide ebb period and a change in direction (outflow) is experienced. In the shallower section of Bocachica, higher current velocity in negative direction (outflow), during the rising tide period can be seen.

Considering that during the wet season, when the channel flow rate is maxima and the vertical exchange of the water is minima due to the absence of wind, a strong pycnocline is formed (*Tuchkovenko et al., 2003*), during the dry season the presence of the trade winds increases the vertical water exchange reducing the strong pycnocline what allows an improvement of the water exchange through the bay's entrances.

The Dique Channel discharge induces water level differences along the bay; higher water level is obtained close to the shore (continent), decreasing from the east to the west and increasing from the south to the north. This water level anomaly is in the order of 2 cm during high Dique Channel flow rate discharge; however this anomaly can be increased or decreased depending on the wind direction. Northern wind can produce an additional water level anomaly, pilling up the water against the southern shore of the bay in the order of 0.5 cm.

During December – March the predominant wind (North – trade winds), as was explained before, pushes the superficial water against the southern shore; in the northern part of the bay, the water level decreases (at this time of the year the Dique Channel experiences low flow rate levels); in the following months the wind force decrease. During September – December, the wind direction changes (southwest) and the Dique Channel flow rate discharge increase; that situation produces an increase in the order of 2 cm in the water level at the eastern shore of the bay.

During extreme Dique Channel flow rate discharge events (La Niña phenomenon), at the continental shore in the bay, the water level anomaly could reach a value in the order of 3 cm; however wind anomalies associated to the phenomenon have to be taken into consideration.

The effect of the Dique Channel in the Cartagena Bay water level is in the order of 10%, which does not explains the sea level rise throughout the year, in about 15 cm. Comparing the measured water level in Cartagena Bay with the data obtained by the IDEAM (National Institute of Meteorology) in Rosario Island, situated 40 km southwest of Cartagena (fig. 75), both time series show the same trend and similar water level magnitudes, indicating the presence of other forcings for the water level increment different than the Dique Channel discharge. Andrade C.A (personal communication) has hypothesised the role of cyclonic or anticyclonic circulation causing seasonal water level anomalies, since there is a mesoscale variability in the Caribbean related with eddies travelling close to the coast (*Nystuen and Andrade, 1993; Andrade and Barton, 2000; Jouanno et al., 2008; Jouanno et al., 2009*) and sea level variability at the coast is expected (Andrade, 2000).

Using ROMS_AGRIF that hypothesis could be confirmed. However, the wind regime in the bay and the effect of Tierrabomba Island should be evaluated. It is recommended to use a higher resolution grid in order to avoid problems related with the bathymetry, in a way that more realistic bottom topography can be used, considering its effects on the water exchange in the entrances of the bay.

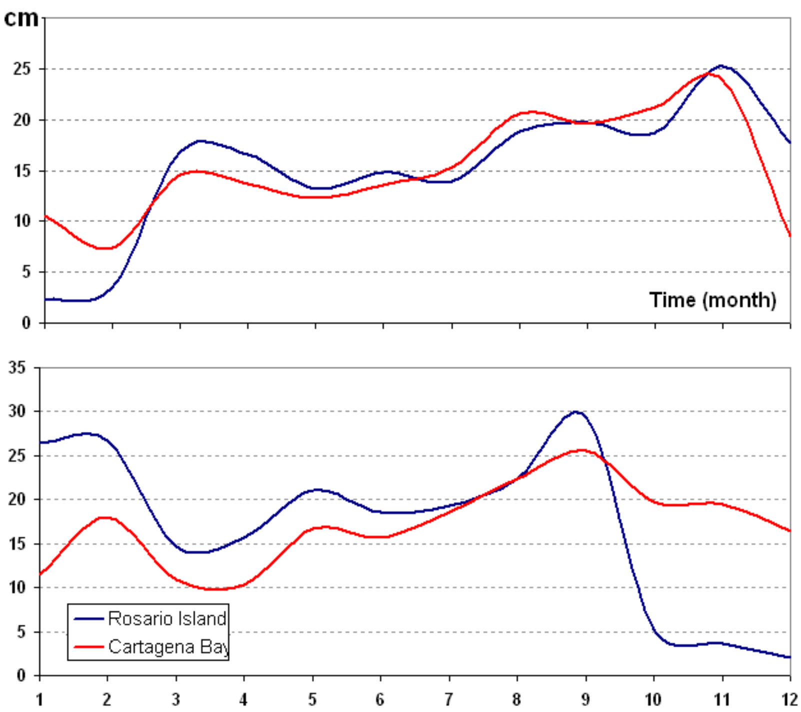

Figure 75. Monthly averaged water level at Rosario Island (blue) and Cartagena Bay (red). Above: 1999; below: 1997.

The calibration and validation of the model (ROMS) can be improved by monitoring water levels and currents at the entrances of the bay, considering that CODEGO was calibrated and validated by ecological surveys at Cartagena Bay (*Tuchkovenko et al., 2003*). Are required direct measurements of the Dique Channel flow rate at the mouth, considering that the values used in the present study were obtained using hydrodynamic modelling of the Dique Channel due to the lack of measurements (UNAL, 2007), which presents another source of uncertainty.

8 REFERENCES

Alexandre, L., Francoi, T., Paul, D., Torres, R., Andrade, C.A. 2008. Variabilidad del nivel del mar desde 1950 hasta el 2000 y riesgos asociados a episodios de mar de leva en las penínsulas de Bocagrande y Castillogrande, Cartagena de Indias, Colombia. [*Variability in the sea level between 1950 and 2000 and risks associated to events of swell in the Bocagrande and Castillogrande Peninsula*]. Bol. Cient. CIOH 26, 71-78.

Alvarez, R., Andrade, C.A., Aguilera, J., Nowak, P. 1995. Caracterización general de la zona de afloramiento de la Península de la Guajira [*General characterisation of the upwelling zone in the Guajira Peninsula*], J. Colombian Academy of Exact Physics and Natural Sciences, Vol. XIX, No.75, 679-694.

Andrade, C.A. 1993. Análisis de la velocidad del viento sobre el Mar Caribe, [*Analysis of the surface-wind speed over the Caribbean Sea*], Bol. Cient. CIOH 13, 33-44.

Andrade, C.A. 2000. The Circulation and variability of the colombian basin in the Caribbean Sea. PhD Thesis, School of Ocean Sciences, University of Wales. 248.

Andrade, C.A., Barton, E. 2000. Eddy development and motion in the Caribbean sea. J. Geophys. Res., 105(C11), 26191-26201.

Andrade, C.A., Barton, E., Mooers, C. 2003. Evidence for an eastward flow along the Central and South American Caribbean Coast. J. Geophys. Res., 108(C6), 3185, doi:10.1029/2002JC001549.

Antonov, J. I., Locarnini, R. A., Boyer, T. P., Mishonov, A. V., Garcia, H. E. 2006. World Ocean Atlas 2005, Volume 2: Salinity. S. Levitus, Ed. NOAA Atlas NESDIS 62, U.S. Government Printing Office, Washington, D.C., 182.

Arabelos, D., Asteriadis, G., Contadakis, M., Spatalas, S., Sachsamanoglou, H. 1997. Atmospheric tides in the area of Thessaloniki. J. Geodynamics 23. No.1., 65-75.

Blumberg, A.F., G.L. Mellor. 1987. A Description of a three-dimensional coastal ocean circulation Model, in three-dimensional coastal ocean models. American Geophysical Union. 4, 208.

Cheng R., Gardner, J. 1985. Harmonics analysis of tides and tidal currents in south San Francisco Bay, California. Estuarine. Coastal and Shelf Science 21, 57-74.

CIOH. 1997. Estudios que identifican la condición ambiental del ecosistema, grado de impacto sobre los componentes biológicos, potencial de la capacidad de recuperación y acciones de rehabilitación del sistema de la Bahía de Cartagena. [*Studies to identify the environmental condition of the ecosystem and the degree of impacts on the biological components, potential recovery capacity and actions to rehabilitate the Cartagena Bay system*]. Project: GEF/RLA/93/G41. Final Report.

CIOH. 1998. Numerical modelling of the coastal circulation and their application in the study of the processes of the transport of substances and contaminated particulates in the Colombian Caribbean coastal zone. CIOH-COLCIENCIAS Cod.0140-09-347-95. Final Report.

CIOH. 1999. Executive report. Project: Diseño preliminar del modelo numérico 2D-3D de calidad de aguas para el Canal del Dique y sus sistemas lagunares. [*Preliminary design for a Dique Channel 2D-3D water quality numerical model*] . 24 pp.

CIOH. 2004 – 2010. Monthly Meteomarine Weather Report. Internet: http://www.cioh.org.co/index.php?option=com_content&task=view&id=61&Itemid=185

CIOH. 2005. Naval Academy. Faculty of Marine Sciences – (Undergraduate project: Forecasting the behaviour of hurricanes over the Caribbean Sea for the 2006 cyclonic season. 42 pp.

CLIVAR/VAMOS/PACS .1998. Workshop on field programs and CLIVAR/VAMOS Panel Meeting-1 (VPM-1). Instituto Oceanográfico, University of São Paulo, São Paulo, Brazil March 30 - April 2, 1998. In: http://www.atmos.ucla.edu/~mechoso/VPM.html

CNR – (Compagnie Nationale du Rhône). 2007. Estudio de factibilidad y anteproyecto para el programa de restauración del Canal del Dique en Colombia [*Feasibility study for the restoration program of the Dique Channel*]. Final report – Apendix (4/6). N°: DI-EE 07-262a.

DaSilva, A., Young, A., Levitus, S. 1994. Atlas of surface marine data 1994, volume 1: Algorithms and procedures.," Tech. Rep. 6, U.S. Department of Commerce, NOAA, NESDIS.

DiMego, G.J., Bosart, L.F., Enderson, G.W. 1976. An examination of the frequency and mean conditions surrounding frontal incursions into the Gulf of Mexico and the Caribbean Sea: Monthly Weather Review 104, 709-718.

Egbert, G., Erofeeva, L. 2002. Efficient inverse modeling of barotropic ocean tides. J. Atmos. Ocean. Technol. 19, 183-204.

El Tiempo. Colombian Newspaper. 2010. Marea alta tiene locos a los habitantes de Cartagena. [*High tide is driven the Cartagena inhabitants mad*]. September 23rd 2010. In: http://www.eltiempo.com/archivo/documento/CMS-4684541.

Fine, R.A., Molinari, R.L. 1988. A continuous deep western boundary current between Abaco (26.5 N) and Barbados (13 N). Deep Sea Res. 35, 1444 – 1450.

Foreman, M. 1996. Manual for tidal heights analysis and prediction. IOS, Pacific Marine. Science Report 77. pp 66.

Garay, T., Giraldo L. 1997. Influencia de los aportes de materia orgánica externa y autóctona en el decrecimiento de los niveles de oxigeno disuelto en la Bahía de Cartagena, Colombia. [*Influence of the autochthonous and external organic matter inputs in the decreasing levels of dissolved oxygen in the Bay of Cartagena, Colombia*]. Bol. Cient. CIOH 18, 1-13.

Gianinni, A., Kushnir, Y., Cane, M. 2000. Interannual variability of Caribbean rainfall, ENSO, and the Atlantic Ocean.. Journal of Climate 13, pp 15.

Haney, R. L. 1991. On the pressure gradient force over steep topography in sigma coordinate ocean models. J. Phys. Oceanogr. 21, 610– 619.

Hedström, K. 2009. DRAFT Technical Manual for a Coupled Sea-Ice/Ocean Circulation Model (Version 3). Arctic Region Supercomputing Center. University of Alaska Fairbanks, 161 pp.

Hess, K.W., 1985. Assessment model for estuarine circulation and salinity. NOAA Technical Memorandum NESDIS AISC3—National Environmental Satellite, Data, and Information Service, USA, Washington, DC, 39 pp.

Holcombe, T.S., Moore W.S. 1977. Paleocurrents in the eastern Caribbean: Geophysical evidence and interpretations. Mar. Geol. 23, 35-56.

Hu, L., Liu, L., Sun,H. 2007. Comments on “analysis and prediction of ocean tides by the computer program VAV” by B. Ducarme, A.P. Venedikov, J. Arnoso and R. Vieira. J. Geodynamics 44, 91-95.

IDEAM. 1995. Atlas Climatológico Nacional. 285 pp.

Jouanno, J., Sheinbaum, J., Barnier, B., Molines, J. 2009. The mesoscale variability in the Caribbean Sea. Part II: energy sources. Ocean Modelling 26, 226 – 239.

Jouanno, J., Sheinbaum, J., Barnier, B., Molines, J.M., Debreu, L., Lemarié, F., 2008. The mesoscale variability in the Caribbean Sea. Part I: simulations with an embedded model and characteristics. Ocean Modelling 23, 82–101.

Kazakov A.L., Lezhenin, A.A., Spreranzkiy, L.S. 1996. Resultados preliminares del estudio de la capa límite meso-meteorológica de la atmósfera en la costa norte colombiana aplicando un modelo numérico. [*Preliminary results on the study of the atmosphere meso-meteorological limit layer on the north coast of Colombia applying a numerical model*]. Bol. Cient. CIOH 17, 17-26.

Kjerfve, B. 1981. Tides in the Caribbean Sea, J. Geophys. Res., 86(C5), 4243 – 4247.

Large. W., McWilliams, M., S. C. Doney. 1994. Oceanic vertical mixing: a review and a model with a nonlocal boundary layer parameterization. Rev. Geophys., 32, 363–403.

Leaman, K., Donoso, M. 2001. Tropical intraseasonal and longer-period variability of precipitation in the isthmus of Panama. J. Hydro. Sci.. Tech.. 7 (1-4), 203-222.

Lemaitre, E. 1998. Caminos reales de Colombia. El tránsito del Canal del Dique. [*Royal ways of Colombia. The transit f the Dique Channel*]. Fondo Fen. 1998.

Lee, T.N., Johns W. E., Zantopp, R. J., Fillenbaum, E.R. 1996. Moored observations of western boundary current variability and thermohaline circulation at 26.5° N in the subtropical North Atlantic. J. Phys. Oceanogr., 26, 962-983.

Locarnini, R. A., Mishonov, A. V., Antonov, J. I., Boyer, T. P., Garcia, H. E. 2006. World Ocean Atlas 2005, Volume 1: Temperature. S. Levitus, Ed. NOAA Atlas NESDIS 61, U.S. Government Printing Office, Washington, D.C., 182 pp

Lonin, S.A., 1997. Cálculo de la transparencia del agua en la Bahia de Cartagena. [*Evaluation of the water transparency in Cartagena Bay*]. Bol. Cient. CIOH 18, 85–92.

Lonin, S.A., Giraldo, L. 1995a. Circulación de las aguas y transporte de contaminantes en la Bahia Interna de Cartagena. [*Water circulation and transport of contaminants in the Cartagena's internal bay*]. Bol. Cient. CIOH 16, 25-56.

Lonin, S.A., Giraldo, L. 1995b. Influencia del intercambio térmico a través del fondo marino en el régimen de temperaturas en zonas costeras. [*The influence of the temperature exchange through the sea bottom in the coastal zone temperature*]. Bol. Cient. CIOH 16, 57-72.

Lonin, S.A., Giraldo, L. 1996. Influencia de los efectos térmicos en la circulación de la bahía interna de Cartagena. [*The influence of the thermal effects in the circulation of the Cartagena's internal bay*]. Bol. Cient. CIOH 17, 47-56.

Maul, G.A. 1993. Climatic Change in the Intra-Americas Sea. United Nations Environment Program, Edward Arnold Publishers, London. 389 pp.

Mellor, G., Yamada, T. 1974. A hierarchy of turbulence closure models for planetary boundary layers. J. Atmos. Sci., 31, 1791–1806.

Mesa O., G. Poveda, L.F. Carvajal. 1997. Introducción al clima de Colombia. Universidad Nacional de Colombia. Sede Medellín. Facultad de Minas.

Mofjeld, H.O., Wimbush, W. 1977. Bottom pressure observations in the Gulf of Mexico and Caribbean Sea. Deep Sea Res., 24, 987-1004.

Molares, R. 2004. Clasificación e identificación de las componentes de marea del Caribe colombiano. [*Identification and classification of the Colombian Caribbean tide components*]. Bol. Cient. CIOH 22, 105-114.

Molinari, R.L., Fine, R.A., Johns, E. 1992. The deep western boundary current in the tropical North Atlantic Ocean, Deep Sea Res., 39, 1967-1984.

Nystuen, J.A., Andrade, C.A. 1993.Tracking mesoscale ocean features in the Caribbean Sea using GEOSAT altimetry. J. Geophys. Res., 98, 8389-8394.

Ordoñez, J., Cubillos, E., Forero, G. 2007. Balance hídrico y sedimentológico del Canal del Dique y sus efectos sobre la sedimentación de la bahía de Cartagena. [*The Dique Channel hydraulic and sedimentary balance and their effects on the Cartagena bay sedimentation*]. Third regional symposium in hydraulics on rivers. 18 pp.

Penven, P., Marchesiello, P., Lefevre, J. 2008. Software tools for pre- and post-processing of oceanic regional simulations. Environmental Modelling & Software 23, 660-662.

Penven, P., Cambon, G., Tan, T., Marchesiello, P., Debreu, L. 2010. ROMS AGRIF / ROMSTOOLS User’s Guide. Institut de Recherche pour le Développement (IRD). 91 pp.

Poveda, G. 2004. La hidro-climatología de Colombia: Una síntesis desde la escala interdecadal hasta la escala diurna. [*The hydro-climatology of Colombia: A review from the inter-decadal to the diurnal scale*]. Rev. Acad. Colomb. Cienc., 28, 201-222.

Poveda, G., Mesa, O. J. 1997. Feedbacks between hydrological processes in tropical South America and large-scale ocean-atmosphere processes. J. Climate, 10, 2690-2702.

Pujos, M., Pagliardini, J.L., Steer, R., Vernette, G., Weber, O. 1986. Influencia de la contra-corriente norte colombiana para la circulación de las aguas en la plataforma continental y su acción sobre la dispersión de los efluentes en suspensión del rio Magdalena [*Influence of the north Colombian counter-current on the circulation of the continental platform: its action on the dispersion of effluents in suspension from the Magdalena River*] Bol. Cient. CIOH 6, 3-15.

Rivera, S., Molares, R. 2003. Evidencias de la oscilación del tipo Madden-Julian en el Caribe colombiano [*Evidences of the Madden Julian Oscillation in the Colombian Caribbean Sea*]. Bol. Cient. CIOH 21, 101-113.

Restrepo, J., Lopez, S. 2008. Morphodynamics of the Pacific and Caribbean deltas of Colombia, South America. Journal of South American Earth Sciences 25, 1–21

Seemüller, W., Seitz, M., Sánchez, L., Drewes, H. 2009. The position and velocity solution SIR09P01 of the IGS Regional Network Associate Analysis Centre for SIRGAS (IGS RNAAC SIR). DGFI Report 85. 96 pp.

Shchepetkin, A., McWilliams, J. C. 2005. The regional ocean modelling system (ROMS): A split-explicit, free-surface, topography-following coordinates oceanic model. Ocean Modelling, 9, 347–404.

Shi, W., L’Heureux, M., Halpert, M. 2011. Climate Diagnostic Bulletin – NOAA. Report April 2011, 90.

Smith, W. H. F., Sandwell, D.T. 1997. Global sea floor topography from satellite altimetry and ship depth soundings. Science 277, 1957-1962.

Song, Y., Haidvogel, D. B. 1994. A semi-implicit ocean circulation model using a generalized topography-following coordinate system. J. Comp. Phys., 115 (1), 228-244.

Stommel, H. 1965. The Gulf Stream. University of California Press, 2nd Ed., 248pp.

Sutherland, M., Dare, P., Miller, K. 2008. Monitoring sea level change in the Caribbean. Geomatica 62 (4), 428-436.

Tuchkovenko, Y., Lonin, S.A., Calero, L. 2002. Modelo de eutrofización de la Bahía de Cartagena y su aplicación práctica. [*Cartagena Bay eutrofication model and it´s practical application*]. Bol. Cient. CIOH 20, 28-44.

Tuchkovenko, Y., Lonin, S.A. 2003. Mathematical model of the oxygen regime of Cartagena Bay. Ecological Modelling 165, 91–106.

UNAL. 2007. Project: Study and research about the works for environmental and navigational restoration for the Dique Channel. Report CM-CD-2. 97 pp.

UNAL. 2008. Flow rate reduction alternative of the Dique Channel through the narrowing of the channel section by sectors and the construction of the lock of Paricuica. Final report CM-513. Vol. 1.

Umlauf, L., Burchard, H. 2001. A generic length-scale equation for geophysical turbulence models. J. Marine Res., 61, 235–265.

Vides, M.P. 2008. Sea-level rise coastal adaptation. Technical Report NCAP Colombia Project. ETC Project Number 032135. Marine and Coastal Research Institute. INVEMAR. Santa Marta, Colombia. 290 pp.

Zerbini, S., Plag, H., Baker, T., Becker, M., Billiris, H., Biirki, B., Kahle, H., Marson, I., Pezzoli, L. Richter, B., Romagnoli, C., Sztobryn, M., Tomasi, P., Tsimplis, M., Veis, G., Verrone, G. 1996. Sea level in the Mediterranean: a first step towards separating crustal movements and absolute sea-level variations. Global and Planetary Change 14, 1-48.